

DTIC FILE COPY

12

AD-A181 178

TGAL-86-5

MODELS OF THE FREQUENCY DEPENDENCE OF Q IN THE MANTLE UNDERLYING TECTONIC AREAS OF NORTH AMERICA, EURASIA AND EASTERN PACIFIC

Z.A. Der, W.W. Chan, A.C. Lees, and M.E. Marshall
Teledyne Geotech Alexandria Laboratories
314 Montgomery Street
Alexandria, Virginia 22314-1581

OCTOBER 1986



FINAL TECHNICAL REPORT:

ARPA ORDER NO: 4511

PROJECT TITLE: Frequency Dependence of Q

CONTRACT: F08606-85-C-0023

Approved for Public Release; Distribution Unlimited.

Prepared for:
DEFENSE ADVANCED RESEARCH PROJECTS AGENCY
1400 Wilson Boulevard
Arlington, VA 22209

Monitored By:
AFTAC/TGR
PATRICK AFB
FLORIDA 32925-6001

The views and conclusions contained in this report are those of the authors and should not be interpreted as representing the official policies, either expressed or implied, of the Defense Advanced Research Projects Agency or the U.S. Government.

87

6

4

019

UNCLASSIFIED

SECURITY CLASSIFICATION OF THIS PAGE

REPORT DOCUMENTATION PAGE

Form Approved
OMB No. 0704-0188
Exp. Date: Jun 30, 1986

1a REPORT SECURITY CLASSIFICATION UNCLASSIFIED			1b. RESTRICTIVE MARKINGS		
2a SECURITY CLASSIFICATION AUTHORITY			3 DISTRIBUTION/AVAILABILITY OF REPORT Approved for public release; distribution unlimited.		
2b DECLASSIFICATION/DOWNGRADING SCHEDULE					
4 PERFORMING ORGANIZATION REPORT NUMBER(S) TGAL-86-5			5. MONITORING ORGANIZATION REPORT NUMBER(S)		
6a NAME OF PERFORMING ORGANIZATION Teledyne Geotech Alexandria Laboratories		6b OFFICE SYMBOL (if applicable)	7a. NAME OF MONITORING ORGANIZATION AFTAC/TGR		
6c. ADDRESS (City, State, and ZIP Code) 314 Montgomery Street Alexandria, Virginia 22314-1581			7b. ADDRESS (City, State, and ZIP Code) Patrick Air Force Base Florida 32925-6001		
8a. NAME OF FUNDING / SPONSORING ORGANIZATION DARPA		8b. OFFICE SYMBOL (if applicable) GSD	9. PROCUREMENT INSTRUMENT IDENTIFICATION NUMBER F08606-85-C-0023		
8c. ADDRESS (City, State, and ZIP Code) 1400 Wilson Blvd. Arlington, VA 22209			10. SOURCE OF FUNDING NUMBERS PROGRAM ELEMENT NO 62714E	PROJECT NO. PA DT/5122	TASK NO. WORK UNIT ACCESSION NO.
11. TITLE (Include Security Classification) Models of the Frequency Dependence of Q in the Mantle Underlying Tectonic Areas of North America, Eurasia and Eastern Pacific					
12. PERSONAL AUTHOR(S) Z.A. Der, W.W. Chan, A.C. Lees and M.E. Marshall					
13a. TYPE OF REPORT Final Technical Report		13b. TIME COVERED FROM Mar 85 TO Sep 86		14. DATE OF REPORT (Year, Month, Day) 1986 October 30	
15. PAGE COUNT 171					
16. SUPPLEMENTARY NOTATION					
17. COSATI CODES			18. SUBJECT TERMS (Continue on reverse if necessary and identify by block number)		
FIELD	GROUP	SUB-GROUP	Attenuation, Frequency Dependence Q, Magnitude, Eurasia, North America, E. Pacific		
08	11				
17	10				
19. ABSTRACT (Continue on reverse if necessary and identify by block number)					
<p>The results of wide-band data analyses for the determination of frequency dependent Q models of the mantle under the tectonic areas of Eurasia, North America and the Eastern Pacific are presented. For tectonic areas of Eurasia, the spectra of short period P waves from Kazakh explosions are used to estimate t^* in the 1 to 8 Hz range. For shield to tectonic paths, $t_p^* \sim 0.35$ sec which gives $t_p^* \sim 0.6$ sec for tectonic to tectonic paths. P wave rise times from the same events give upper bounds on the estimates of t_p^* to be ~ 0.8 sec. The large difference between the spectral and rise time estimates may be due to scattering. In the 0.5 to 1.3 Hz range, PP and P amplitude ratios give $t_p^* \sim 0.5$ sec for PP's relative to surface reflection points under the Eurasian shield. Amplitude ratios of long period multiple ScS phases were used to estimate attenuation in the 0.3 to 0.9 Hz band. Under tectonic Eurasia, these analyses gave $(t_{ScS}^*) \sim 3.9 \pm 0.4$ sec. Thus, for Eurasia, $t^*(f)$ for tectonic paths is approximately parallel to, but approximately 0.25 sec (for t_p^*) greater than $t^*(f)$ under the shield. <i>→ next page</i></p>					
20 DISTRIBUTION/AVAILABILITY OF ABSTRACT <input checked="" type="checkbox"/> UNCLASSIFIED/UNLIMITED <input type="checkbox"/> SAME AS RPT <input type="checkbox"/> DTIC USERS			21. ABSTRACT SECURITY CLASSIFICATION UNCLASSIFIED		
22a. NAME OF RESPONSIBLE INDIVIDUAL Dr. Dean Clauter			22b. TELEPHONE (Include Area Code) (305) 494-5263		22c. OFFICE SYMBOL TGR

DD FORM 1473, 84 MAR

B3 APR edition may be used until exhausted
All other editions are obsoleteSECURITY CLASSIFICATION OF THIS PAGE
UNCLASSIFIED

+ or -
+ sub ScS of approx.
+ sub p

(19. Continued)

For North America, the amplitudes of long period multiple ScS phases were analyzed for two type of paths. Multiple ScS amplitudes recorded in the Northeastern US for events in the Aleutians (paths across the Canadian shield) give $t_{scs}^* \sim 1.1 \pm 0.4$ sec. Similar data recorded in the Southeastern US for a Central American event, gives $t_{scs}^* \sim 4.0 \pm 0.9$ sec. These data analyses show that the attenuation in the long period band in North America varies in the same sense regionally as shown in previous work in the short period band. For Eastern Pacific the upper mantle attenuation appears to be the highest of all regions studied with t^* uniformly higher than in the two "tectonic" continental areas discussed above.

These findings support the general idea proven for continental North America by Der and Lees (1985) that $t^*(f)$ curves for teleseismic paths crossing the upper mantle in various areas of the world generally do not converge towards the long period end of the seismic spectrum as implied by some "absorption band shift" models. Instead, the $t^*(f)$ curves tend to run quasi-parallel throughout the seismic frequency band as one would expect if the lateral Q variations in the upper mantle are caused by changes in temperature and chemical composition over large depth ranges (Minster and Anderson, 1980; Jordan 1975). These broad-band frequency dependent attenuation models must be known when applying attenuation correction to yield estimates.

SUMMARY

The results of wide-band data analyses for the determination of frequency dependent Q models of the mantle under the tectonic areas of Eurasia, North America and the Eastern Pacific are presented. For tectonic areas of Eurasia, the spectra of short period P waves from Kazakh explosions are used to estimate t^* in the 1 to 8 Hz range. For shield to tectonic paths, $\overline{t_p^*} \sim 0.35$ sec which gives $\overline{t_p^*} \sim 0.6$ sec for tectonic to tectonic paths. P wave rise times from the same events give upper bounds on the estimates of $\overline{t_p^*}$ to be ~ 0.8 sec. The large difference between the spectral and rise time estimates may be due to scattering. In the 0.5 to 1.3 Hz range, PP and P amplitude ratios give $\overline{t_p^*} \sim 0.5$ sec for PP's relative to surface reflection points under the Eurasian shield. Amplitude ratios of long period multiple ScS phases were used to estimate attenuation in the 0.3 to 0.9 Hz band. Under tectonic Eurasia, these analyses gave $t_{ScS}^* \sim 3.9 \pm 0.4$ sec. Thus, for Eurasia, $t^*(f)$ for tectonic paths is approximately parallel to, but approximately 0.25 sec (for t_p^*) greater than $t^*(f)$ under the shield.

For North America, the amplitudes of long period multiple ScS phases were analyzed for two type of paths. Multiple ScS amplitudes recorded in the Northeastern US for events in the Aleutians (paths across the Canadian shield) give $t_{ScS}^* \sim 1.1 \pm 0.4$ sec. Similar data recorded in the Southeastern US for a Central American event gives $t_{ScS}^* \sim 4.0 \pm 0.9$ sec. These data analyses show that the attenuation in the long period band in North America varies in the same sense regionally as shown in previous work in the short period band. For Eastern Pacific the upper mantle attenuation appears to be the highest of all regions studied with t^* uniformly higher than in the two "tectonic" continental areas discussed above.

These findings support the general idea proven for continental North America by Der and Lees (1985) that $t^*(f)$ curves for teleseismic paths crossing the upper mantle in various areas of the world generally do not converge towards the long period end of the seismic spectrum as

implied by some "absorption band shift" models. Instead, the $t^*(f)$ curves tend to run quasi-parallel throughout the seismic frequency band as one would expect if the lateral Q variations in the upper mantle are caused by changes in temperature and chemical composition over large depth ranges (Minster and Anderson, 1980; Jordan 1975). These broad-band frequency dependent attenuation models must be known when applying attenuation correction to yield estimates.



Accession For	
NTIS CRA&I	<input checked="" type="checkbox"/>
DTIC TAB	<input type="checkbox"/>
Unannounced	<input type="checkbox"/>
Justification	
By	
Distribution /	
Availability Codes	
Dist	Avail and/or Special
A-1	

TABLE OF CONTENTS

	Page
SUMMARY	iii
LIST OF FIGURES	vii
LIST OF TABLES	xi
INTRODUCTION	1
ANALYSES OF MULTIPLE ScS DATA IN ALL REGIONS	7
Background	7
Methodology	9
Data Analysis	12
Discussion of the ScS Results	41
ANALYSES OF DATA FROM THE TECTONIC AREAS OF EURASIA	44
Analyses of P Wave Spectra from Nuclear Explosions	44
Analyses of Short Period PP/P Spectral Ratios	50
Rise Times of P Waves from Nuclear Explosions	51
Analyses of SS/S Amplitude Ratios	56
Frequency Dependent t^* Model for Eurasia	59
ANALYSES OF DATA FROM NORTH AMERICA	62
Review of Previous Data Analyses in the Short and Intermediate Period Bands	62
Summary of Results for North America	62
ANALYSES OF DATA FROM THE EASTERN PACIFIC	65
Review of Previous Data Analyses in the Short and Intermediate Period Bands	65

PP/PKP Spectral Ratios	65
SSS/SS Amplitude Ratios	70
Final Model for E. Pacific	74
DISCUSSION OF THE BROAD-BAND RESULTS	76
POSSIBLE $t^*(f)$ and $Q(f,r)$ MODELS AND YIELD ESTIMATION	78
CONCLUSIONS	81
REFERENCES	84
Appendix A. Time Domain Analyses of Multiple ScS Phases.	89
Appendix B. Analyses of PP/P and PP/PKP Spectral Ratios.	123
Appendix C. Rise Time Analyses.	145
DISTRIBUTION LIST	

LIST OF FIGURES

Figure No.	Title	Page
1	A summary for the various $t^*(f)$ models for N. America. These models are identified as strongly convergent (CS), weakly convergent (CW) and quasi-parallel (QP) for shield to shield path (S-S) and shield to tectonic paths (S-T) in each case. It is assumed that $t^* = 4t_p^*$	2
2	Example of ScS_N phases matched with synthetic constructed by convolving the first observable phase with multiples of t^* . (a) A deep focus event at Tonga-Fiji recorded at AFI. (b) A deep focus S. American event recorded at ZOBO.	10
3	Examples of seismograms showing the decay rate of ScS with multiples. ScS multiples are observable up to ScS_4 for shield S. America and W. Pacific paths whereas ScS_4 is into the noise for path crossing the E. Pacific.	13
4	Map of the tectonic regions in the Pacific Ocean. The French nuclear test site located at Tuamotu is identified.	15
5	Map indicating the location of events and stations used in the ScS_N study for E. Pacific. The bounce points are indicated for all ScS_N phases as + 's for ScS_2 , X 's for ScS_3 , and Y 's for ScS_4 .	16
6	Map indicating the location of events and stations used in the ScS_N study for W. Pacific. The bounce points are indicated for all ScS_N phases as + 's for ScS_2 , X 's for ScS_3 .	17
7	Map showing the location of events and stations in S. America and the associated bounce points for all the ScS_N phases used are shown in + 's for ScS_2 phases, and X 's for ScS_3 .	19
8	Map showing the location of events and stations in the Kurile and Japan region as used by Nakanishi (1979). The bounce points for all the ScS_N phases used are also shown as + 's for ScS_2 , X 's for ScS_3 and Z 's for ScS_4 .	20

9	Map showing the location of events and stations in the Western Pacific as used by Sipkin and Jordan (1977). The bounce points for all the ScS_N phases used are shown for paths across (a) Western Pacific (b) Northern Pacific as +’s for ScS_2 , X’s for ScS_3 and Z’s for ScS_4 .	21
10	Map of the tectonic regions in Eurasia. The nuclear test sites are identified.	25
11	Map of WWSSN stations and multiple ScS bounce points for the Hindu-Kush earthquakes.	26
12	Tracings of multiple ScS phases followed by the corresponding $sScS$ multiples at the WWSSN station EIL for the Hindu-Kush earthquake of 7/03/74.	29
13	Tracings of multiple ScS phases followed by the corresponding $sScS$ multiples at the WWSSN station SHI for the Hindu-Kush earthquake of 7/03/74.	30
14	Tracings of multiple ScS phases followed by the corresponding $sScS$ multiples at the WWSSN station JER for the Hindu-Kush earthquake of 8/20/79.	31
15	Summary of the ScS analyses for Eurasia. Shield paths give the mean t^* value of 2.5 sec (triangles) while the best fit for "tectonic" bounce points is 3.9 sec.	33
16	Map of the tectonic regions in North America. The nuclear test site is identified.	34
17	Map of sources, bounce points and WWSSN stations used in the analyses of ScS attenuation under North America.	37
18	Tracings of multiple ScS arrivals with the corresponding $sScS$ phases at the WWSSN station WES. These phases have relatively short periods and low decay rates thus indicating a high Q path.	38
19	Tracings of multiple ScS arrivals with the corresponding $sScS$ phases from the 4/05/71 Aleutian event as recorded at the WWSSN station BLA.	39

20	Tracings of multiple ScS arrivals with the corresponding sScS phases from the 3/06/74 Central American earthquake as recorded at the WWSSN station TUC. These phases have a rapidly decreasing amplitude due to high attenuation in the mantle under Mexico.	40
21	Summary of multiple ScS analyses for North America. The mean t^* for Canadian shield paths is 1.1 sec while the value for Mexico is 4.0 sec.	42
22	Samples of P wave spectra from Kazakh nuclear explosions. + 's are the signal and o 's are the noise. (a) Event of 1976241 recorded at MAIO, (b) event of 1979301 recorded at ANTO, and (c) event of 1979230 recorded at KONO.	45-47
23a	Map of t^* values for direct paths to SRO stations and PP arrivals (plotted at the bounce point). The values of 0 near two bounce points indicate low attenuation under the shield.	53
23b	Map of the bounce points (+ 's) within the tectonic Eurasia as used for the SS/S amplitude ratio study.	58
24	Plot of SS/S amplitude ratios versus epicentral distance. The amplitude ratios have been corrected for radiation pattern. The theoretical predictions of the SNA model (Grand and Helmberger, 1984) for a number of t^* values are also shown for comparison.	60
25	Summary of the results for tectonic Eurasia compared to the predictions of our Q model for the Eurasia shield (solid curves).	61
26	Summary of our results for North America as related to previous estimates of t^* from P and S wave spectral and waveform analyses in the short and intermediate period bands. The boxes and bars correspond to data for the Central American-Southwestern US path (top) and the Aleutian-Northeastern US path (bottom). The dotted lines are estimated t^* models for the two paths. The lower curve is estimated t^* model for the shield paths while the upper one is for "tectonic" N. America.	64
27	Map for E. Pacific showing locations of events used for the PP/PPK amplitude ratio study. The bounce points where the PP are sampling are indicated.	67

28	An example of a least squares fit to the PP/PKP amplitude ratios for a path across the E. Pacific. The ratios are plotted in $\log(\text{PP/PKP})$ against frequencies. The best fitting least squares line indicates a t_p^* of 0.67 sec.	69
29	Map for E. Pacific showing locations of events used for the SSS/SS amplitude ratio study. The bounce points for the SSS are in X's while those for SS are +'s.	71
30	Plot of SSS/SS amplitude ratios versus distance. The theoretical fits to these data are obtained for an J-B oceanic model.	73
31	Summary of our results for E. Pacific as related to estimates of t^* obtained from amplitude waveform matching, spectral ratio study and amplitude ratio method.	75
32	A summary of all models shown in this study for different tectonic and shield regions.	79
Appendix A	Time Domain Analyses of Multiple ScS phases.	89
Appendix B	Analyses of PP/P and PP/PKP spectral ratios.	123
Appendix C	Rise Time Analyses.	145

LIST OF TABLES

Table No.	Title	Page
1	Parameters of Earthquakes Used in ScS Study of Tectonic Pacific	14
2	A Summary of ScS _N Phases Used and t_{ScS}^* for All Regions.	23
3	Event Parameters for Far Eastern Events Used in Estimating t_{ScS}^* Under the Eurasian Shield	27
4	Event Parameters for Hindu Kush Events Used in Estimating t_{ScS}^* Under Eurasian Tectonic Areas.	28
5	Event Parameters for Aleutian Events Used in Estimating t_{ScS}^* Under North America.	35
6	Event Parameters for Central American Event Used in Estimating t_{ScS}^* Under North America.	36
7	Event Parameters for East Kazakh Explosions.	48
8	$\overline{t_p^*}$ Estimates for Paths from East Kazakh to Eurasian Stations for Shield - Tectonic Paths.	49
9	$\overline{t_p^*}$ and $\overline{t_{pp}^*}$ Estimates for Eurasian Stations for Tectonic-Tectonic Paths.	52
10	Parameters of Earthquake Used in SS/S Study of Tectonic Eurasia.	57
11	Parameters of Earthquakes Used in PP/PKP Study of Tectonic Pacific.	68
12	Parameters of Earthquakes Used in SSS/SS Study of Tectonic Pacific.	72
13	Comparison of Long Period ScS and Short Period P Attenuation Results.	77

(THIS PAGE INTENTIONALLY LEFT BLANK)

INTRODUCTION

This final report describes the functional forms of frequency dependence of Q in the mantle under various regions of the Earth. The study is exploratory in nature; resolution of finer details in the Q structures within each of the major regions studied are beyond the scope of this limited project. The motivation for studies of this nature is given by the fact that the form of $t^*(f)$ for various paths determines how m_b depends on the measured values of the apparent $t^* (\bar{t}^*)$ derived from spectral analyses. For some, albeit hypothetical, forms of frequency dependence of regional $t^*(f)$ models, the relationships between the measured \bar{t}_p^* and m_b may be quite complex, thus affecting our ability to measure attenuation-related source and station biases from spectral measurements (Hadley and Mellman, 1983). It is therefore important to prove that the corresponding forms of frequency dependence of t^* are inconsistent with the data if we are to utilize spectral methods to estimate magnitude bias. Moreover, if the apparent t^* is not strongly frequency dependent even though the absolute t^* is, then it is possible to estimate source region biases from some quite simple spectral measurements (Der *et al.*, 1979, 1982a,b; Der and Lees, 1985) for the purpose of yield estimation.

The appropriate models for $t^*(f)$ can be delineated by making measurements of attenuation in different frequency bands using various types of data and piecing together the most likely functional forms of $t^*(f)$ and outlining the most likely models of $Q(f,r)$ of the given regions. Our measurements in the long period band also have relevance to acceptable forms of $Q(f,r)$ to be used for correcting surface wave data for attenuation (Stevens, 1986; Der, 1986).

Various types of $t^*(f)$ models have been proposed for use in correcting yield estimates for attenuation. In Figure 1, we summarize a few of these models for central and southwestern United States. These models include the strongly convergent models proposed by Lay and Helmberger (1981) and Butler (1984), the weakly convergent models, (that is less frequency

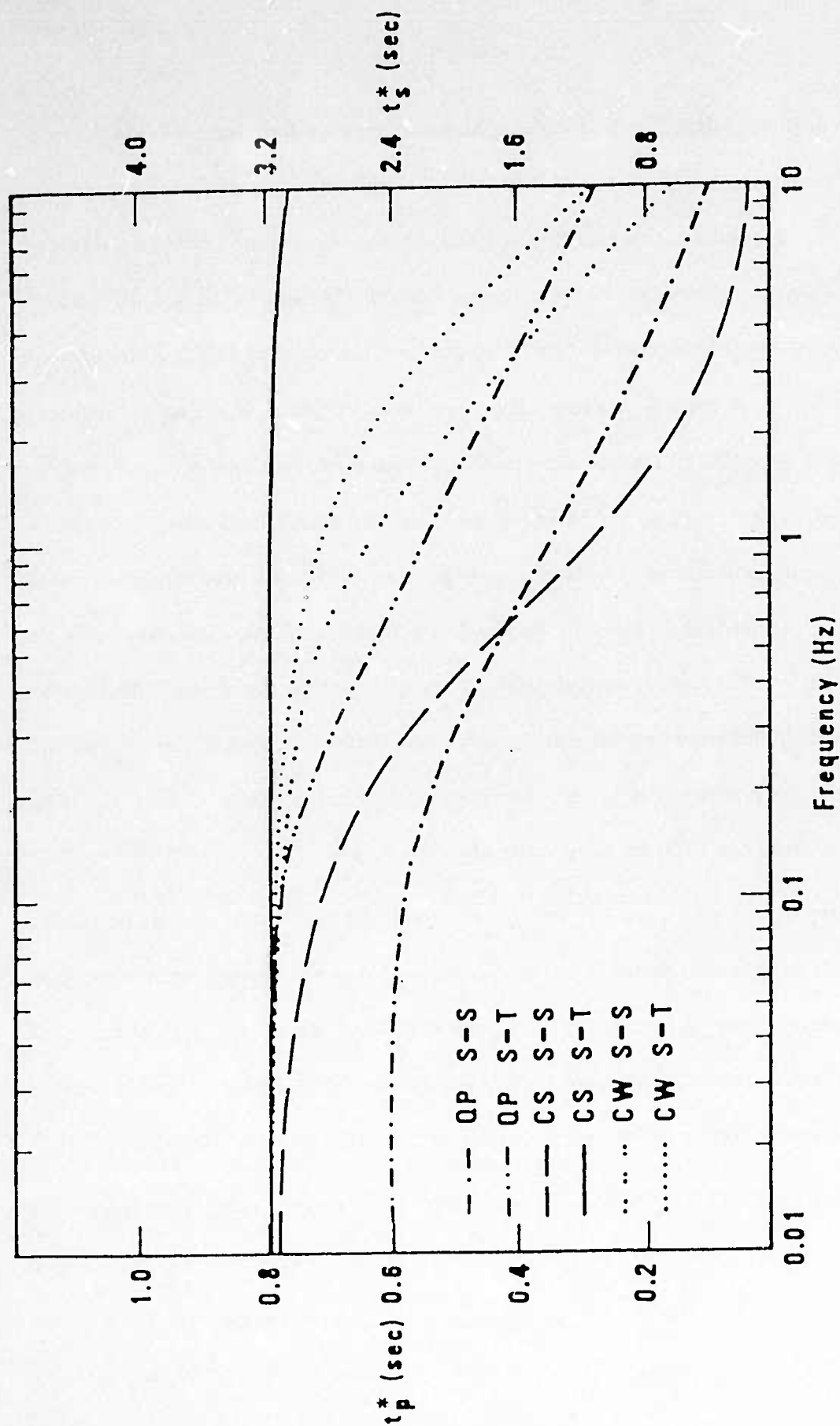


Figure 1. A summary of the various $t(f)$ models for N. America. These models are identified as strongly convergent (CS), weakly convergent (CW) and quasi-parallel (QP) for shield to shield path (S-S) and shield to tectonic paths (S-T) individually. It is assumed that $t_S^* = 4t_p^*$

dependent than the earlier pairs) as proposed by Hadley and Mellman (1983) and the quasi-parallel models by Der and Less (1986). These models have been constructed using mainly short period data; the long period extrapolation has a very strong effect on how these curves may diverge or converge and on m_b also. It is the objective of this study to settle such questions for all the areas studied.

In studies of this kind we are not looking for subtle differences in attenuation, but rather for changes in upper mantle Q by factors exceeding two in depth ranges exceeding 100 km. It is doubtful that any lateral changes less pronounced than this could be detected at all by any currently used methodology, especially in the long period band where the wave amplitudes are less sensitive to Q. Any measurements of Q must be, by the nature of the problem, much cruder than measurements of the seismic velocities in the Earth, for example. Since the detectable changes in t^* at teleseismic distances must be at least of the order of two and are mainly due to lateral changes of Q in a relatively thin upper mantle layer (250-300 km), the Q in this layer must change by factors considerably larger than two. Our survey of the seismological literature indicates that some of the best documented (indeed classical) studies of the upper mantle support lateral variations in Q by about two orders of magnitude in the depth range of 100-300 km. Since our broad band study encompasses both the short and long period bands our results are relevant to yield estimation from both short period body waves and long period surface waves.

In studying "tectonic", or any regionalized data, a word of caution is in order. Clearly, any such concept as a "tectonic" region is an abstraction that will have to be discarded in the near future as detailed three-dimensional velocity models of the Earth from tomographic studies (Dziewonski and Anderson, 1981) assume concrete forms. In any case, "shields" correspond to the upper mantle regions of high velocity with deep "roots" in the tomographic results.

There is evidence indicating that tectonic areas are more heterogeneous than shields with respect to Q.

In studies of this sort, the most difficult task is to extract relevant data from a mass of recordings and to overcome the severe limitations imposed on the scientist by geography and availability of suitable stations and events. Expectations with regard to the availability of certain kinds of arrivals are often not met. In continental areas, our experience parallels that of Sipkin and Jordan (1980) who have found that ScS phases are often masked by a high background consisting of continental higher and fundamental mode waves excited by the event. In our experience, only a fraction (less than one third) of the events examined have yielded useful ScS data even when the data set was restricted to very large and deep events. In general, one has to search through all plausible events in a region recorded over many years to gather sufficient data for a study. The film library of the Center for Seismic Studies covers the years 1970-1982 fairly well by acting as the main source of analog data. Outside this time period the coverage is sporadic and it was necessary to acquire data from other sources during this project (more complete sets of film chips exist at Lamont-Doherty Geological Observatory).

In previous work we have investigated the shield areas of Eurasia using broad-band t^* measurements and determined a frequency dependent Q model for this region (Der *et al.*, 1985b). This model gives us a useful basis of reference for comparing the frequency dependence of Q in various areas of the world chosen for this project. Following the methodology of our shield studies, this study avoids mixing global and regional data in order to arrive at Q models applicable to each region.

The general plan of this study is to make t^* estimates in several overlapping limited frequency bands and combine them to construct the best fitting $Q(r,f)$ models that are the most compatible with the various kinds of measurements. Since thus far no convincing evidence has

surfaced favoring rapid variation in the derivative of Q (or t^*) with respect to frequency, the use of quasi-constant apparent Q in narrow frequency bands is not likely to introduce appreciable errors in the construction of a broad-band Q(f) model. Moreover, since we have made a thorough study of some shield regions, we may now make relative comparisons of attenuation estimates between the tectonic regions and the known shield regions. There is also hardly any need to analyze additional short period data for North America in constructing frequency dependent Q models for the region since it has been well studied in this frequency band (Lay and Helmberger, 1981; Der *et al.*, 1982). We will concentrate in obtaining new long period estimates of Q to supplement the available short period estimates from previous studies to construct a broad-band Q(f) model for North America.

Both amplitude and spectral measurements are important in this study of Q. In our data analyses we make a distinction between results for the absolute t^* and the apparent t^* defined as \bar{t}^* . At a constant frequency, t^* can be determined from the change in amplitude spectrum of an arrival,

$$A = e^{-\pi f t^*}, \text{ where } t^* = \int \frac{d(\text{travel time})}{Q}. \quad (1)$$

Waveforms and spectral ratios are mostly shaped by the apparent t^* defined as \bar{t}^* , which can be written as:

$$\bar{t}^* = t^* + f \frac{\delta t^*}{df} = \frac{-1}{\pi} \frac{d(\ln A)}{df}. \quad (2)$$

over a narrow frequency band. We also assume the relationship

$$t_S^* \approx 4t_P^*, \quad (3)$$

which corresponds to losses in shear deformation only (Lay and Helmberger, 1981; Der *et al.*,

1980, 1982a). This relationship can best be tested in the 0.1 to 2 Hz frequency range where attenuative effects are observable in both P and S waves.

In studies of this kind the most difficult part of the work is the finding of suitable data. When searching for data, certain paths are hard to access due to the location of the available earthquakes and geophysical and political constraints. We will be investigating all possible data analysis schemes to process the available data to obtain attenuation measurements covering as broad a frequency band as possible.

In the first part of this report we shall describe the results obtained for multiple ScS waves. This is followed by our data analyses for all of our individual regions and some surrounding but relevant areas. The report is concluded by defining the most likely forms of $t^*(f)$ for each individual region and present our conclusions as to what the results imply for yield estimation.

The reason for this manner of presentation is that the methodology for determining Q from multiple ScS data by various workers is quite varied and the results are not directly comparable, and we thus have decided that the regional variations in the Q_{ScS} should be presented first using a uniform methodology for its estimation. By bringing all of our ScS results together, as well as reworking some of the data from other authors, we are able to define regional patterns and compare our results to other work within the framework of a common methodology. We follow this by an extension of the results to shorter periods by combining a variety of new data with known regional attenuation patterns for most of the regions included in this study (Der *et al.*, 1982b; Lay and Helmberger, 1981). All data spanning both long and short period bands are then combined to construct the most likely $t^*(f)$ curves for the regions of interest.

ANALYSES OF MULTIPLE ScS DATA IN ALL REGIONS

Background

The quality factors derived from the analysis of multiple ScS provide a sampling of the whole mantle. Since, presumably, most of the attenuation probably occurs in the upper mantle, the measurement of Q_{ScS} is likely to be the most indicative of the dissipation of energy within the upper mantle low Q zone. Although some researchers postulated a low Q region near the core-mantle boundary (Anderson and Given, 1982), the existence of such feature is still being debated. Prominent multiple ScS phases with impulsive signatures are frequently present on recordings of earthquakes with hypocenters below the lithosphere, these arrivals are obscured by high amplitude surface waves for shallower events. The SH component of these arrivals is eminently suited for attenuation studies because of the lack of S-P conversions at the free surface or the core mantle boundary. This study analyzes multiple ScS phases in the time domain to obtain Q_{ScS} for different paths across the tectonic S. Pacific, continental S. America and N. America and, in doing this, to detect any regional variations of Q_{ScS} .

Various authors have utilized ScS arrivals to obtain average Q values for the whole mantle. The methodologies applied vary considerably. Jordan and Sipkin (1977) applied a stacking method in the spectral domain to obtain a statistical measurement of Q_{ScS} for different parts of the world. Nakanishi (1979) obtained Q_{ScS} for the Sea of Okhotsk, Sea of Japan and the Izu-Bonin region using a maximum likelihood estimates on spectral ratios between multiple ScS phases from seismic recordings in Japan. Sato and Espinosa (1967) obtained a lower bound for Q_{ScS} for paths from S. America to N. American stations using essentially a spectral ratio technique. They also obtained estimates of the core viscosity and postulated the frequency dependence of Q. Similar finding was reported by Yoshida and Tsujiura (1975). It is quite difficult to compare the results obtained by the various authors since all methods have various

degrees of inherent bias. The method used to estimate Q from multiple ScS is largely a matter of personal preference and philosophy.

Estimates of Q_{ScS} from the shapes of the spectra as opposed to the decay of absolute amplitudes in the successive ScS arrivals are heavily influenced by the ever-present scattered surface wave background on the long period seismograms. The ScS pulses are of very short duration thus making the window-carpentry for spectral analyses very difficult. Such noise contamination will result in overestimates of Q. Spectral stacking methods may de-emphasize the high frequency content of the data thus biasing the Q values to be lower.

We have used two time domain approaches to estimate Q_{ScS} for different regions of the world. A robust measurement of Q_{ScS} is introduced in this study using a time domain waveform matching scheme to obtain the Q operator that produces both the broadening and decrease in amplitude of the successive multiply reflected ScS phases. By processing a large amount of data from various parts of the world we obtained Q estimates that are comparable because of the identical processing method applied. By reprocessing the data from some earlier analyses we are also able to compare various regions of the earth in a common framework.

The other approach has been used in our earlier work on Q under the Eurasian shield (Der *et al.*, 1984) utilizing WWSSN photographic records to obtain Q_{ScS} . For these we used a simplified method of analysis by fitting the decay rate of the successive ScS pulses (corrected for geometrical spreading effects) graphically to values of t^* . In such analyses we assumed that the ScS pulses have a dominant frequency and that the pulses are monochromatic. This method was found to be generally compatible with the more precise time domain fitting methods applied to our digital data. This method is mainly used for N. America and Eurasia where the station and earthquake configurations prevent us to obtain adequate digital data to perform the time domain waveform matching scheme. Results on t^* for North America and

Eurasia are mostly obtained using this method. Although hand-digitization was attempted on some of the photographically recorded data, the lack of precision in lining up the horizontal components for rotation, prevented us to gain any more precision compared to the simplified analysis.

Methodology

The time domain waveform matching scheme compares the entire waveform of ScS with all of its multiples. We convolve the first well recorded, clear ScS_H phase with succession of t^* operators such that the convolved phase will have the same amplitude decay rate and waveform characteristics as those of the succeeding multiples. These ScS_N phases are identified with the aid of the J-B travel time table. After correcting for geometrical spreading effects, we add for each increase of multiplicity a trial value for the contribution to the t^* for a single passage through the mantle multiplied by a factor of two. The observed amplitude of each convolved phase is compared to the observation and the trial value is changed until a good fit is obtained. Due to the low amplitude of the last observable ScS multiples, comparisons performed to these phases act mainly as constraints on the decay rate. Most of the amplitude and phase information is utilized in the analysis if the waveforms fit also, which is usually the case. Examples for two circum-Pacific deep focus events are shown in Figure 2 to indicate the ease of the method.

This method has the advantage over spectral shape measurements in being simple and yields much more stable measurements. We feel that the spectral shapes and the waveforms are heavily influenced by the scattered background and any Q values that conflict with the gross amplitudes of successive ScS arrivals should be considered suspicious. Often we are able to put upper limits to Q by measuring the background level at the expected arrival time of the next ScS_n pulse after the last observable arrival. ScS pulses and their associated surface

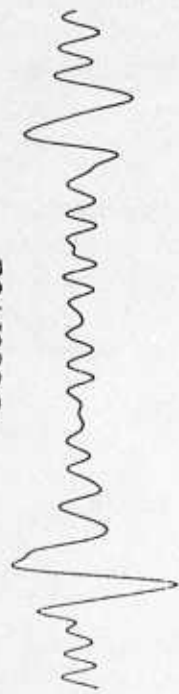
AFI

84322

W. Pacific

ScS

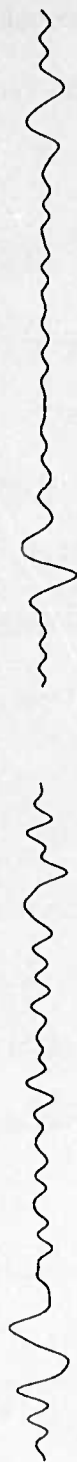
Observed



ScS convolved with t^*

ScS2

$t^* = 3.0$



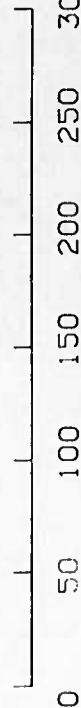
ScS3

$t^* = 6.0$



ScS4

$t^* = 9.0$



sec

Figure 2a. Examples of ScS_N phases matched with synthetic constructed by convolving the first observable phase with multiples of t^* for a deep focus event at Tonga-Fiji recorded at AFI.

ZOBO

77035

Shield S. America

ScS2

Observed



ScS₂ convolved with t^*

ScS3

$t^* = 2.5$



ScS4

$t^* = 5.0$



ScS5

$t^* = 7.5$

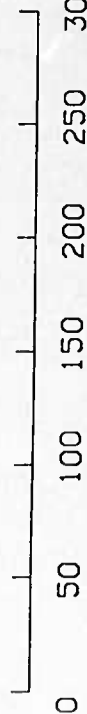
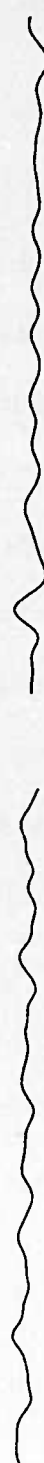


Figure 2b. Examples of ScS_N phases matched with synthetic constructed by convolving the first observable phase with multiples of t^* for a deep focus S. American event recorded at ZOBO.

reflections often form characteristic pairs which can be recognized even at low amplitudes. Some of the examples of such $ScSn-sScSn$ pairs are shown in Figure 3.

Data Analysis

We have collected data from a variety of tectonic environments around the world. Multiple ScS phases are the best seen for deep earthquakes for which the surface waves that commonly mask ScS phases are not strongly excited. Event parameters for all the earthquakes used are given in Table 1. The first region we shall study is the E. Pacific Ocean. The tectonic subdivision of the Pacific Ocean is shown in Figure 4. Seven earthquakes are used for the E. Pacific path (Figure 5). They are mostly deep focus earthquakes associated with the Tonga-Fiji trench and recorded at digital stations ZOBO and BOCO in S. America. The bounce points of these events are also shown in Figure 5. From the figure, it is observed that the bounce points are located away from the E. Pacific Rise where active spreading and upwelling of magma are occurring. Any average of t^* including measurement of the upper mantle beneath or very near E. Pacific Rise may be biased towards low Q. The phases used for these events are mostly ScS_2 , ScS_3 , ScS_4 . The first ScS is not used in this part of the study since it is either not observed (shadow zone) or arrives too close to the S phase in time. The waveforms and their matchings are shown in Appendix A. In most cases, the amplitudes of the multiple ScS decay quite rapidly as the number of bounces increases as shown in Figure 3 and other examples in Appendix A. The values of t_{ScS}^* across the S. Pacific are generally high and average about 7.0 sec.

To constrain our measurements, we have also applied the same method to other regions and some published data. Eight events in the Tonga-Fiji trench recorded at digital stations, AFI, HON, CTA and GUMO (Figure 6, Table 1) have been used to study the Q_{ScS} for the tectonic S.W. Pacific. These phases are ScS , ScS_2 , ScS_3 and ScS_4 with surface reflection

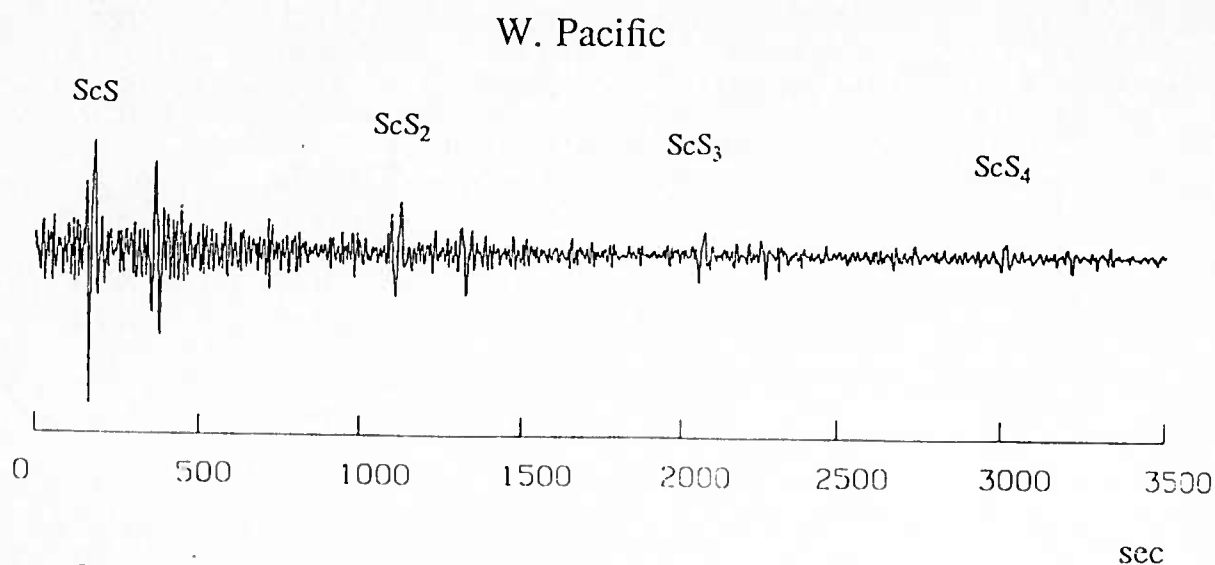
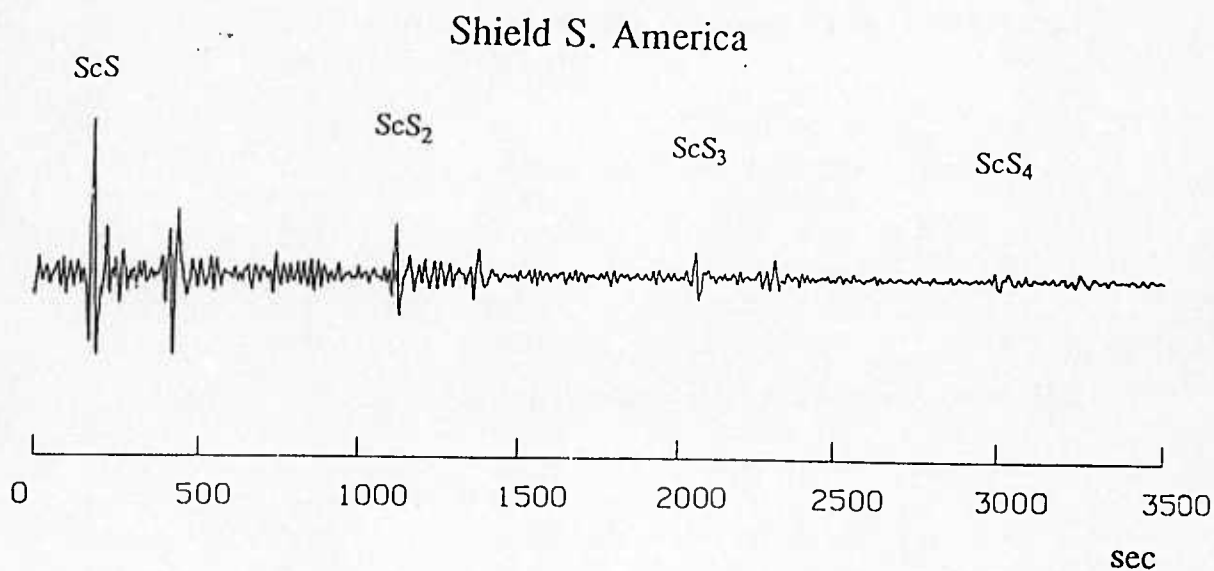
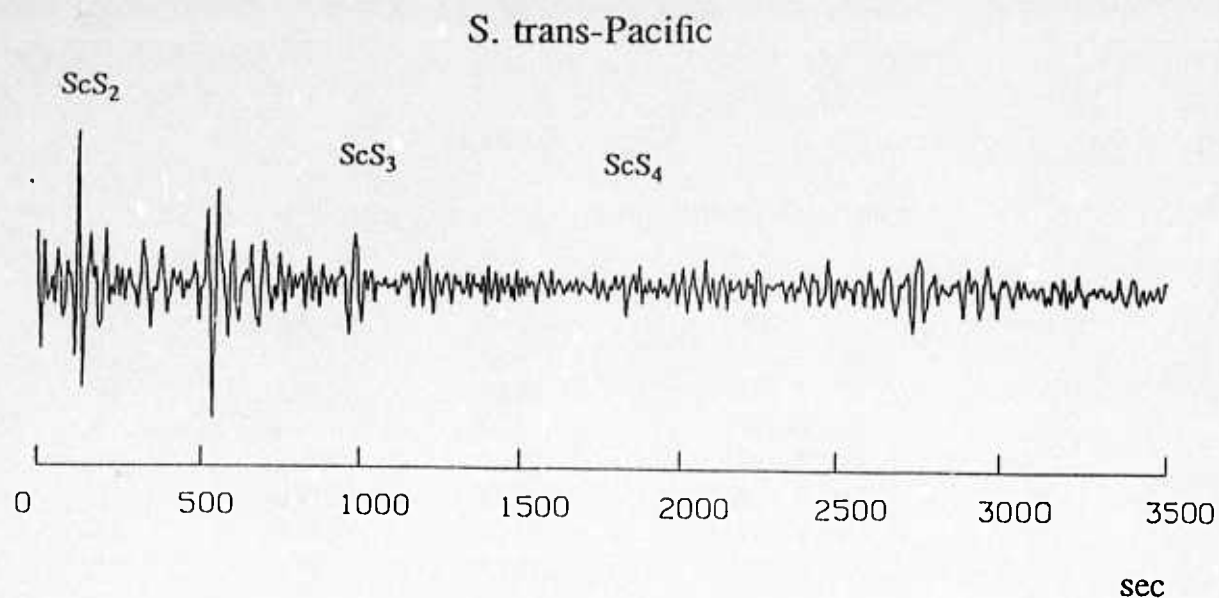


Figure 3. Examples of seismograms showing the decay rate of ScS_N with multiples. ScS multiples are observable up to ScS_4 for shield S. America and W. Pacific paths whereas ScS_4 is into the noise for path crossing the E. Pacific.

Table 1

Parameters of earthquakes used in ScS study of tectonic Pacific

Path: Fiji-Tonga events recorded at ZOBO and BOCO

Event #	date	latitude	longitude	depth	m _b
1	Nov 25, 1976	-19.50	-177.70	424	6.0
2	Jul 17, 1978	-23.63	-179.96	519	5.4
3	Apr 24, 1979	-20.82	-178.67	596	5.9
4	Jul 20, 1980	-17.88	-178.61	596	5.9
5	Sep 28, 1981	-29.33	-179.04	323	6.0
6	Nov 25, 1981	-20.94	-178.86	614	5.9
7	Sep 16, 1983	-24.03	-179.80	510	6.0

Path: Fiji-Tonga events recorded at AFI, HON and GUMO

Event #	date	latitude	longitude	depth	m _b
8	Sep 28, 1981	-29.33	-179.04	323	6.0
9	Jan 19, 1984	-23.64	-178.32	332	5.8
10	May 30, 1984	-04.84	151.58	174	6.2
11	Aug 26, 1984	-23.59	179.07	560	5.9
12	Nov 17, 1984	-18.79	-178.03	451	6.1
13	Nov 22, 1984	-17.78	-178.05	646	5.9
14	Dec 12, 1985	-21.66	-176.38	155	5.9
15	Aug 28, 1985	-21.01	-178.98	625	6.1

Path: South American events recorded at ZOBO and BDF

Event #	date	latitude	longitude	depth	m _b
16	Feb 04, 1977	-22.66	-63.39	555	5.9
17	May 21, 1979	-15.44	-70.05	209	5.9
18	Jan 10, 1983	-22.01	-68.47	121	5.6
19	Jun 02, 1983	-09.51	-71.25	599	5.9
20	Dec 21, 1983	-28.19	-63.17	602	6.2
21	May 01, 1985	-09.20	-71.23	600	6.0
22	Jun 10, 1985	-27.96	-66.99	151	5.8
23	Nov 29, 1985	-22.76	-63.62	521	5.3

Path: Events used by Nakanishi (1979) for NW Pacific

Event #	date	latitude	longitude	depth	m _b
24	Jun 26, 1975	+31.90	+138.20	394	5.3
25	Dec 21, 1975	+51.90	+151.60	546	6.0
26	Aug 12, 1975	+32.10	+137.90	399	5.6
27	Jul 28, 1973	+50.50	+148.90	585	5.5

Path: Events used by Sipkin and Jordan (1977) for the Pacific

Event #	date	latitude	longitude	depth	m _b
28	Apr 10, 1976	-17.10	-178.46	548	5.7
29	Nov 25, 1976	-19.50	-177.70	424	6.0
30	Jan 9, 1976	-15.80	+167.85	173	5.7

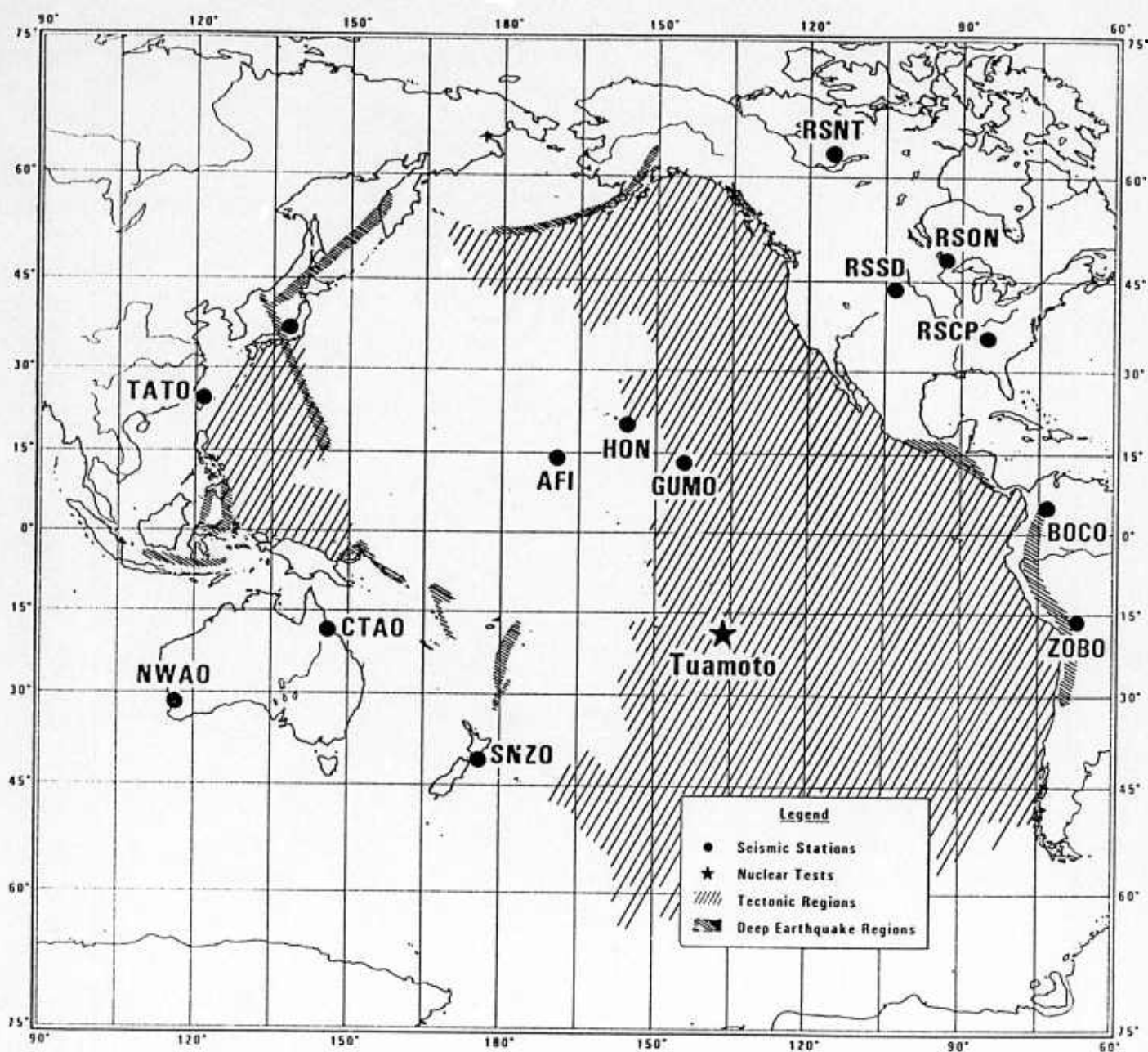


Figure 4. Map of the tectonic regions in the Pacific Ocean. The French nuclear test site located at Tuamotu is identified.

SE. Pacific ScS_N bounce points

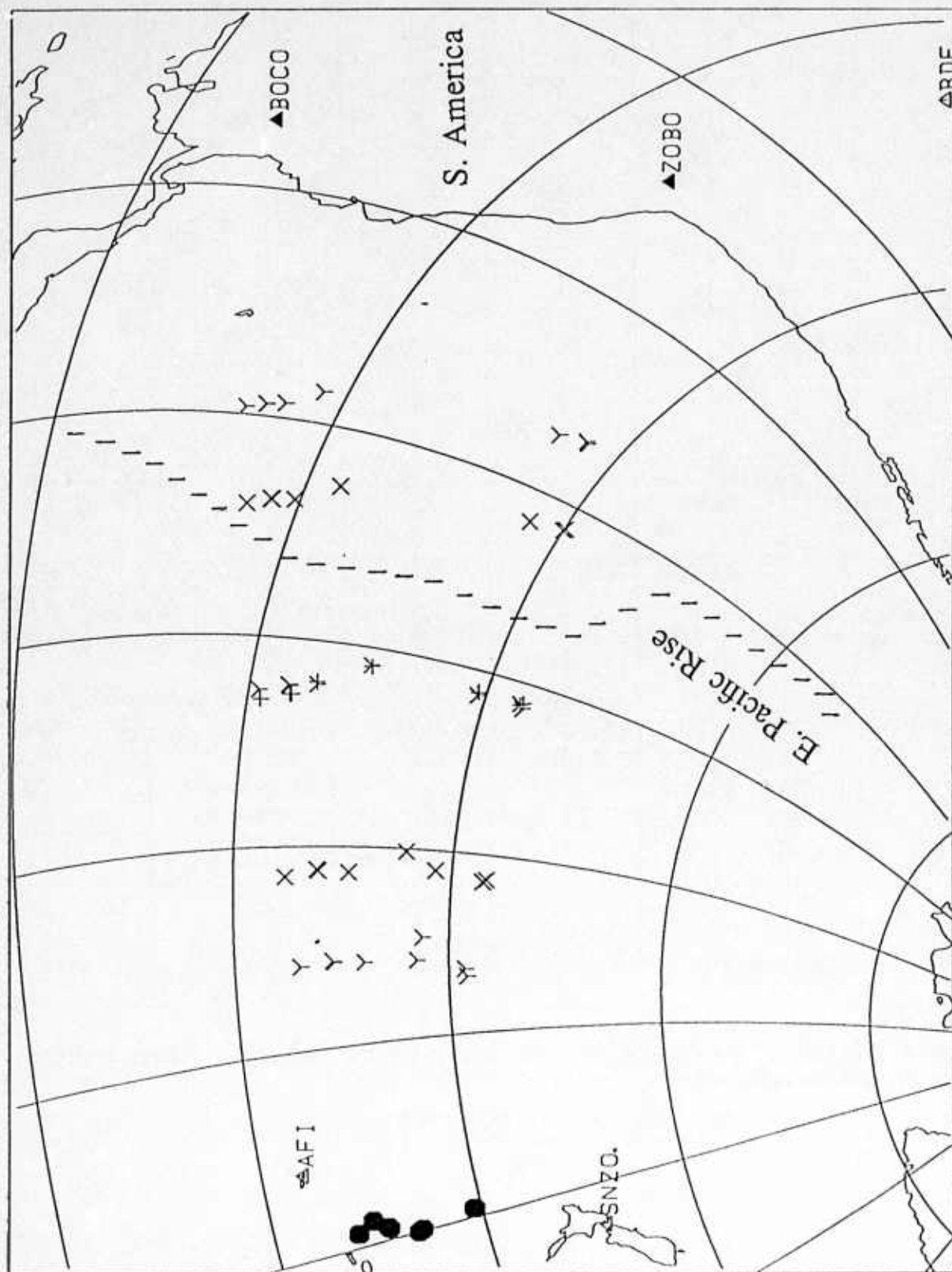


Figure 5. Map indicating the location of events and stations used in the ScS_N study for E. Pacific. The bounce points are indicated for all ScS_N phases as +’s for ScS₂, X’s for ScS₃ and Y’s for ScS₄.

W. Pacific

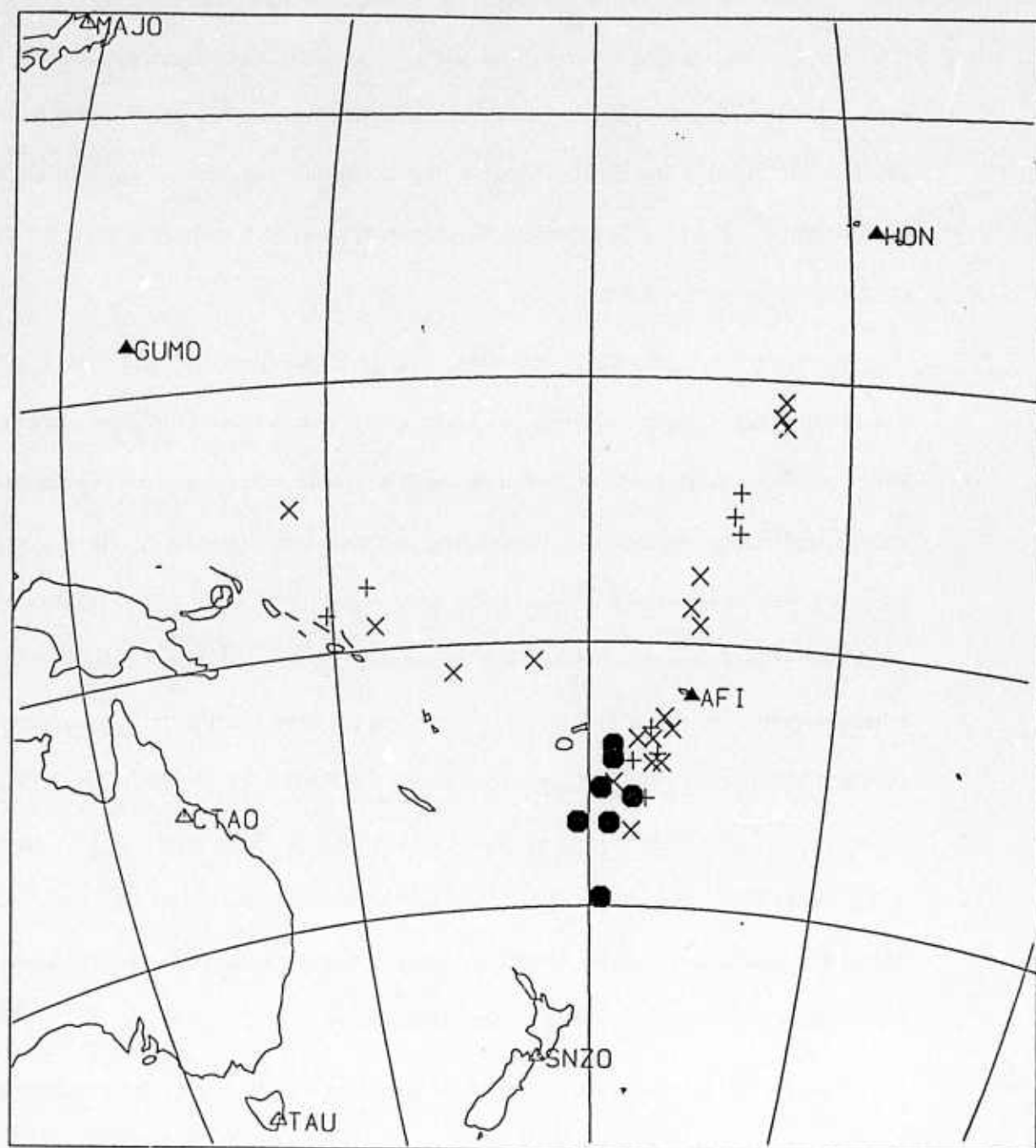


Figure 6. Map indicating the location of events and stations used in the ScS_N study for W. Pacific. The bounce points are indicated for all ScS_N phases as '+'s for ScS_2 and 'X's for ScS_3 .

points within the S.W. Pacific. The seismograms and waveform matches are presented in Appendix A. The resulting average t_{ScS}^* for this relatively limited region is about 4.0 sec.

We have also applied the method to shield S. America. Deep focus S. American trench earthquakes recorded at digital stations ZOBO and BDF with bounce points within the region are shown in Figure 7 and listed in Table 1. The waveforms and data analysis runs are shown in Appendix A. The t_{ScS}^* for the shield S. America is around 2.0 seconds whereas for the tectonic paths, t_{ScS}^* is up to 5.0 sec.

We have also re-analyzed some data used by Nakanishi(1979) and Sipkin and Jordan(1980). These include Izu-Bonin and Kurile events recorded at HGLP digital station MAT with ScS , ScS_2 , ScS_3 and ScS_4 sampling the NW Pacific. Figure 8 shows the locations of stations and reflection points with the seismograms shown in Appendix A. The t_{ScS}^* obtained for this region is around 4.0 sec and being very close to Nakanishi (1979) results. Several paths studied by Sipkin and Jordan (1980) are reprocessed here and the locations of the surface reflection points are shown in Figure 9. Two paths are shown in Figure 9a sampling the W. Pacific and one path with ScS_N bounces across the Pacific are shown in Figure 9b. The waveforms and data analysis runs are shown in Appendix A. Most results are similar, but the values derived by Sipkin and Jordan (1980) tend to be somewhat higher than ours. All t_{ScS}^* results are summarized in Table 2 and are compared to those obtained by the amplitude decay method for Eurasia and N. America as summarized below.

Multiple ScS data were also collected for deep Hindu Kush earthquakes observed at various WWSSN station. Figure 10 shows the tectonic and shield regions of Eurasia. These paths sample two of our chosen regions fairly well as indicated by the map in Figure 11. The event parameters are listed in Tables 3 and 4. We have presented some examples of the ScS and $sScS$ multiples in Figures 12-14. The plots of ScS phases, normalized to ScS_2 and plotted

S. America

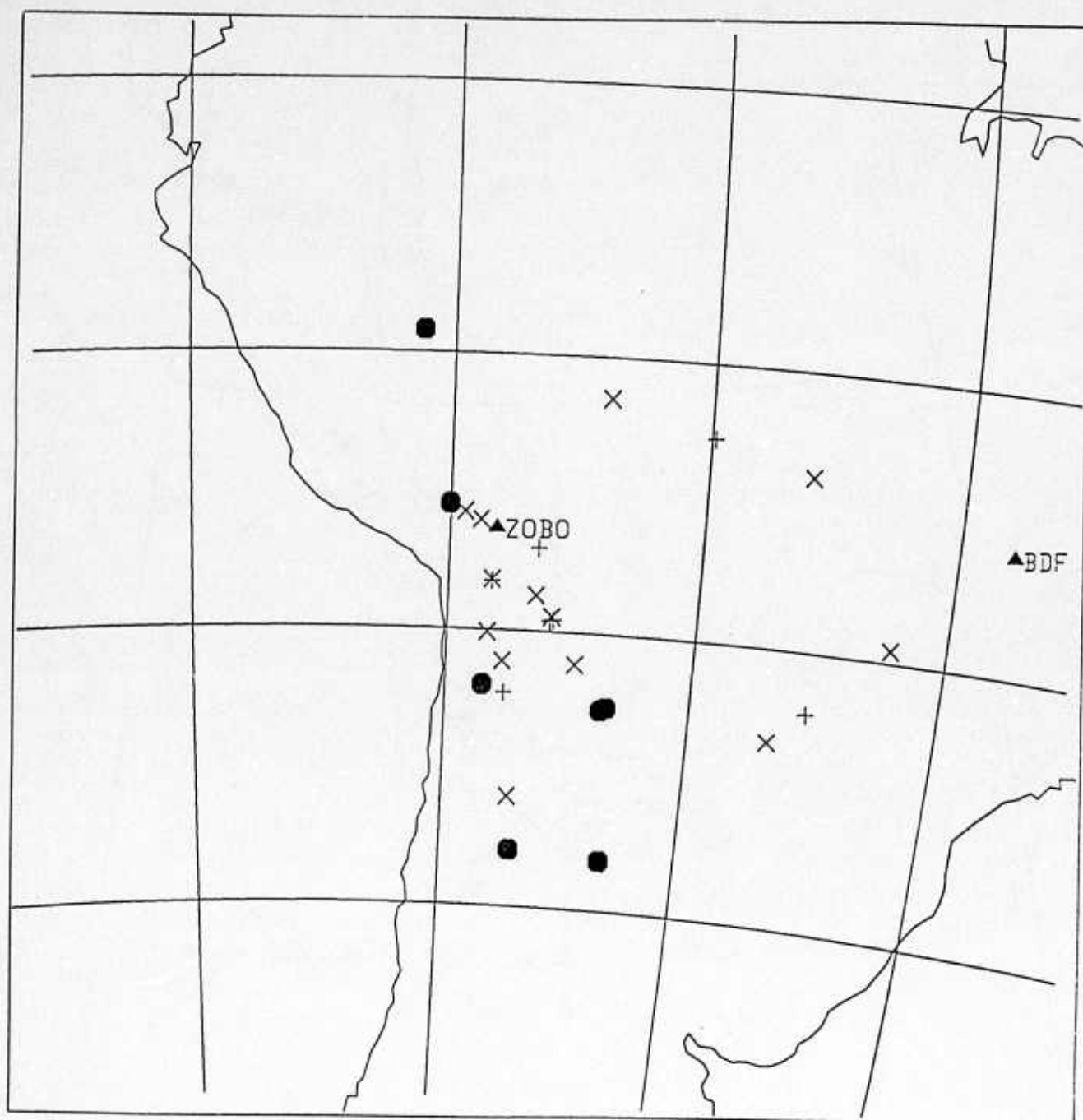


Figure 7. Map showing the location of events and stations in S. America and the associated bounce points for all the ScS_N phases used are shown in +’s for ScS_2 phases, and X’s for ScS_3 .

NW. PACIFIC



Figure 8. Map showing the location of events and stations in the Kurile and Japan region as used by Nakanishi (1979). The bounce points for all the ScS_N phases used are shown as +’s for ScS_2 , X’s for ScS_3 and Z’s for ScS_4 .

W. PACIFIC

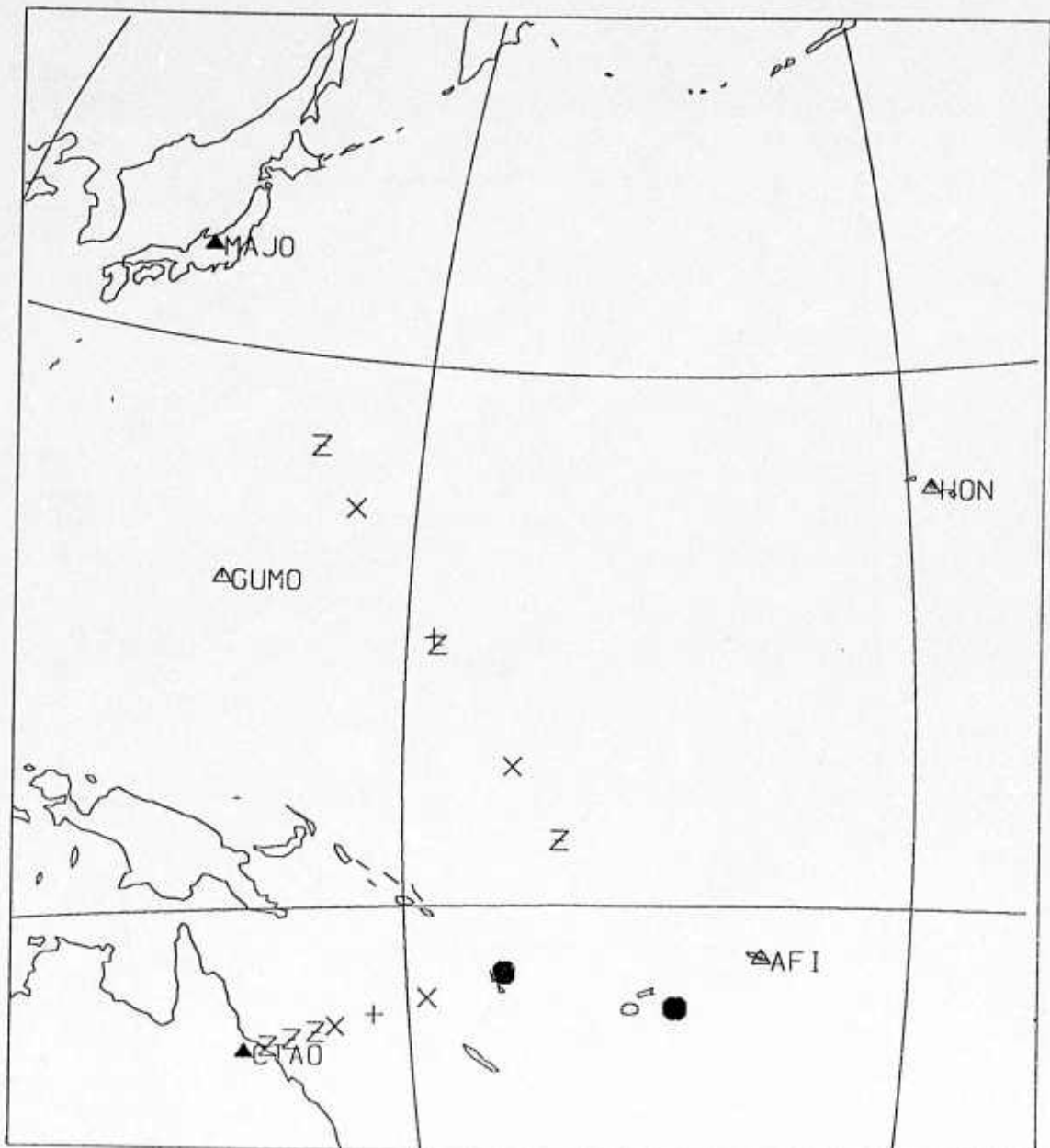


Figure 9a. Map showing the location of events and stations in the Western Pacific as used by Sipkin and Jordan (1977). The bounce points for all the ScS_N phases used are shown as +’s for ScS_2 , X’s for ScS_3 and Z’s for ScS_4 .

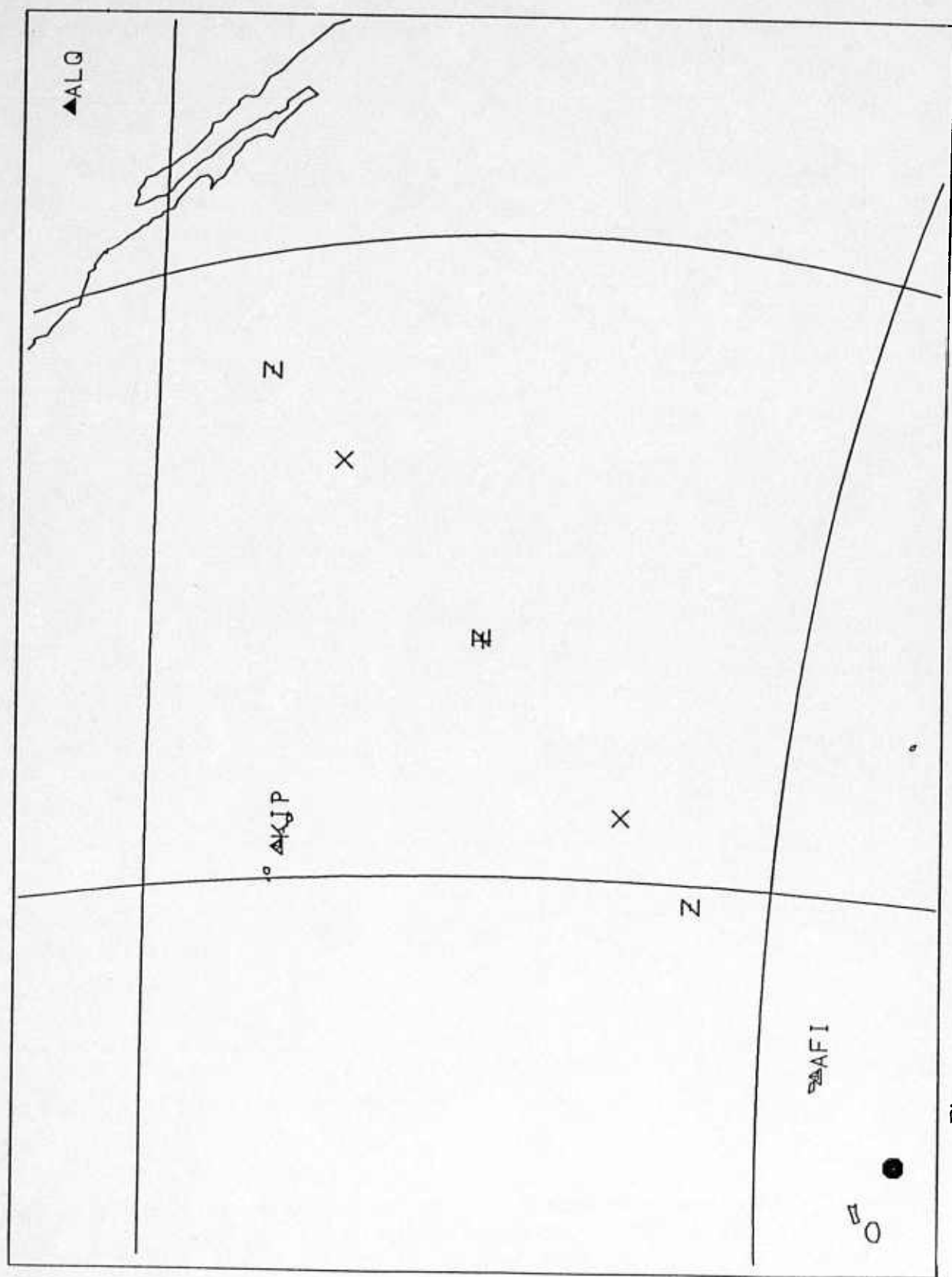


Figure 9b. Map showing the location of event and station for a path across the Pacific as used by Sipkin and Jordan (1977). The bounce points for all the ScS_N phases used are shown as '+'s for ScS_2 , X's for ScS_3 and Z's for ScS_4 .

Table 2
A summary of ScS_N phases used and t_{ScS}^* for all regions

Region: E. Pacific

Event #	Station	Observed phase type				δt_{ScS}^*
		ScS	ScS ₂	ScS ₃	ScS ₄	
1	ZOBO		•	•		7.0
2	ZOBO			•	•	7.0
	BOCO			•	•	7.0
3	BOCO			•	•	5.0
4	BOCO		•	•	•	5.0
5	BOCO		•	•	•	5.0
6	BOCO			•	•	7.0
7	ZOBO			•	•	7.0

Region: SW Pacific

Event #	Station	Observed phase type				δt_{ScS}^*
		ScS	ScS ₂	ScS ₃	ScS ₄	
8	AFI	•	•	•	•	4.0
9	AFI	•	•			5.0
10	HON			•	•	5.0
	GUMO		•	•	•	5.0
11	AFI	•	•	•	•	5.5
12	AFI	•	•	•	•	2.5
13	HON	•	•	•		7.0
14	AFI	•	•	•		5.0
15	HON	•	•	•		2.5
29	CTA	•	•	•	•	5.0 # (6.6)

Region: Shield S. America

Event #	Station	Observed phase type				δt_{ScS}^*
		ScS	ScS ₂	ScS ₃	ScS ₄	
16	ZOBO	•	•	•	•	2.5
17	ZOBO	•	•	•	•	4.0
18	ZOBO	•	•	•	•	2.5
19	ZOBO	•	•	•		3.0
20	BOCO	•	•	•	•	2.5
	BDF		•	•	•	2.5
21	BDF	•	•			2.0
22	ZOBO	•	•	•	•	3.0
23	ZOBO	•	•	•	•	3.0

Table 2 (cont'd)

Region: NW Pacific

Event #	Station	Observed phase type				δt_{ScS}^*
		ScS	ScS ₂	ScS ₃	ScS ₄	
24	MAT	•	•			4.5 * (1.5)
25	MAT	•	•	•	•	4.0 * (3.8)
26	MAT	•	•	•		4.0 * (3.4)
27	MAT	•	•			5.0 * (3.5)
28	MAT		•	•	•	2.5 # (5.8)

Region: N. Trans-Pacific

Event #	Station	Observed phase type				δt_{ScS}^*
		ScS	ScS ₂	ScS ₃	ScS ₄	
29	ALQ			•	•	2.5 # (5.8)

Region: Shield Eurasia

 δt_{ScS}^*

2.5

Region: Tectonic Eurasia

 δt_{ScS}^*

3.0-3.9

Region: Shield North America

 δt_{ScS}^*

1.1-2.5

Region: Tectonic N. America

 δt_{ScS}^*

4.0-4.5

() value from Sipkin and Jordan (1977)

* () value from Nakanishi (1979)

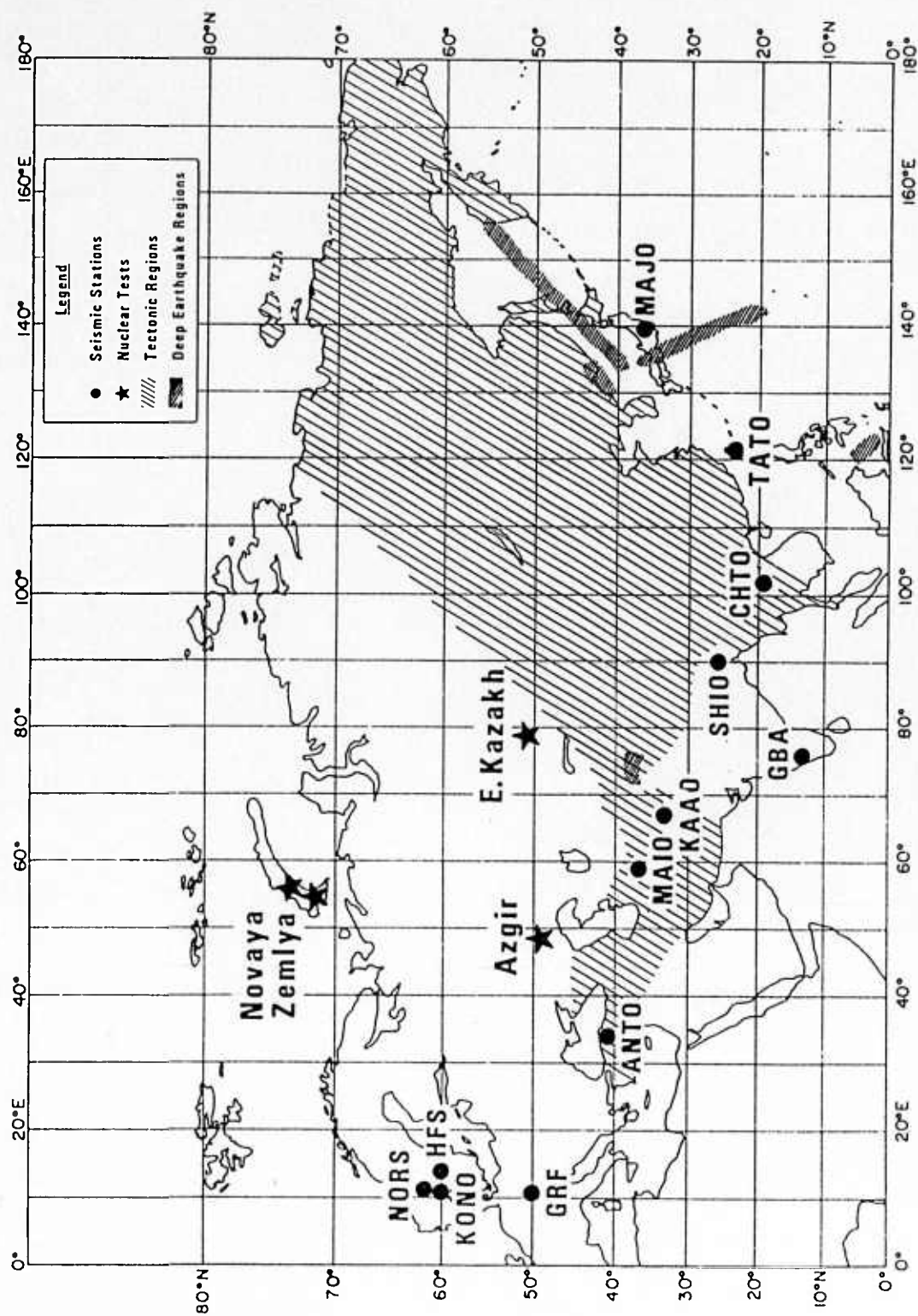


Figure 10. Map of the tectonic regions in Eurasia. The nuclear test sites are identified.

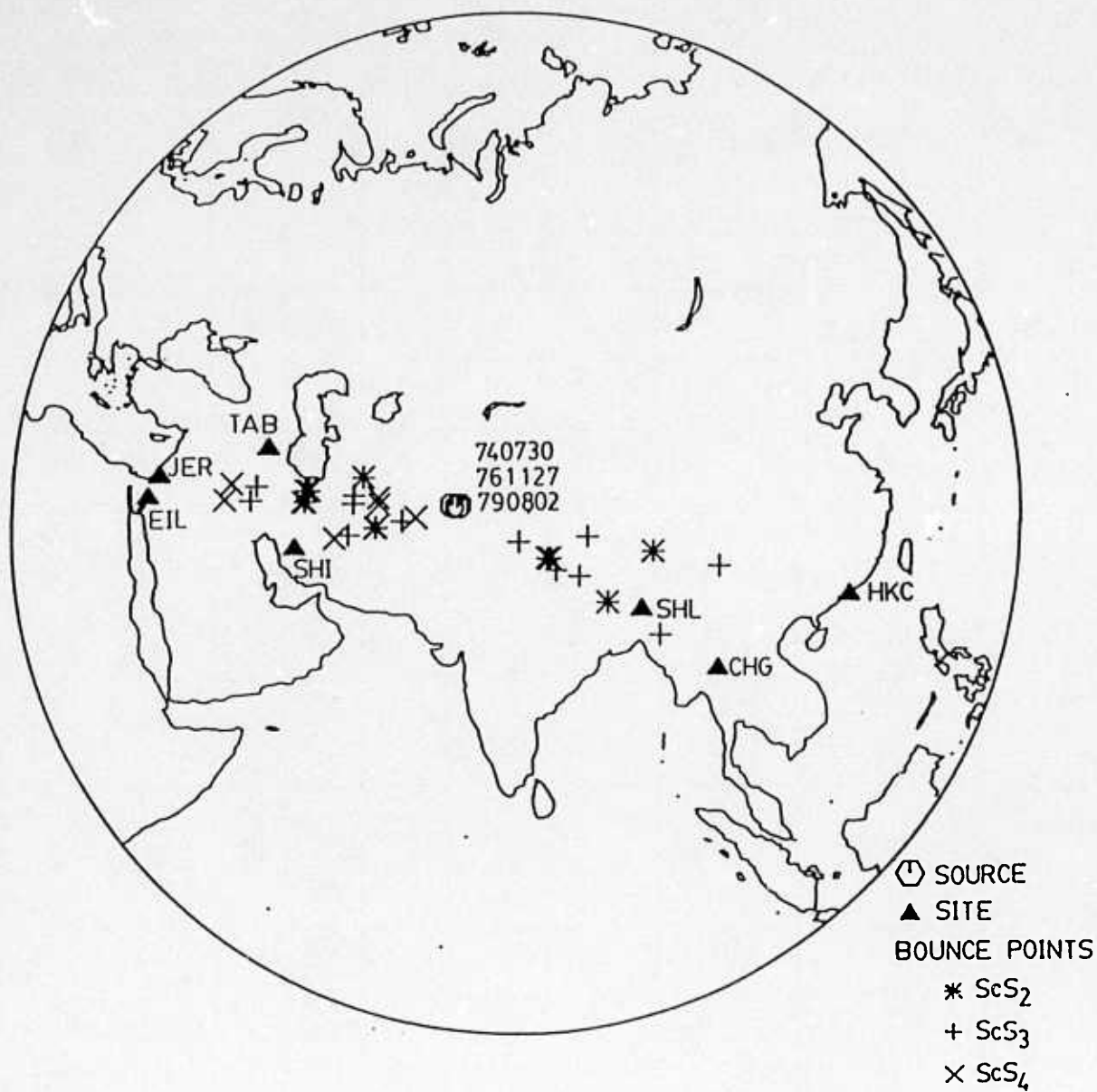


Figure 11. Map of WWSSN stations and multiple ScS bounce points for the Hindu-Kush earthquakes.

Table 3

Event Parameters for Far Eastern Events
Used in Estimating t_{scs}^* Under the Eurasian Shield

date	origin time (sec)	latitude (degrees)	longitude (degrees)	depth (km)	m_b (ISC)
660606	07:46:16.1	36.4	71.1	221.0	6.2
731017	03:16:18.6	36.4	71.2	221.0	5.5
740730	05:12:40.6	36.4	70.8	211.0	6.5
780421	15:22:57.9	36.63	71.26	229.6	5.8
790816	21:31:26.3	41.81	130.19	588.0	6.1
810502	16:05:02.2	36.8	70.99	229.0	5.9

Table 4

Event Parameters for Hindu Kush Events
Used in Estimating t^*_{scs} Under Eurasian Tectonic Areas

date	origin time (sec)	latitude (degrees)	longitude (degrees)	depth (km)	m_b (ISC)
740730	05:12:40.6	36.35	70.76	211.0	6.5
761127	21:42:12.1	36.52	71.04	190.2	6.2
790820	03:50:52.3	36.48	70.15	230.5	5.9

740703 EIL NS

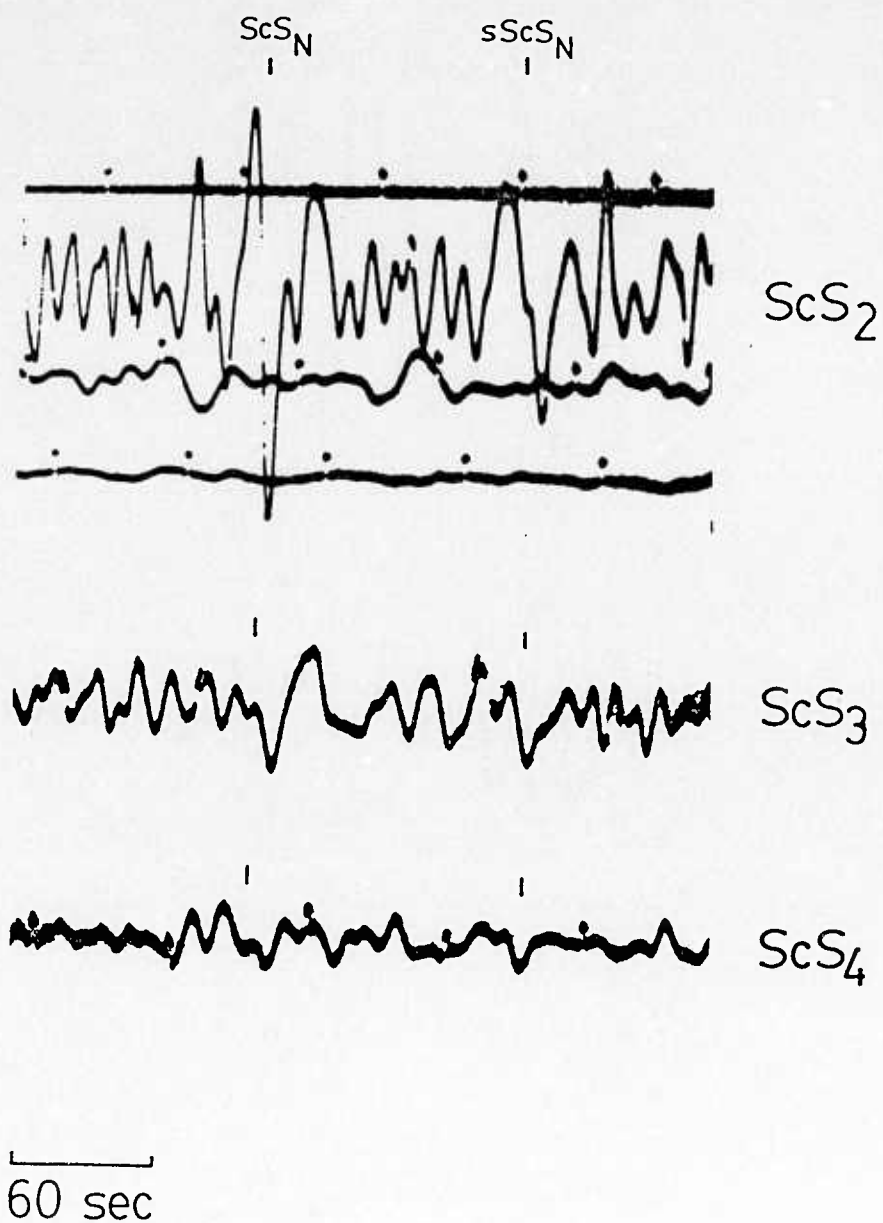


Figure 12. Tracings of multiple ScS phases followed by the corresponding sScS multiples at the WWSSN station EIL for the Hindu-Kush earthquake of 7/03/74.

740703

SHI

NS

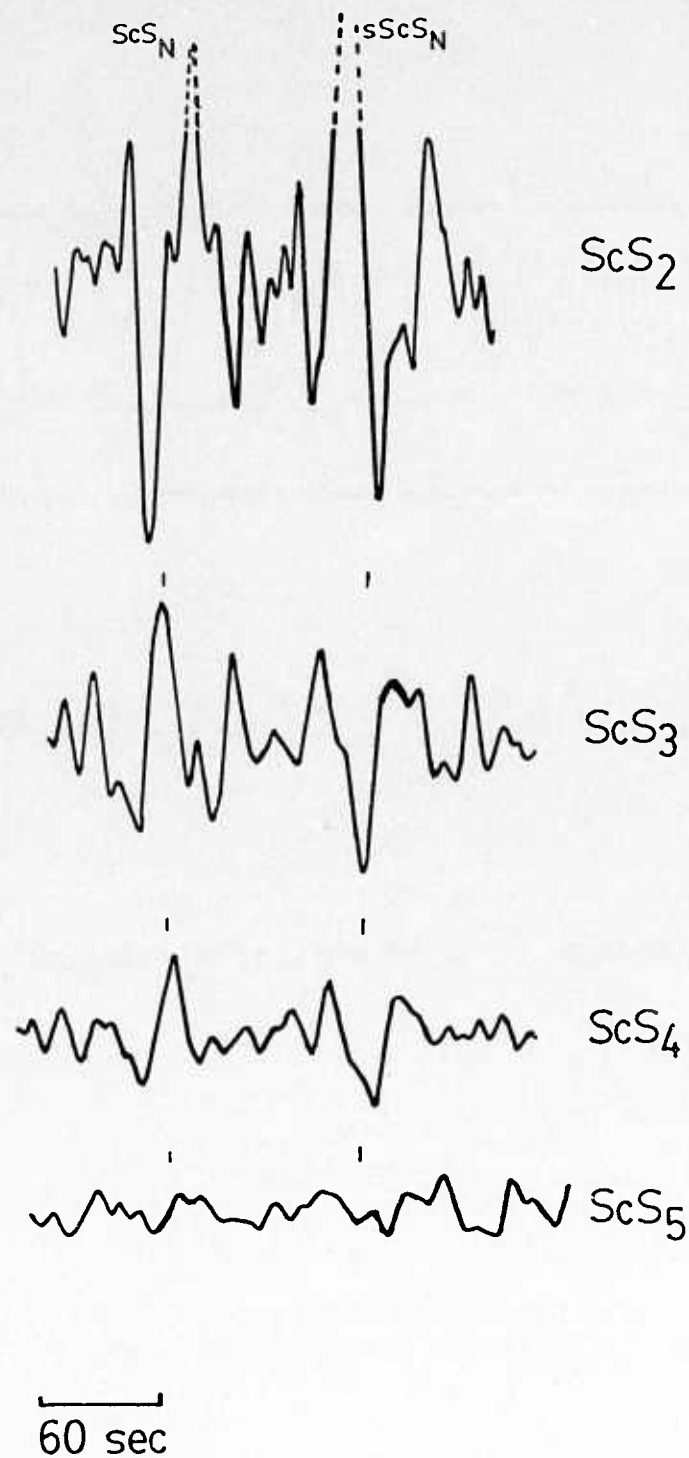


Figure 13 Tracings of multiple ScS phases followed by the corresponding sScS multiples at the WWSSN station SHI for the Hindu-Kush earthquake of 7/03/74.

790820

JER

NS

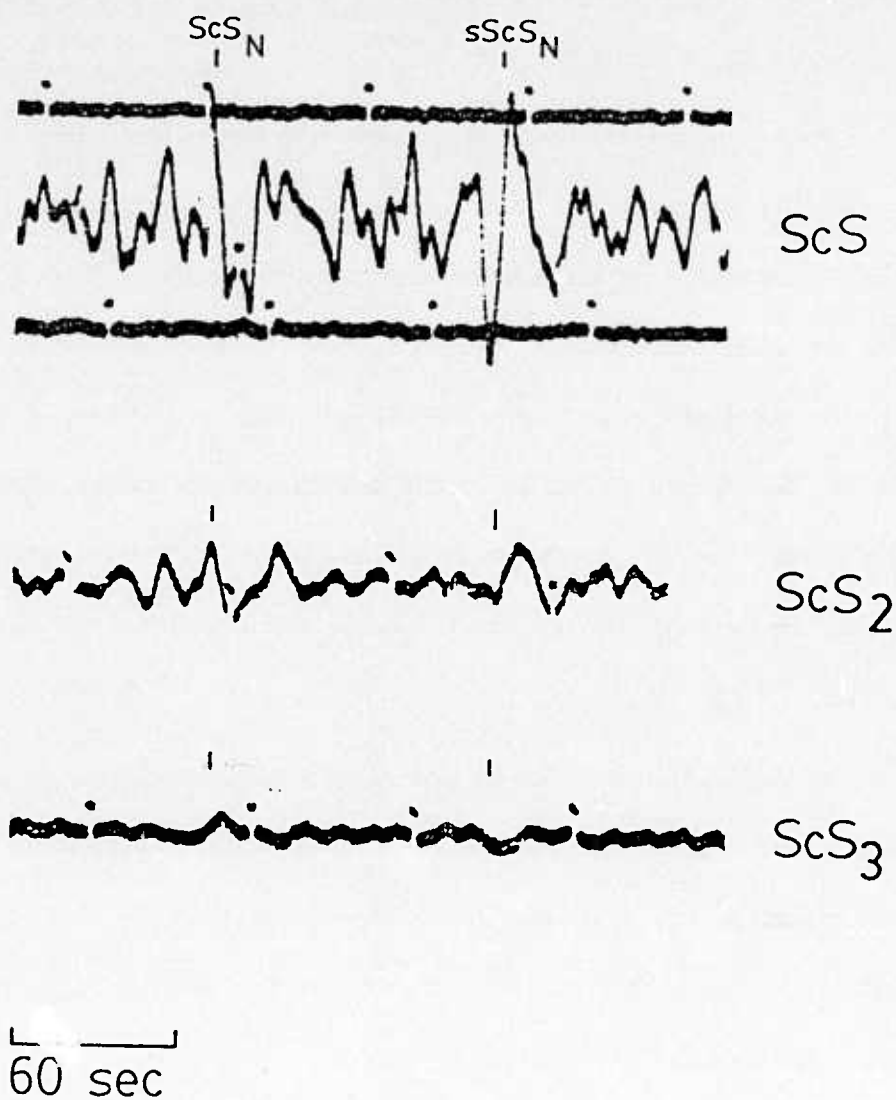


Figure 14 Tracings of multiple ScS phases followed by the corresponding $sScS$ multiples at the WWSSN station JER for the Hindu-Kush earthquake of 8/20/79.

against $f(N-2)$ where f is frequency and N is the order of ScS phase are shown in Figure 15 for the two source regions. The resulting fit to the data gives a t_{ScS}^* of 2.5 sec for shield Eurasia and 3.9 sec for tectonic Eurasia.

For North America, the nearby deep earthquake sources are Central America and the Alaskan-Aleutian region. Stations with multiple ScS phase surface reflection point in the tectonic and shield regions are found in the western and eastern United States respectively. The tectonic and shield boundary in N. America is shown in Figure 16. We found it difficult to obtain events in Central America with multiple ScS phases as spectacular as those in Eurasia and Pacific. The deepest earthquakes in this area are relatively shallow, not much more than 100 km in depth and thus surface waves tend to obscure ScS arrivals. Moreover, the event magnitudes are relatively low compared to other regions with deep earthquakes, the seismicity is also relatively low.

In the Alaskan-Aleutian region the sources are somewhat deeper and the seismicity higher but events towards the western end of the Aleutian chain often have surface reflection points for multiple ScS beneath the ocean. The events we judged to be suitable for analysis are listed in Tables 5 and 6 and their locations with the recording stations and the surface reflection points for ScS phases are shown in Figure 17.

Figures 18-20 show some tracings of multiple ScS data for the two source regions. In general, as seen in these figures, the ScS phases for events in Central America with bounce points within the western US fall off with increasing order much faster than those reflecting under the Canadian shield. Moreover, for some of the ScS phases with Canadian paths, the period is quite short and does not change much with increasing multiplicity of ScS. These facts indicate very low attenuation under Canada and much higher attenuation under the tectonically active regions of Mexico and southwestern United States.

EURASIAN STATIONS

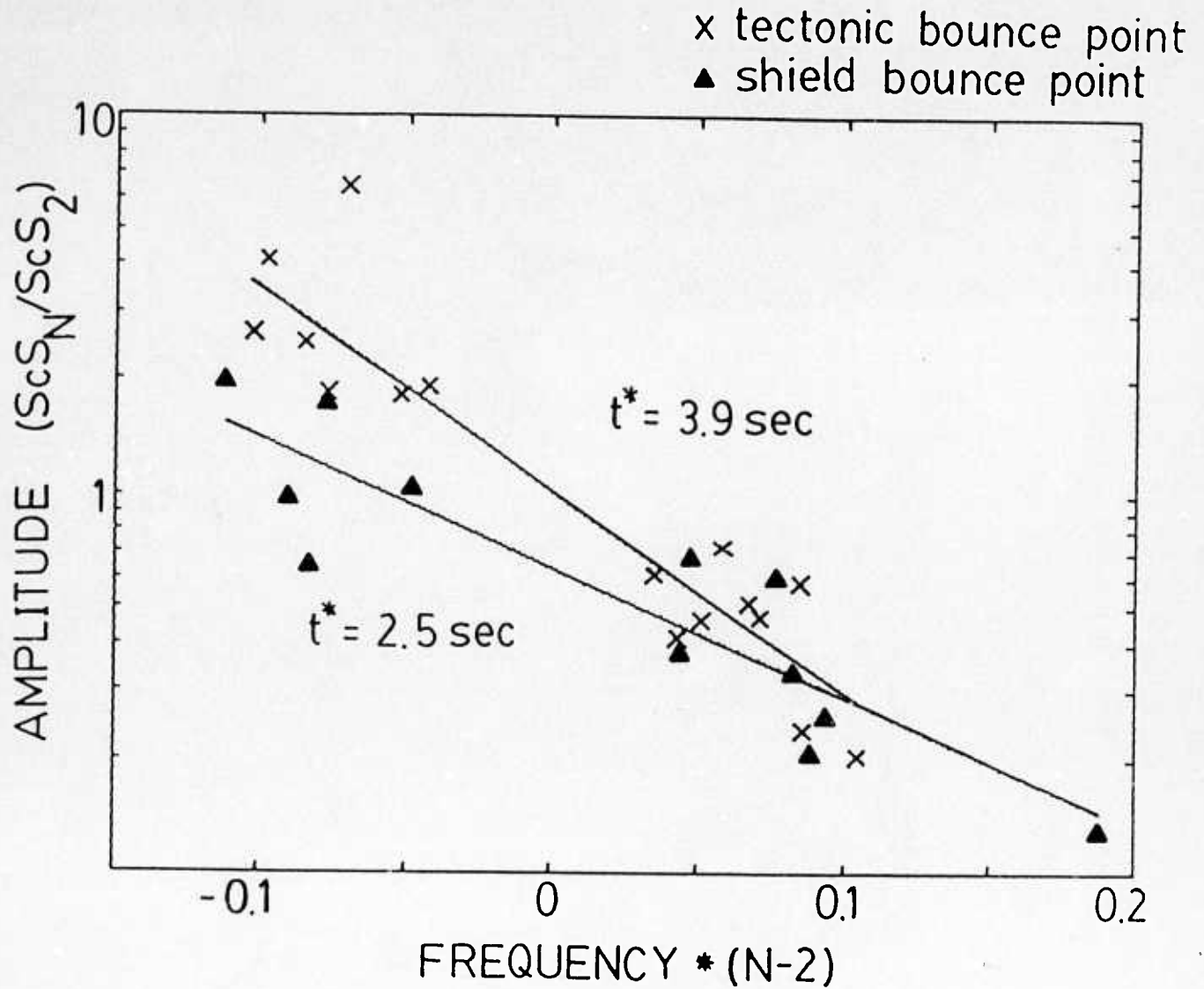


Figure 15. Summary of the ScS analyses for Eurasia. Shield paths give the mean t^* value of 2.5 sec (triangles) while the best fit for "tectonic" bounce points is 3.9 sec.

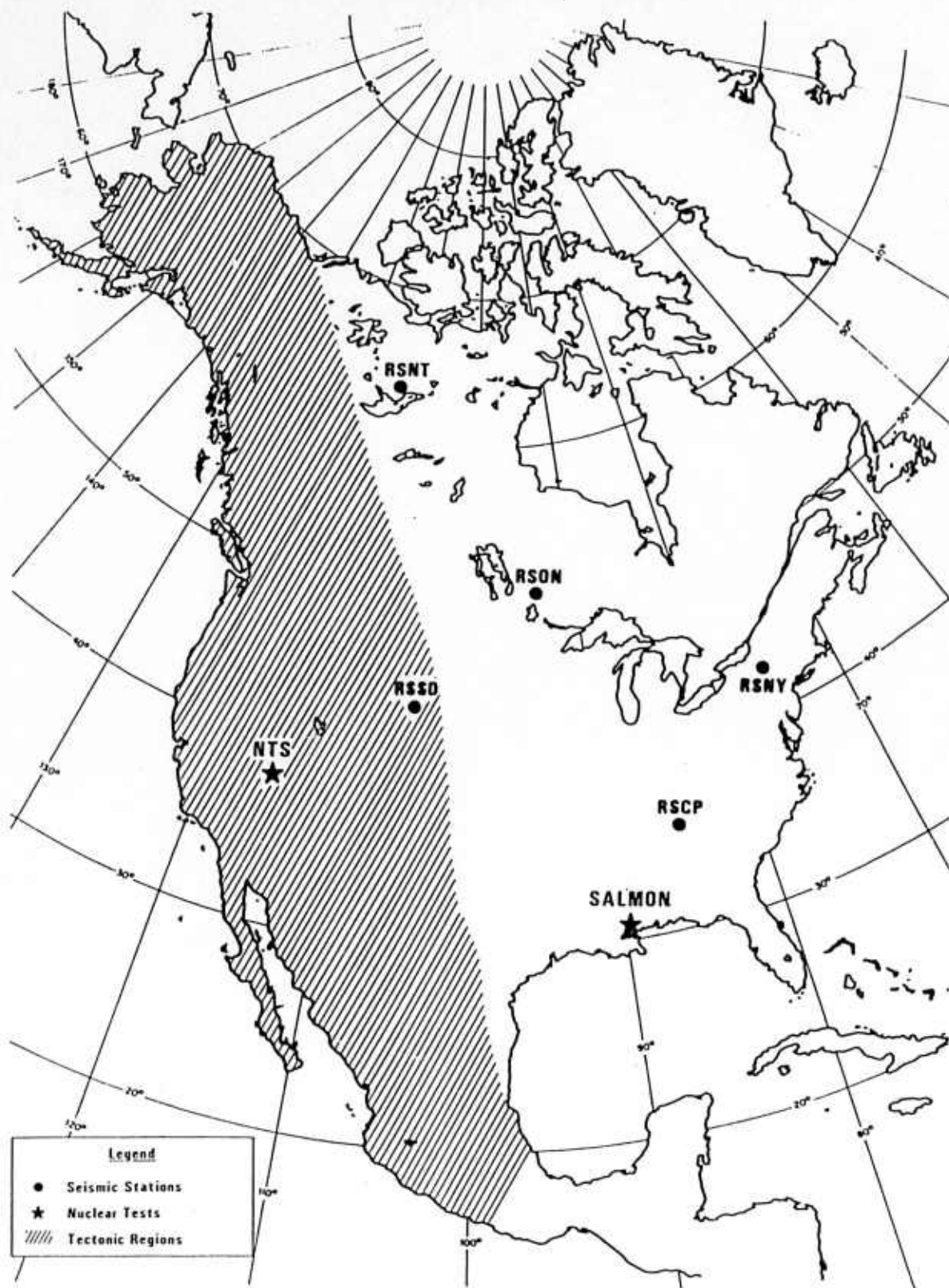


Figure 16. Map of the tectonic regions in North America. The nuclear test site is identified.

Table 5

**Event Parameters for Aleutian Events Used in Estimating
 t^*_{ScS} Under North America**

date	origin time (sec)	latitude (degrees)	longitude (degrees)	depth (km)	m_b (ISC)
700228	10:52:31.2	52.70	-175.10	162.	6.1
710405	09:04:42.8	53.36	-170.55	153.	5.8
710904	15:53:25.4	54.98	-163.36	107.	5.8

Table 6

Event Parameters for Central American Event Used
in Estimating t^*_{scs} Under North America

date	origin time (sec)	latitude (degrees)	longitude (degrees)	depth (km)	m_b (ISC)
740306	01:40:26.4	12.29	-86.39	110.	5.8

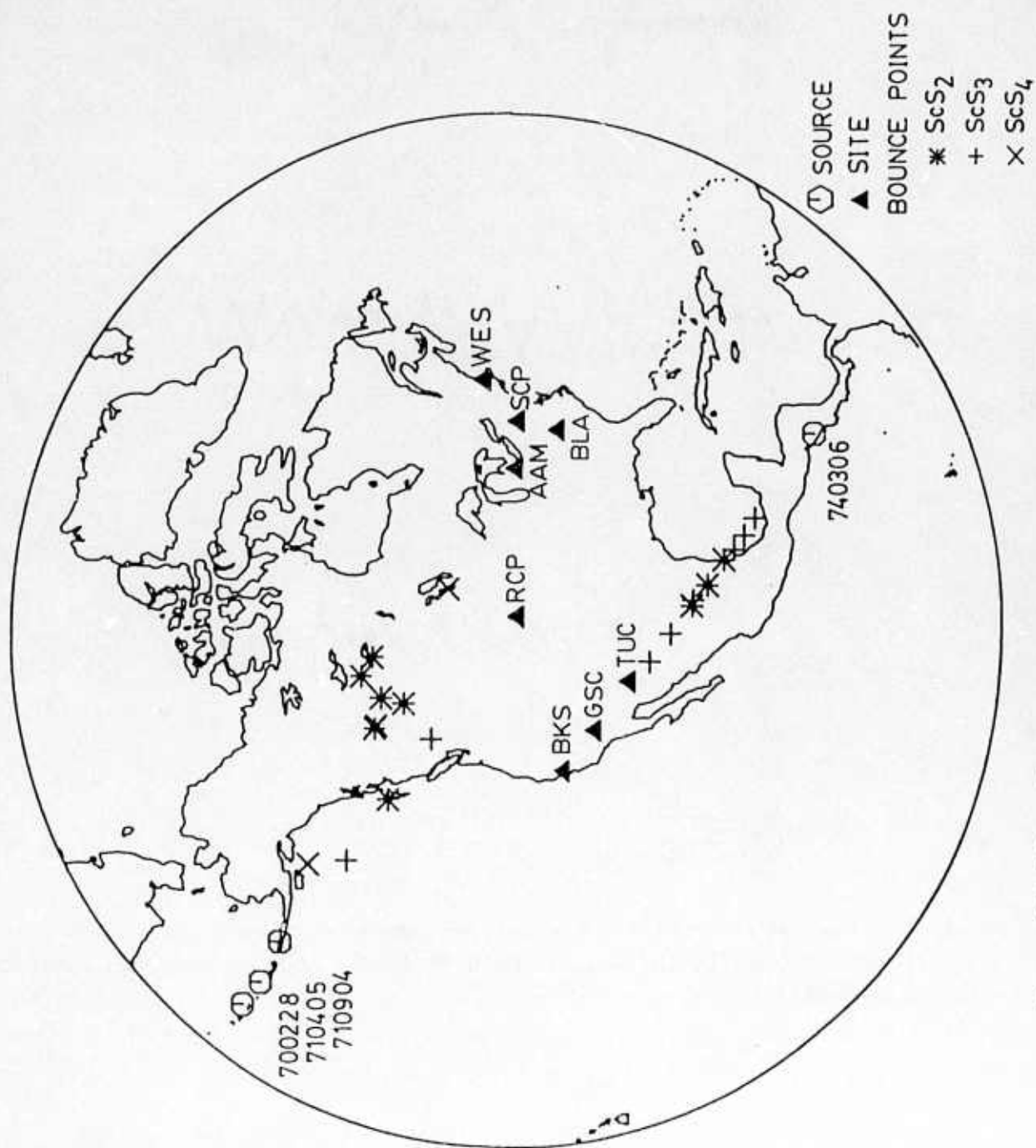


Figure 17. Map of sources, bounce points and WWSSN stations used in the analyses of ScS attenuation under North America.

720421

WES

EW

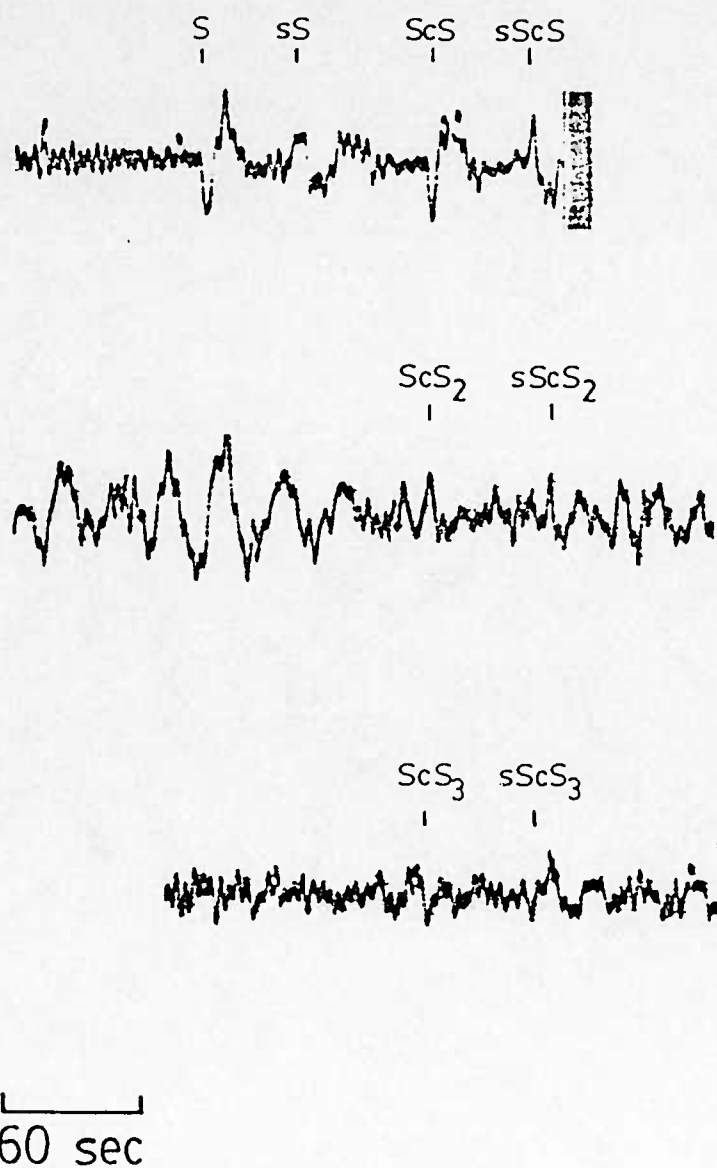


Figure 18. Tracings of multiple ScS arrivals with the corresponding sScS phases at the WWSSN station WES. These phases have relatively short periods and low decay rates thus indicating a high Q path.

710405

BLA

NS

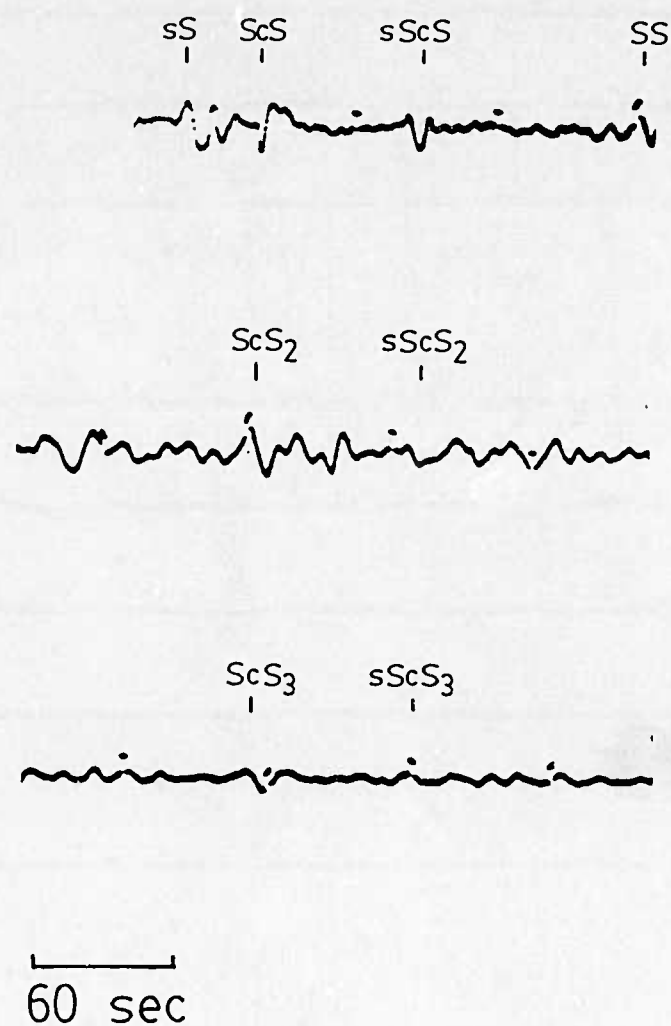


Figure 19. Tracings of multiple ScS arrivals with the corresponding sScS phases from the 4/05/71 Aleutian event as recorded at the WWSSN station BLA.

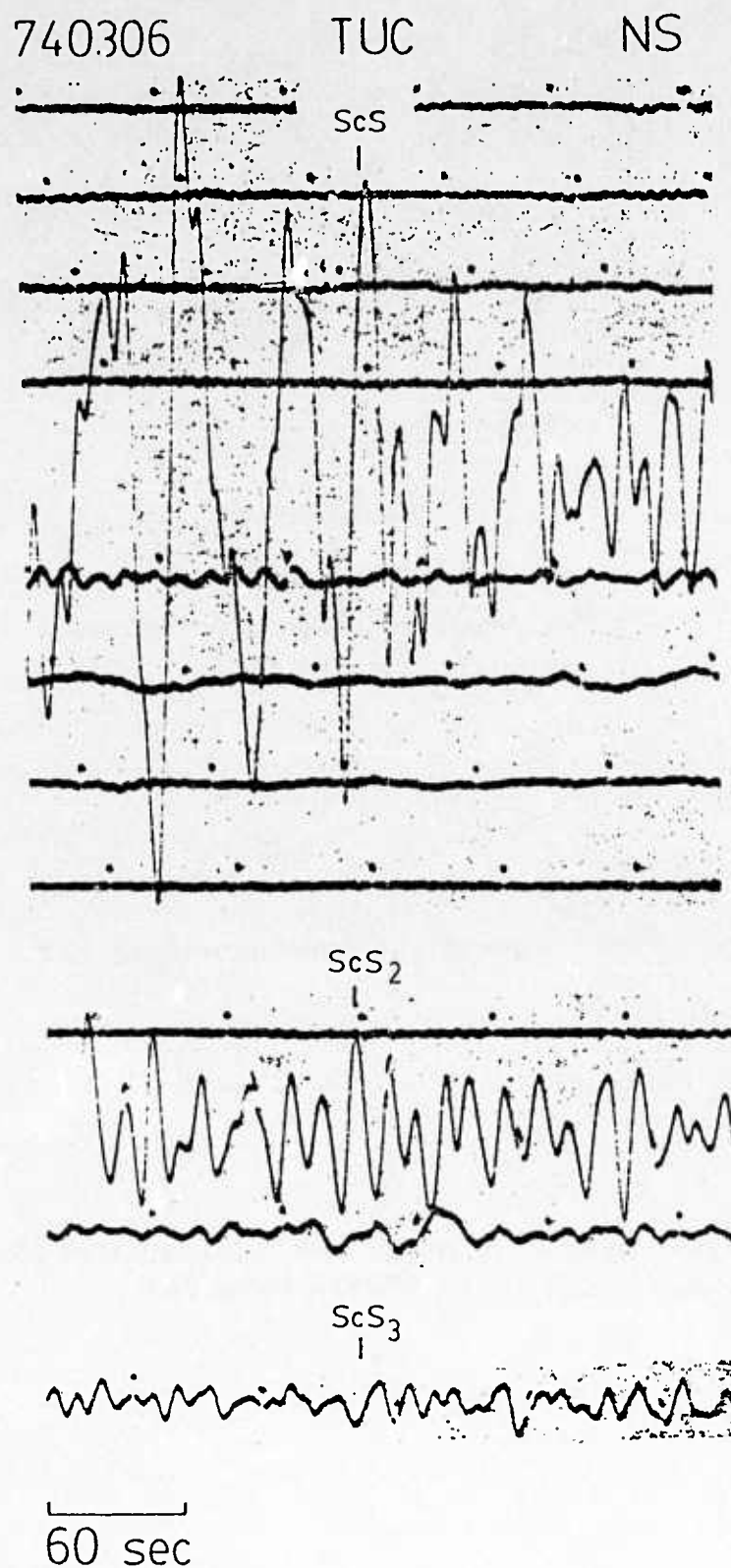


Figure 20. Tracings of multiple ScS arrivals with the corresponding sScS phases for the 3/06/74 Central American earthquake as recorded at the WWSSN station TUC. These phases have a rapidly decreasing amplitude due to high attenuation in the mantle under Mexico.

The plots of ScS phases, normalized to ScS_2 and plotted against $f(N-2)$ where f is frequency and N is the order of ScS phase are shown in Figure 21 for the two source regions. These data give t_{ScS}^* values of 1.1 sec for a single ScS leg under Canada and 4.0 sec under Mexico-Arizona. It appears that the regional Q differentials are no less significant and are of the same sign in the long period band as in the short period band in accordance with the hypothesis of quasi-parallel $t^*(f)$ curves (Der and Lees, 1985). The results are summarized in Table 2.

In summary, the regional differentials in attenuation are similar in sense that those reported in earlier studies. We have obtained an average t_{ScS}^* of 7.0 sec for paths across the E. Pacific while the SW Pacific and the NW Pacific are characterized by moderate attenuation with t_{ScS}^* values close to 4.0 sec. The results for the Eurasian, North and South American shield areas are significantly lower in t_{ScS}^* values, mostly in the 2-3 sec range. The tectonically active continental areas of Eurasia and North America are characterized by higher t_{ScS}^* estimates typically near 4.0 sec.

Discussion of the ScS Results

The range of variations in the average t_{ScS}^* contributed by the passage of SH waves through the upper mantle seems to be at least 3.5:1. Although this range may be increased by the inevitable scatter in any t_{ScS}^* estimation procedures, the differences are significant. The measurement of mantle averaged Q values does not provide enough information about the forms of the depth dependence of Q in the regions studied. It is reasonable to assume, however, that most of the lateral variation in the mantle Q is associated with the lateral changes in the properties of the upper mantle within a zone 200-300 km thick, since this is the vertical extent of the largest lateral variations of the seismic velocities as well (Dziewonski and Anderson, 1981; Grand and Helmberger, 1984; Jordan, 1975), presumably due to a common cause,

NORTH AMERICAN STATIONS

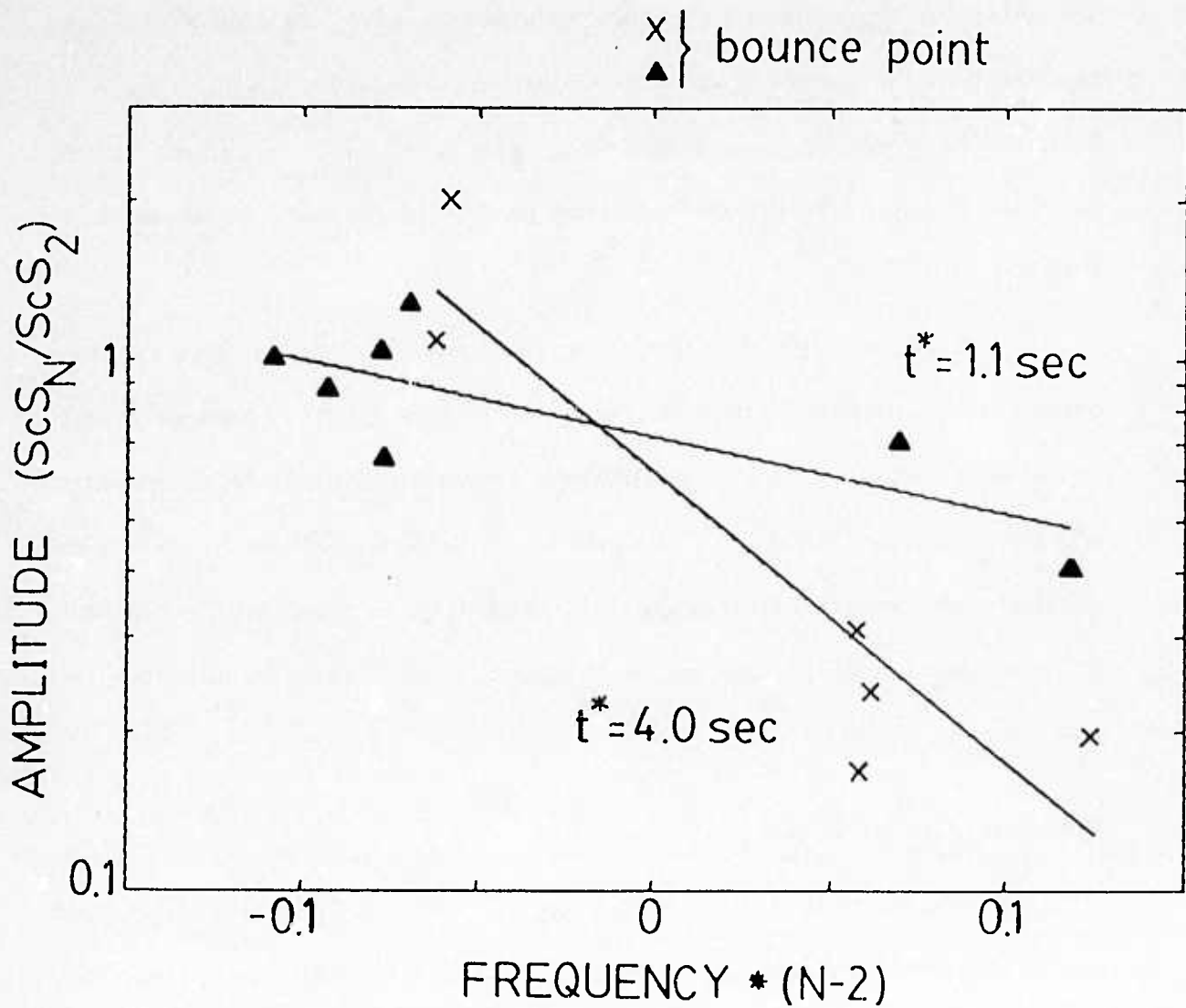


Figure 21. Summary of multiple ScS analyses for North America. The mean t^* for Canadian shield paths is 1.1 sec while the value for Mexico is 4.0 sec.

lateral changes in temperature or chemical composition. The large variations in the mantle averaged Q values imply much larger proportional changes in the upper mantle Q in this layer.

Our analyses of multiple ScS data show, similarly to other previous studies, that the attenuation properties in the mantle vary considerably from region to region. This variation is similar to the corresponding variations in the short period band (Der *et al.*, 1982b) in sign. Our Q values vary similarly to those reported by Sipkin and Jordan (1980) but are significantly higher than theirs as shown in Table 2. From ScS data alone we cannot, of course, delineate a complete profile of the depth dependence of Q, nor any frequency dependence of Q in the narrow frequency band we have been working in.

The results are important with regards to possible $Q_{ScS}^*(f)$ models. Assuming that the lateral variations in Q we observe with the multiple ScS data are confined in a 200-250 km thick layer in the upper mantle, wherever the lateral velocity variations are the most pronounced, presumably due to the same causes, temperature and chemical variations in the upper mantle, (Jordan, 1975) these results imply lateral variations in Q_{ScS} of up to an order of magnitude.

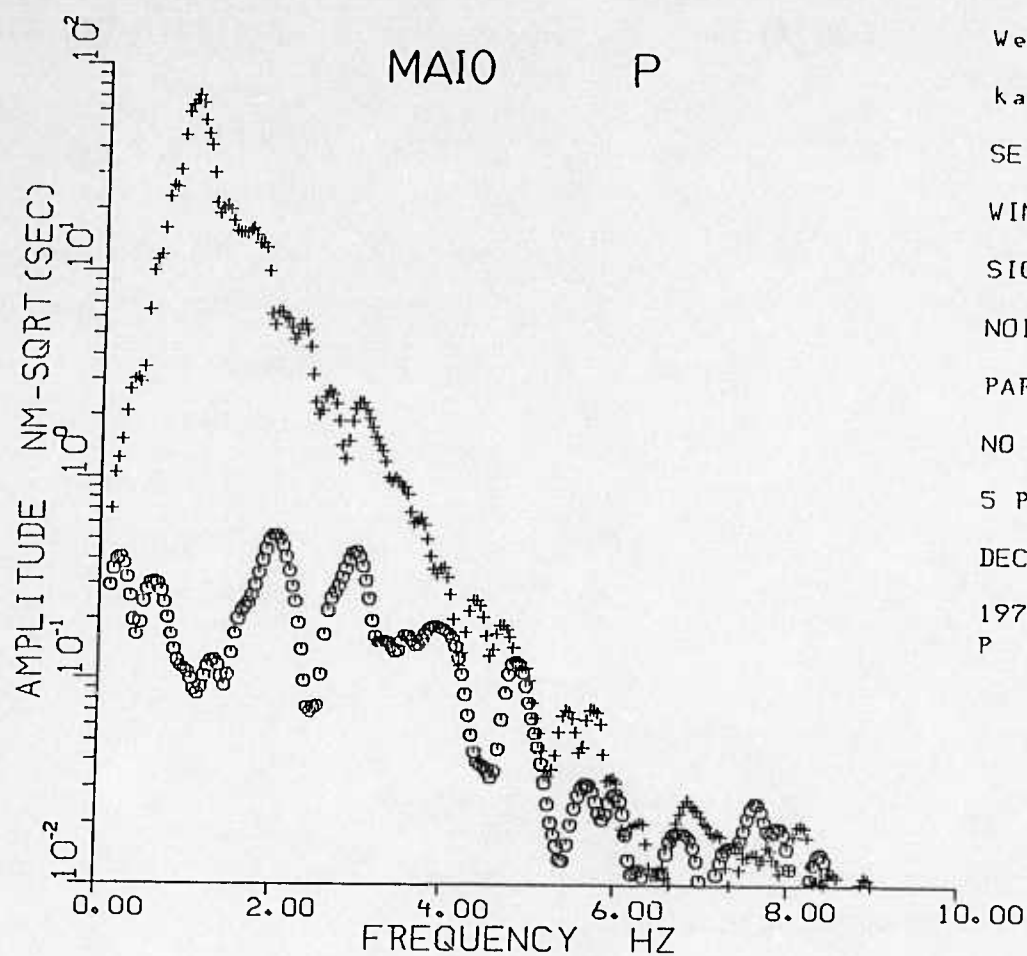
ANALYSES OF DATA FROM THE TECTONIC AREAS OF EURASIA

Analyses of P Wave Spectra from Nuclear Explosions

Analyses of P wave spectra of nuclear explosions in Kazakh consist of estimating the best fitting $\overline{t_p^*}$ values from the spectra. The instrument response and a von Seggern-Blandford (1972) explosion source are removed from the spectra of each P wave and the slope of a linear least squares fit line through the reduced spectrum within the region of good signal-to-noise ratio provides an estimate of $\overline{t_p^*}$. Sample P wave spectra are shown in Figure 22 for the tectonic stations MAIO and ANTO and the shield station KONO. The average t_p^* obtained for the shield-tectonic path is around 0.28 sec. The tectonic stations show a much more limited range of good signal to noise than does KONO. Except for TATO, at least 10 observations were used for each station. The event parameters for the explosions used in this study are in Table 7 and the values obtained are given in Table 8.

The values in Table 8 are not dissimilar to those quoted by Der *et al.* (1985b) and are not particularly high. They are definitely less than t^* values for paths involving the upper mantle under the Basin and Range (Der *et al.*, 1985b; Bache *et al.*, 1985). Since t^* values for paths between Kazakh and Scandinavia are near 0.15 sec, only values for the stations ANTO, CHTO, GRFO and MAIO can be called higher than the typical values for shields. Since the sources of these events were in high Q area, the additional attenuation must be attributed to attenuation in the mantle under these stations.

These findings are in agreement with some results of one of our previous studies (Der *et al.*, 1982b) in which we found that unlike the shields, the so called "tectonic" areas of the world are quite heterogeneous with respect to Q and both high and low Q paths are possible through such regions. This manifests itself in the large scatter in the t^* estimates for paths



Wed Sep 11 21:09:22
 kazqp1
 SEIS # 2
 WINDOW = 512
 SIGNAL 295 512
 NOISE 199 256
 PARZEN TAPER
 NO INST CORRECTION
 5 PT SMOOTHING
 DECIMATED BY 1
 1976241 maio
 P 2

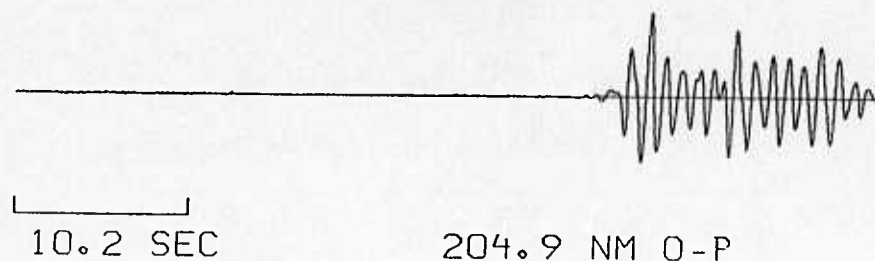
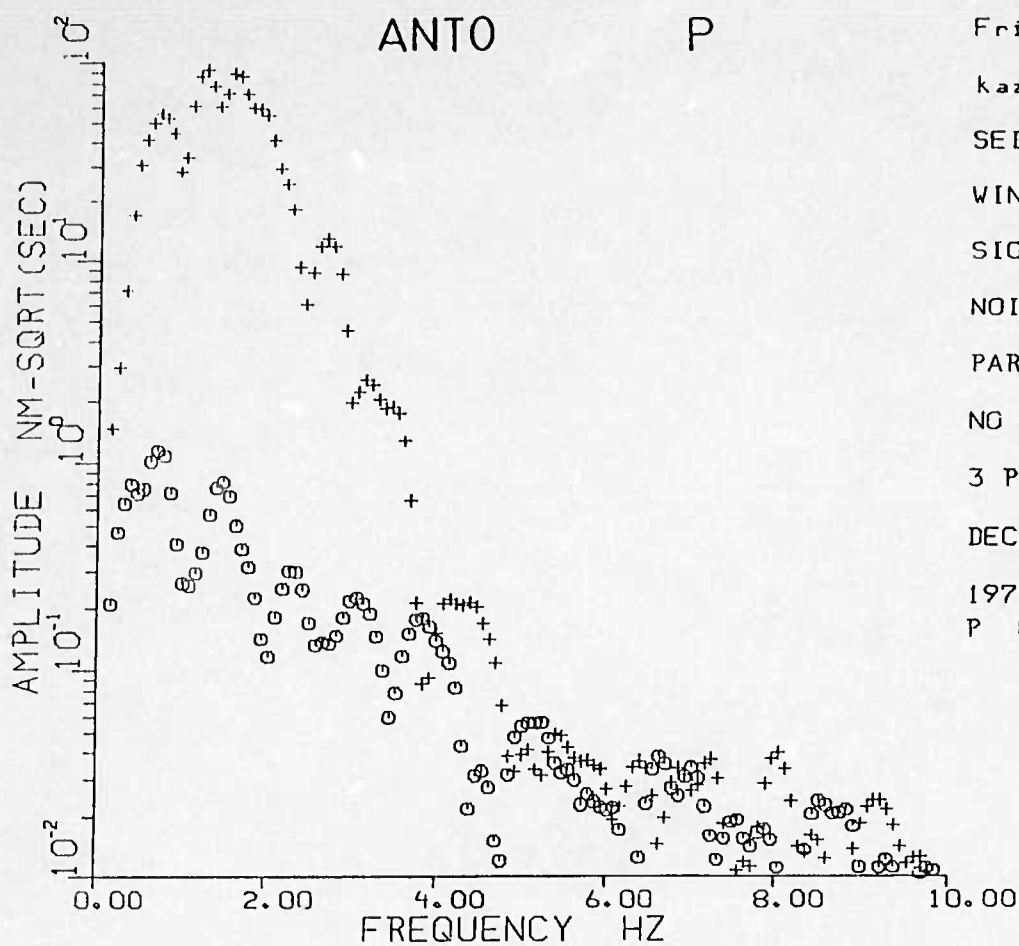


Figure 22a. Samples of P waves spectra from Kazakh nuclear explosions. +'s are the signal and the o's are the noise level for an event 1976241 recorded at MAIO.



Fri Sep 13 01:03:43

kazpq2

SEIS # 8

WINDOW = 256

SIGNAL 613 256

NOISE 437 256

PARZEN TAPER

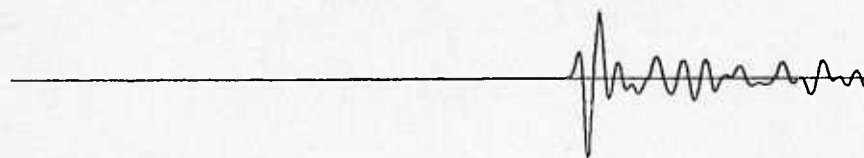
NO INST CORRECTION

3 PT SMOOTHING

DECIMATED BY 1

1979301 anto

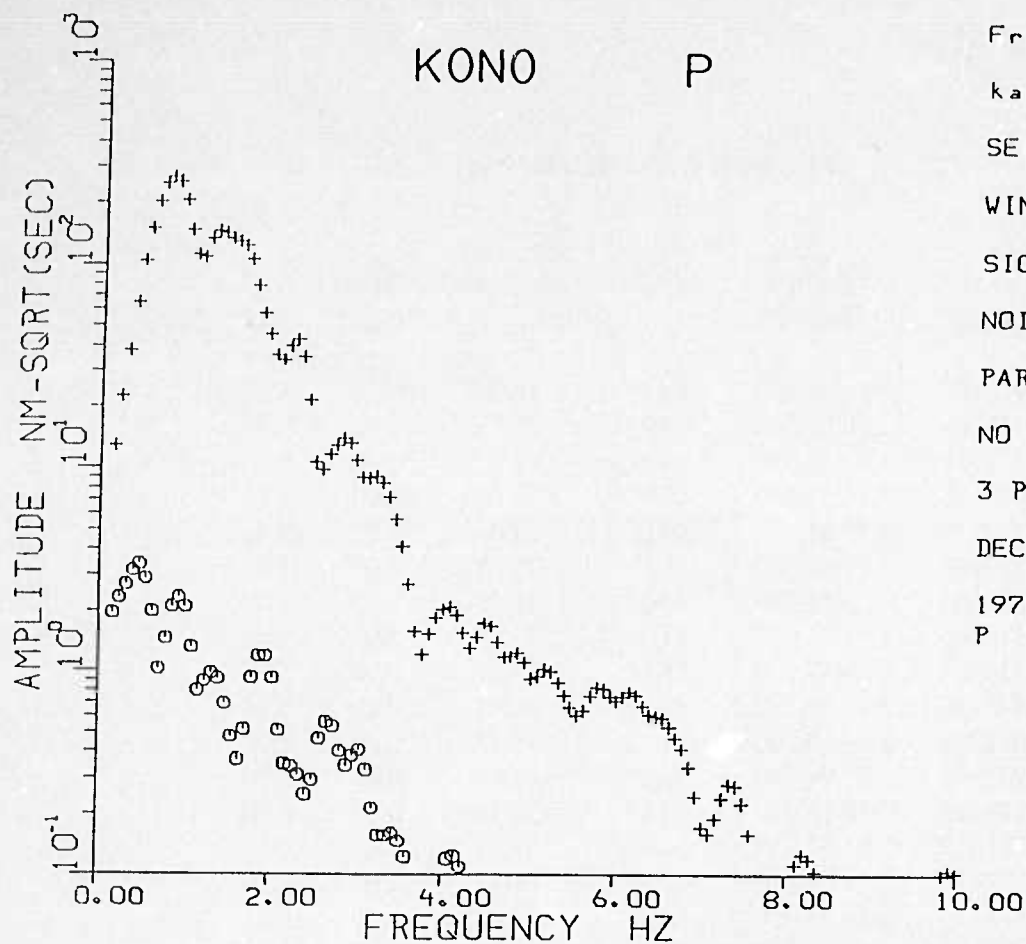
P 8



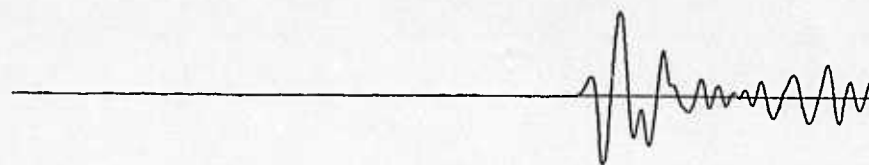
5.1 SEC

627.5 NM O-P

Figure 22b. Samples of P waves spectra from Kazakh nuclear explosions. +'s are the signal and the o's are the noise level for an event 1979301 recorded at ANTO.



Fri Sep 13 01:02:20
 kazpq2
 SEIS # 5
 WINDOW = 256
 SIGNAL 400 256
 NOISE 224 256
 PARZEN TAPER
 NO INST CORRECTION
 3 PT SMOOTHING
 DECIMATED BY 1
 1979230 kono
 P 5



5.1 SEC

1044.2 NM O-P

Figure 22c. Samples of P waves spectra from Kazakh nuclear explosions. +'s are the signal and the o's are the noise level for an event 1979230 recorded at KONO.

Table 7

Event Parameters for Kazakh Explosions

date	origin time (sec)	latitude (degrees)	longitude (degrees)	depth (km)	m_b (ISC)
1976186	2:56:57.480	49.85	78.97	0.00	5.80
1976241	2:56:57.600	49.95	78.98	0.00	5.80
1976328	5:02:57.470	49.97	79.01	0.00	5.80
1976342	4:56:57.480	49.87	78.89	0.00	5.90
1977149	2:56:57.490	49.85	78.84	0.00	5.80
1977248	3:02:57.760	50.05	78.93	0.00	5.80
1977334	4:06:57.630	49.93	78.89	0.00	6.00
1978085	3:56:57.690	49.71	78.06	0.00	5.60
1978162	2:56:57.800	49.88	78.81	0.00	5.90
1978186	2:46:57.510	49.84	78.91	0.00	5.80
1978209	2:46:57.760	49.73	78.15	0.00	5.70
1978241	2:37:06.380	49.98	79.02	0.00	5.90
1978258	2:36:57.500	49.91	78.94	0.00	6.00
1978308	5:05:57.550	50.03	78.97	0.00	5.60
1978333	4:33:02.870	49.93	78.77	0.00	6.00
1979174	2:56:59.050	49.88	78.92	0.00	6.20
1979188	3:46:57.480	50.05	79.06	0.00	5.80
1979216	3:56:57.250	49.86	78.94	0.00	6.10
1979230	2:51:57.310	49.93	78.98	0.00	6.10
1979301	3:16:57.030	49.96	79.07	0.00	6.00
1979336	4:36:57.620	49.88	78.83	0.00	6.00
1979357	4:56:57.640	49.92	78.80	0.00	6.20
1980116	3:56:57.440	49.92	78.81	0.00	5.50
1980143	3:56:57.780	49.75	78.11	0.00	5.50
1980164	3:26:57.670	49.95	79.05	0.00	5.60
1980181	2:32:57.750	49.90	78.86	0.00	5.70
1980258	2:42:39.300	49.98	78.89	0.00	6.20
1980286	3:34:14.100	49.96	79.08	0.00	5.90
1980349	3:47:06.600	49.93	79.00	0.00	5.90
1980362	4:09:08.200	50.04	79.05	0.00	5.90
1981088	4:03:50.000	50.01	79.02	0.00	5.60
1981112	1:17:11.400	49.90	78.90	0.00	5.90

Table 8

$\overline{t^*_p}$ Estimates for Paths
from East Kazakh to Eurasian Stations
for Shield - Tectonic Paths

station	frequency range (Hz)	$\overline{t^*}$ (sec)
ANTO	0.5-4	0.35±0.04
CHTO	0.5-5	0.29±0.06
GRFO	0.5-4	0.34±0.06
KAAO	0.5-6	0.13±0.03
KONO	0.5-5	0.24±0.05
MAIO	0.5-4	0.28±0.04
MAJO	0.8-5	0.20±0.05
SHIO	0.5-5	0.22±0.04
TATO	1.0-3	0.17±0.07

crossing tectonically active areas.

Analyses of Short Period PP/ P Spectral Ratios

Unlike the analyses of direct P wave spectra which are diagnostic of the upper mantle under the station and source, comparisons of the frequency contents of P and PP will give information about the mantle attenuation under the surface reflection point of PP.

Short period PP arrivals are commonly engulfed in the coda of the first P arrival. Although some successful analyses of PP/P spectral ratios have been made on carefully selected data to determine Q (Shore, 1983), we have found it to be more expedient to estimate Q by band-pass filtering the wavetrain consisting of P and PP arrivals, the same window also includes sP for earthquakes. Moreover, at some distances PcP is often near these arrivals. It is expected that the PP arrival will disappear if the surface reflection point is in highly attenuating regions, and the high frequency expression of the phase should disappear first.

We have processed a number of PP and P pairs with sharply tuned (48 dB/octave) band pass filters to minimize the effect of spectral falloffs of the seismic sources on the outputs. The events used for the PP analyses are all explosions at Kazakh. We chose these because the time functions of these sources are relatively short in duration compared to earthquakes and PP is easier to recognize on the records. Moreover, explosions generally excite high frequency waves more efficiently. The same approach is also used for earthquakes for the Pacific region as discussed elsewhere in this report.

Appendix B shows some of the bandpass-filtered waveforms used for the PP study. At some stations, such as KONO, SHIO, and GRFO, the PP phases appear frequently and can be observed continuously as we go towards bands with increasing center frequency. The PcP phase is also often visible. At other stations, such as CHTO and ANTO, the PP phase is either not observed at all or it disappears into the noise background at higher frequencies. The

locations of the surface reflection points together with the estimated t^* are shown in Figure 23a, and the results are tabulated in Table 9. For some events at GRFO and KONO, the PP/P ratio initially increases with frequency thus making the overall t^* estimates negative. We do not understand the reasons for this, but this is clearly an indication of a high Q mantle under the surface reflection point which lie in the Russian shield. In Figure 23a we designate these with the t^* estimate of zero. Since we do not believe in negative or zero t^* , the zero designation simply means that the t^* involving these surface reflection points is too low to be measured by this method.

In Table 9 and in Figure 23a, the $\overline{t_p^*}$ values have been adjusted to reflect the t^* values expected for a tectonic-tectonic path instead of the shield-tectonic path obtained when the source event is at East Kazakh. A $\overline{t_p^*}$ of 0.15 sec was assumed for a shield-shield path (Bache *et al.*, 1985), so half of this was subtracted from the $\overline{t_p^*}$ estimates for the shield-tectonic paths, and the remainder was doubled, giving an estimate for a tectonic-tectonic path where both tectonic regions are similar to the station site. Looking at the tectonic-tectonic path, values for $\overline{t_p^*}$ allows more direct comparison with the estimates of $\overline{t_{pp}^*}$, and the values of $\overline{t_p^*}$ and $\overline{t_{pp}^*}$ are relatively close, though they do reflect a good deal of variability within the tectonic regions.

The PP/P ratio method is, of course, subject to errors due to the distortion of the spectral ratios by the effects of crustal structure at the reflection points. We also attempted to compute spectral ratios of PP to P directly using the approach followed by Shore (1983). We have found that for most events the band-pass approach was preferable because of the poor S/N ratios of PP (noise means scattered P coda in this case).

Rise Times of P Waves from Nuclear Explosions

Table 9

$\overline{t^*}_p$ and $\overline{t^*}_{pp}$ Estimates for
Eurasian Stations for Tectonic - Tectonic Paths

station	P frequency range (Hz)	$\overline{t^*}_p$ (sec)	PP frequency range (Hz)	$\overline{t^*}_{pp}$ (sec)
ANTO	0.5-4	0.57±0.08	0.5-1.3	0.50±0.09
CHTO	0.5-5	0.43±0.12	0.5-1.3	0.52±0.08
GRFO	0.5-4	0.54±0.12		
KAAO	0.5-6	0.13±0.05		
KONO	0.5-5	0.34±0.10		
MAIO	0.5-4	0.41±0.08		
MAJO	0.8-5	0.25±0.10	0.5-1.3	0.60±0.11
SHIO	0.5-5	0.29±0.08	0.5-1.3	0.32±0.13
TATO	1.0-3	0.19±0.09		

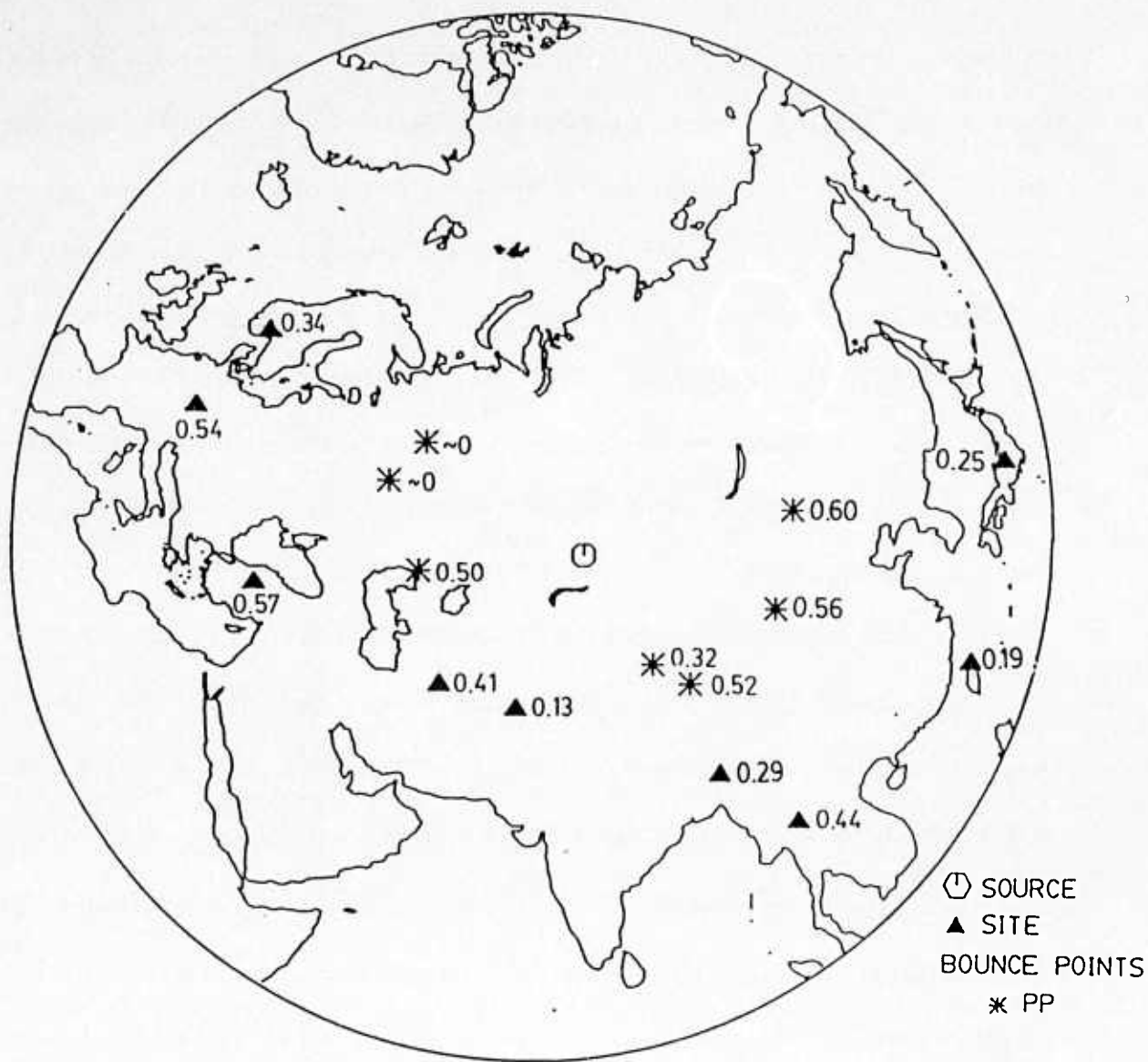


Figure 23a. Map of t^* values for direct paths to SRO stations and PP arrivals (plotted at the bounce point). The values of 0 near two bounce points indicate low attenuation under the shield.

A time domain approach to the estimation of Q for body waves is the matching of rise times (Stewart, 1984). This approach is based on the idea that \bar{t}^* is the controlling factor that determines the gross overall shape of the initial swing of the short period P waveform as characterized by a "rise time". Other factors that may influence the rise time are the shape of the initial source pulse, the time lag between P and pP, and "stochastic dispersion" (Richards and Menke, 1983; McLaughlin *et al.*, 1986). Thus, by assuming that the rise time is due solely to intrinsic attenuation, rise time estimates give upper bounds on \bar{t}^* . For nuclear explosions we have a reasonably good idea about the minimum rise times of the source pulses from near field measurements; these are the shortest for shots in hard rock. The minimum P-pP time lag may be obtained by assuming that the explosion was buried at a relatively shallow scaled depth ($h=0.07Y^{1/3}$, where the depth h is given in km and the explosion yield Y in kilotons) and assuming that the near surface velocities are high. Deeper burial depths and lower uphole velocities would give overly high, conservative upper limits for \bar{t}_p^* .

Rise time is usually defined as the time between the first maximum and the intersection of the tangent to the rising portion of the P waveform with the maximum slope with the zero amplitude level. Since the maximum slope is hard to measure we have used the time between the first break and the first maximum as rise time. We have used the same definition in our theoretical simulations and, therefore, this modification of the procedure has no effect on the conclusions. Theoretical rise times were computed using the cube-root scaled von Seggern and Blandford (1972) granite source model, the minimum scale depth, a range of apparent \bar{t}_p^* from 0 to 1 sec, a surface reflection coefficient of negative unity and an uphole velocity of 5.5 km/sec.

Rise times provide powerful arguments (Stewart, 1984) against high values of \bar{t}^* commonly accepted just a few years ago as valid for the short period band. These high values are

not believed by most seismologists today and the rise times can only be used to put some loose upper bounds on t^* . These upper bounds are not very useful in determining what the most appropriate values of t^* are, although they convincingly rule out the previously accepted high values. We therefore relegated our rise time analyses to Appendix C and did not repeat the same kinds of analyses for the other regions studied in this report. Nevertheless the results in Appendix C should convince the reader that higher t^* values are appropriate for "tectonic" than for "shield" Eurasia.

In Appendix C, the observed rise times are plotted against the apparent t^* values 16 for some of the SRO stations we used in this study. We omitted KAAO and MAIO because these are at regional distances from the Kazakh test site. The four curves in each figure correspond to the theoretical values for four yields derived by measuring synthetic seismograms in a similar manner. The yields used to determine the position of our observational data in these graphs were obtained by taking the m_b values from the seismic bulletin published by the International Seismic Centre and estimating the yields based on the yield-magnitude curve obtained by plotting these magnitudes against the yields estimated by Dahlman and Israelson (1977) for Kazakh explosions. These yield estimates, although crude, are sufficient for predicting the pulse rise times since they are very insensitive to yield.

Each observed rise time is plotted such that the ordinate is equal to the observed rise time, and the point is located between the curves to correspond to its m_b -estimated yield. The projection of each point on the horizontal axis gives an estimate of $\overline{t_p^*}$ which, in view of the conservative assumptions we have used, must be an upper limit. The results in Appendix C indicates that the upper limits of t_p^* are quite variable from station to station. The lowest limits are given by SHIO and ANTO, intermediate limits characterize KONO and GRFO, while high t^* is associated with CHTO. The SHIO results agree with those of Stewart (1984) who

obtained a similar mean value for USSR explosions at YKA, another station situated on a shield region.

The estimate $\overline{t_p^*}$ from rise times is significantly greater than the estimate $\overline{t_p^*}$ generally obtained from spectra. Theoretically, for a minimum phase, causal waveform propagating in an intrinsically anelastic medium, higher frequencies will travel faster than lower frequencies. This will make the rise time *less* than one fourth the full cycle of the first arrival. Observed rise times, however, are often *equal* to or *greater* than one fourth the period of the first full cycle of the P arrival, and it has been observed that often the higher frequencies in the P wave arrive somewhat later than the lower frequencies (McLaughlin and Anderson, 1986; Richards and Menke, 1983). This is due to scattering which can cause reverse apparent dispersion, with the higher frequencies delayed relative to the lower frequencies. Thus, the longer rise times overestimate $\overline{t^*}$ and serve as upper bounds on the attenuation. Recent theoretical work on stochastic dispersion also indicates that such upper limits for $\overline{t_p^*}$ from rise times are probably overestimated (Richards and Menke, 1983; Frankel and Clayton, 1984; McLaughlin and Anderson, 1986; McLaughlin *et al.*, 1986), and therefore impose even more severe constraints on the admissible maximum values of $\overline{t^*}$ than previously thought, since the group delay due to the randomness of media increases with increasing frequency, thus increasing the rise times independently of Q effects.

Analyses of SS/S Amplitude Ratios

A set of S and SS waveforms were collected at various distances. The event parameters are listed in Table 10 and their locations and the associated SS surface reflection bounces are shown in Figure 23b. These have been added to our data for the Eurasian shield using the approach in our previous studies (Der *et al.*, 1985a). The plot of our tectonic data points (stars) together with our previous data for the Eurasian shield (filled circles) is shown in Figure

Table 10

Parameters of earthquakes used in SS/S study of tectonic Eurasia

Event #	date	latitude	longitude	depth	m _b
1	Feb 1, 1984	49.06	+146.59	573.0	5.9
2	Apr 20, 1984	50.12	+148.75	582.0	6.0
3	Apr 23, 1984	47.45	+146.69	414.0	6.0
4	Apr 3, 1985	28.23	+139.52	469.0	5.9

EURASIA



Figure 23b. Map of the bounce points (+'s) within the tectonic Eurasia used for the SS/S amplitude ratio study.

24. Very preliminary results suggest high $t^* > 6$ sec for "tectonic" Eurasia, much higher than the value obtained (~3 sec) previously for the shield (Der *et al.*, 1985b).

Frequency Dependent t^* Model for Eurasia

We have obtained values of t^* for both tectonic and shield Eurasia using the various data sets and methods at various different frequency bands. The short period P wave studies provide information towards the higher frequency band from 0.6 to 10 Hz. The low frequency studies yield t^* information between the frequency band of .04 to .1 Hz. These results are summarized in Figure 25.

In constructing $t^*(f)$ models for Eurasia, we are using the shield curve at the higher frequency band as a basis of reference in order to estimate the Q structure under the tectonic regions of Eurasia. In Figure 25 we show our $t^*(f)$ curve for the Eurasian shield with some of the measurements superposed for paths also involving the tectonically active parts of Eurasia. The new data include some of the direct t^* estimates for the WWSSN stations located in "tectonic" areas. Since these were derived from Kazakh explosion data the associated path is a shield-tectonic one. In order to estimate what the appropriate t^* for a tectonic-tectonic path would be we subtracted the shield contribution (estimated at 0.07 sec) from these values and multiplied the result by two. These values are plotted in the figure. The values from PP/P ratios are directly applicable without adjustments.

The results obtained in our previous studies of the shield regions of Eurasia are plotted together with the new data for the "tectonic" regions. The latter seems to indicate uniformly higher t_p^* values than for the shield. The models are frequency dependent and are quasi-parallel relative to each other. The total picture that emerges from all this is that the *relative* attenuation changes are similar over the whole frequency band studied from .02 to 10 Hz.

EURASIAN SS/S AMPLITUDES

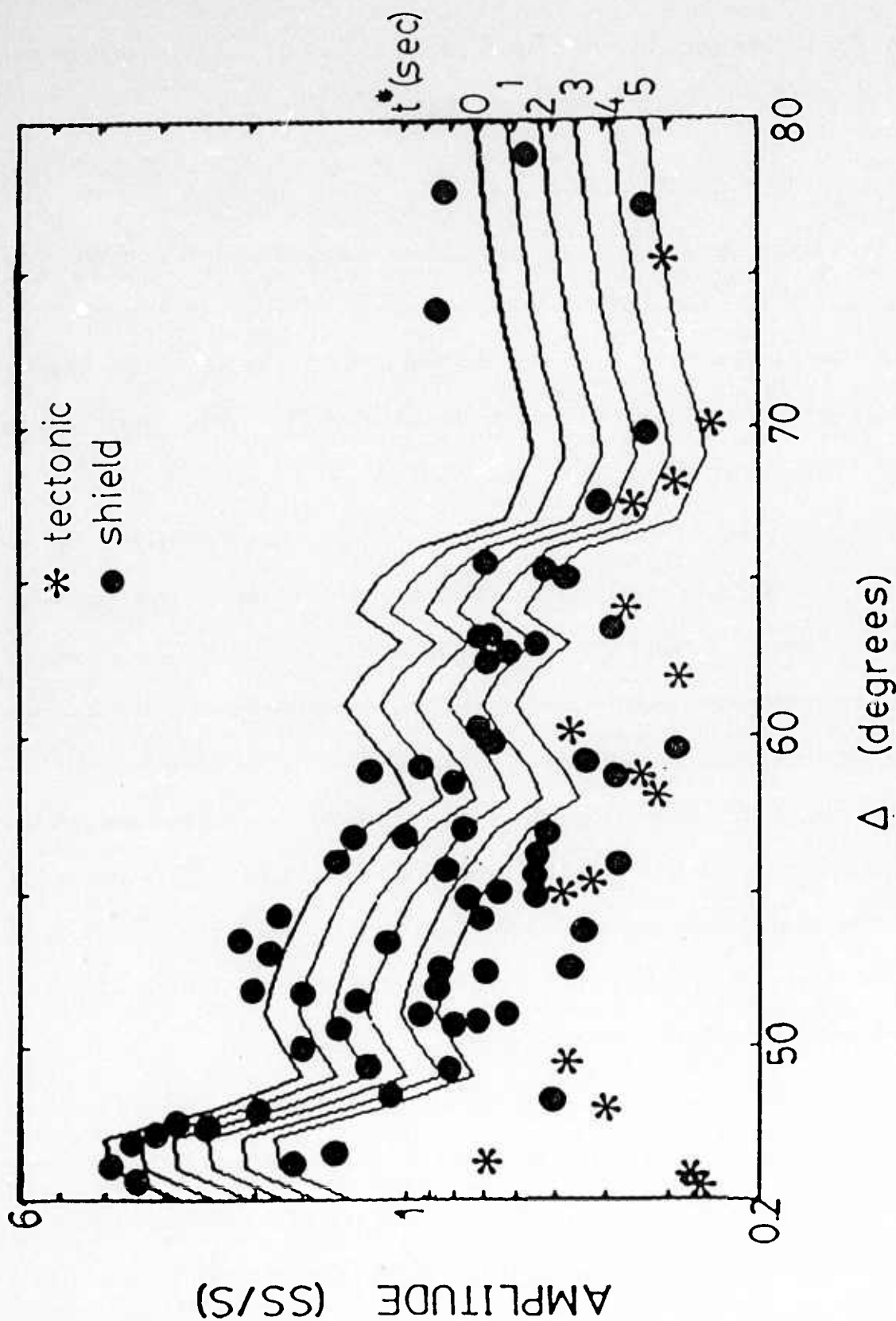


Figure 24. Plot of SS/S amplitude ratios versus epicentral distance. The amplitude ratios have been corrected for radiation pattern. The theoretical predictions of the SNA model (Grand and Helmberger, 1984) for a number of t^* values are also shown for comparison.

EURASIA

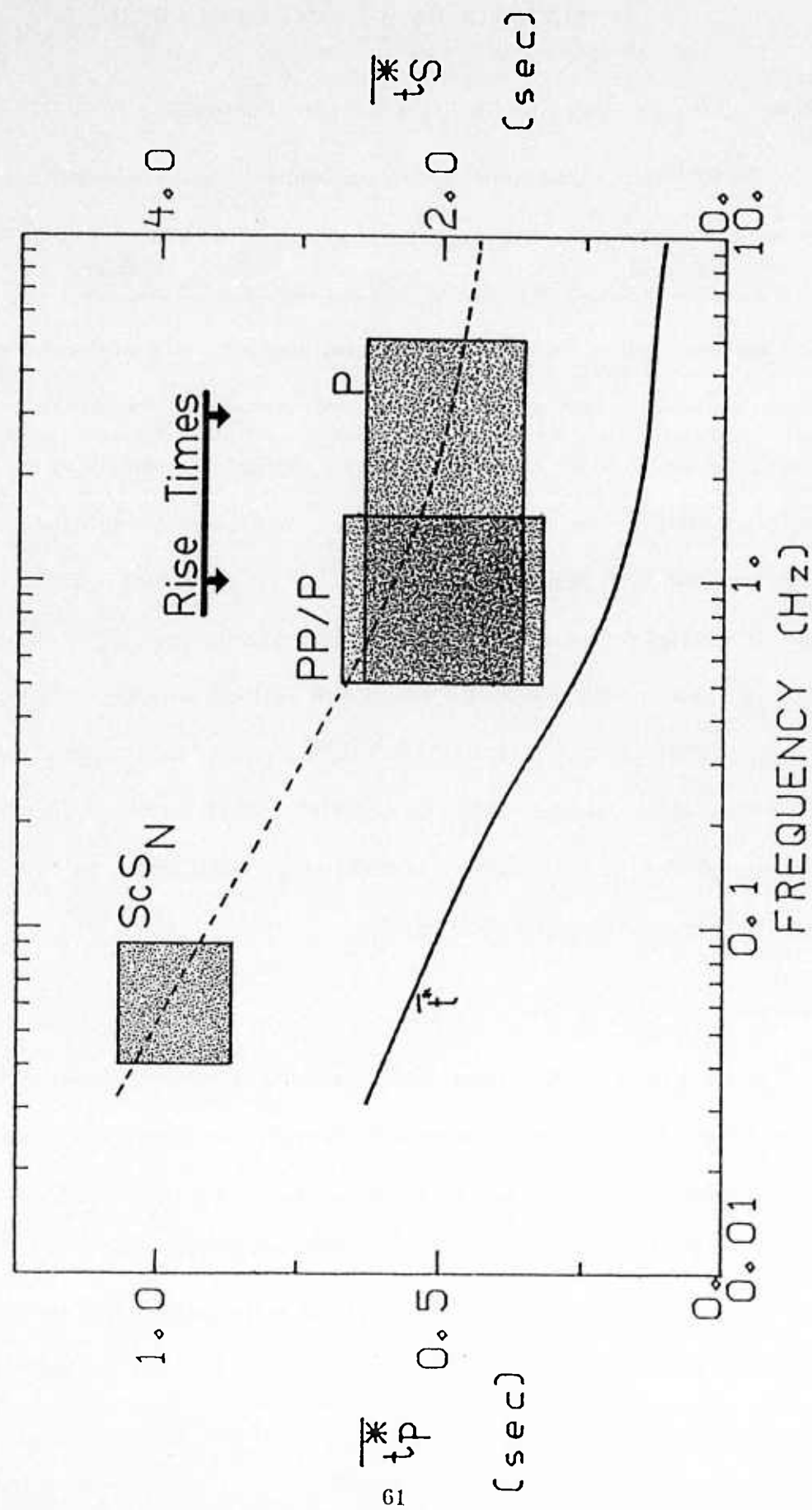


Figure 25. Summary of the results for tectonic Eurasia compared to the predictions of our Q model for the Eurasia shield (solid curves).

ANALYSES OF DATA FROM NORTH AMERICA

Review of Previous Data Analyses in the Short and Intermediate Period Bands

The attenuation-related magnitude bias has been well studied in North America and there is thus hardly any need to redo any of the thorough analyses already in print. The topic has been discussed in a number of papers (Lay and Helmberger, 1981; Der *et al.*, 1980, 1982a; Der and Lees, 1985). The spectral contents and amplitudes of short period P and S waves exhibit some well studied regional patterns (Booth *et al.*, 1974; Lay and Helmberger, 1981; Der *et al.*, 1982a). The P wave amplitudes have amplitude variations of up to factors of 2-3 and short period S waves by factors of up to 8 with corresponding large variations in the dominant periods of these waves for common events. It was pointed out by Der and Lees (1985) that the observed patterns of amplitude and period variations across North America cannot be explained by the models in which the regional $t^*(f)$ variations are solely due to the "corner frequency shift", that is, by the shift of the high frequency cutoff frequency of a single absorption band model of the type described by Minster (1978). Instead, the data require $t^*(f)$ models that are quasi-parallel. In our subsequent syntheses of acceptable models for North America we shall reconform this quasi-parallelism of $t^*(f)$.

Summary of Results for North America

Given the fact that the relative mantle attenuation is fairly well known between the tectonic and shield areas of North America in the short and intermediate period bands, there is no point in redoing much of this work for this region (Solomon and Toksoz, 1970; Lay and Helmberger, 1981; Solomon, 1972; Lee and Solomon, 1975, 1979; Der *et al.*, 1982a; Shore, 1983), the most important problem to solve in this region is for the value of t^* at low frequencies. These can be obtained from the available ScS data. High frequency t^* information will be

acquired from the numerous published data. Attenuation estimates for the shield regions of North America were obtained from PP/P spectral ratios by Shore (1983). By studying 15 events in Eurasia and recorded at N. American stations, Shore (1983) computed spectral ratios of PP/P to arrive at an average t_p^* of approximately 0.29 sec for shield N. America. In addition, Der *et al.* (1982a) have also obtained $\overline{t_p^*}$ in the range of 0.1 to 0.2 sec for shield paths and $\overline{t_p^*}$ differential between shield-to-shield and shield-to-tectonic paths to be of the order of 0.2 s. We shall adopt these results for the short period band to integrate with those obtained for the low frequencies using ScS phases to construct frequencies dependent t^* curves for N. America.

By combining t^* values covering the short and long period bands, we construct $t^*(f)$ curves for tectonic and shield N. America and are plotted together in Figure 26. In this figure we show our best estimates of the $t^*(f)$ curves that fit our short and long period analyses. In compiling this figure we have doubled the SWUS-shield t^* differentials to obtain the appropriate tectonic-tectonic path t^* estimates. While the data for the southwestern US show a clear frequency dependence of t^* , frequency dependence cannot be shown for the Canadian shield from these data. These curves indicate the same quasi-parallel pattern as that observed for Eurasia, with the tectonic region being higher than the shield region. The value of t^* decreases as the frequencies increases in all cases. It is obvious that the two curves are well separated and any systematic bias will not affect their relative shapes.

NORTH AMERICA

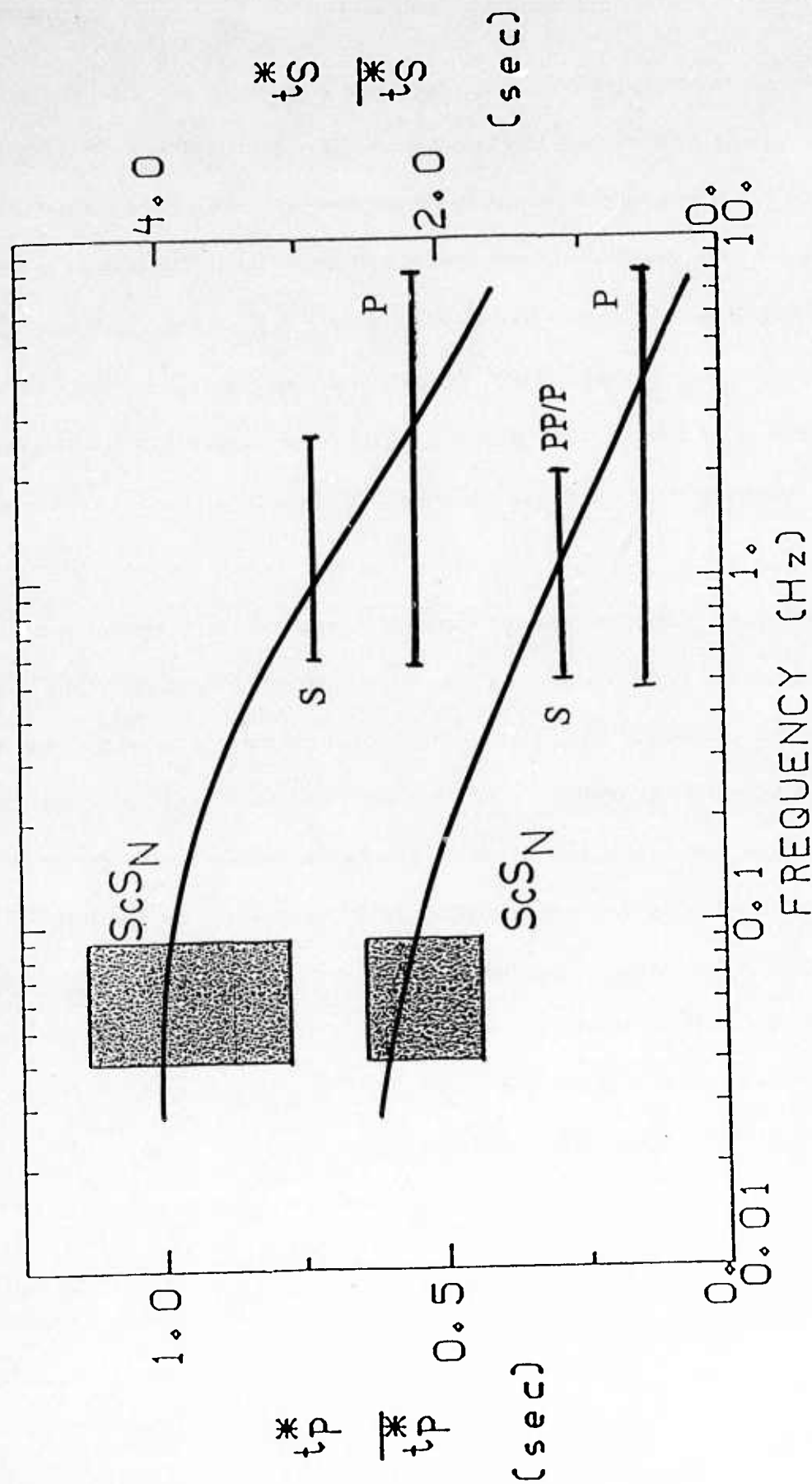


Figure 26. Summary of our results for North America as related to previous estimates of t^* from P and S wave spectral and waveform analyses in the short and intermediate period bands. The boxes and bars correspond to data for the Central American-Southwestern US path (top) and the Aleutian-Northeastern US path (bottom). The lower curve is estimated t^* model for the shield paths while the upper one is for "tectonic" N. America.

ANALYSES OF DATA FROM EASTERN PACIFIC

Review of Previous Data Analyses in the Short and Intermediate Period Bands

Large sets of P wave data have been analyzed from French nuclear explosions from Polynesia by several workers (Der *et al.*, 1985b; Bache *et al.*, 1985). The consensus is that P waves observed at teleseismic distances from this region have spectral characteristics similar to those from NTS thus indicating a low Q under the Tuamotu Archipelago. The t^* contribution to a teleseismic P wave by the upper mantle under Tuamotu was estimated as 0.35 sec by Der *et al.*, (1985b) and by McLaughlin *et al.*, (1986) to be around 0.43 sec.

PP/PKP Spectral Ratios

To study the short period attenuation for the S. Pacific, we employ the similar procedure as used in an earlier section. Shapes of spectral ratio of PP-PKP pairs are computed to obtain $\overline{t_p^*}$ across the S. Pacific Ocean. The PP phase would bounce off the surface and sample the upper mantle near the bounce point with two passages whereas PKP phase would diffract off the core and contains no reflection from the surface of the Earth. The ratio between PP-PKP would provide an estimate of upper mantle attenuation since the Q in the lower mantle and core is high compared to that of the upper mantle. These phases are bandpass filtered in narrow frequency bands between 0.2 to 6 Hz. The bandpass filters allow rapid identification of the phases with estimates of the noise level. Amplitudes are measured in the time domain for each phase and PP/PKP amplitude ratios are computed for each frequency band.

Bi-directional trans-S. Pacific paths are collected for deep focus Fiji-Tonga earthquakes recorded at S. American stations and for deep focus S. American earthquakes recorded at southwestern Pacific stations. We have examined mainly deep focus events associated with the subducting slabs in S. America and Tonga-Fiji regions recorded using digital DWWSSN and

SRO stations. In most of these events, the PP are either highly attenuated or are contaminated by other arrivals.

Short period vertical component recordings from twelve deep focus earthquakes are assembled to study t_p^* for the S. Pacific Ocean using PP/PKP amplitude ratio method. The locations of these events and stations are indicated in Figure 27. The event parameters are listed in Table 11. The surface bounce points for the PP phases are also plotted in the same figure. All of the PP phases have surface reflection bounce points within the S. Pacific and are well away from the axis of the E. Pacific Rise. Due to the long epicentral distance across the Pacific, only multiple PP and PKP phases are observable as all P phases are diffracted. Since the earthquakes used are deep, the ratio of PP and PKP approximately represents the anelasticity properties of the upper mantle in canceling out the source effects.

A similar set of band-pass filters are applied to our data set here and the filtered plots are shown in Appendix B (Figures B9-B20). The arrival times for both phases are identified using the J-B travel time table. The frequency band of PKP ranges from 0.3 to 3 Hz while PP phase generally emerges at a lower frequency ranging from 0.1 to 2.5 Hz. This form of display allows one to measure the amplitudes within good signal to noise level.

The amplitude of these phases is measured from a frequency band of 0.4 to 6 Hz. Where there is too low a signal in either phase, no measurements are attempted to constraint the curve giving rise to bias in constructing the curve. Amplitude ratios for each event are plotted in linear-log scale and an example is shown in Figure 28. A least square fit to the data points gives a best fitting curve through the PP/PKP amplitude ratio data. By averaging the $\overline{t_{pp}^*}$ for all events, we obtained a $\overline{t_{pp}^*}$ of 0.84 ± 0.30 sec for the S. Pacific in close agreement to the value obtained by Der *et al.*, (1985b) and McLaughlin *et al.*, (1986).

SE. Pacific PP/PKP bounce points

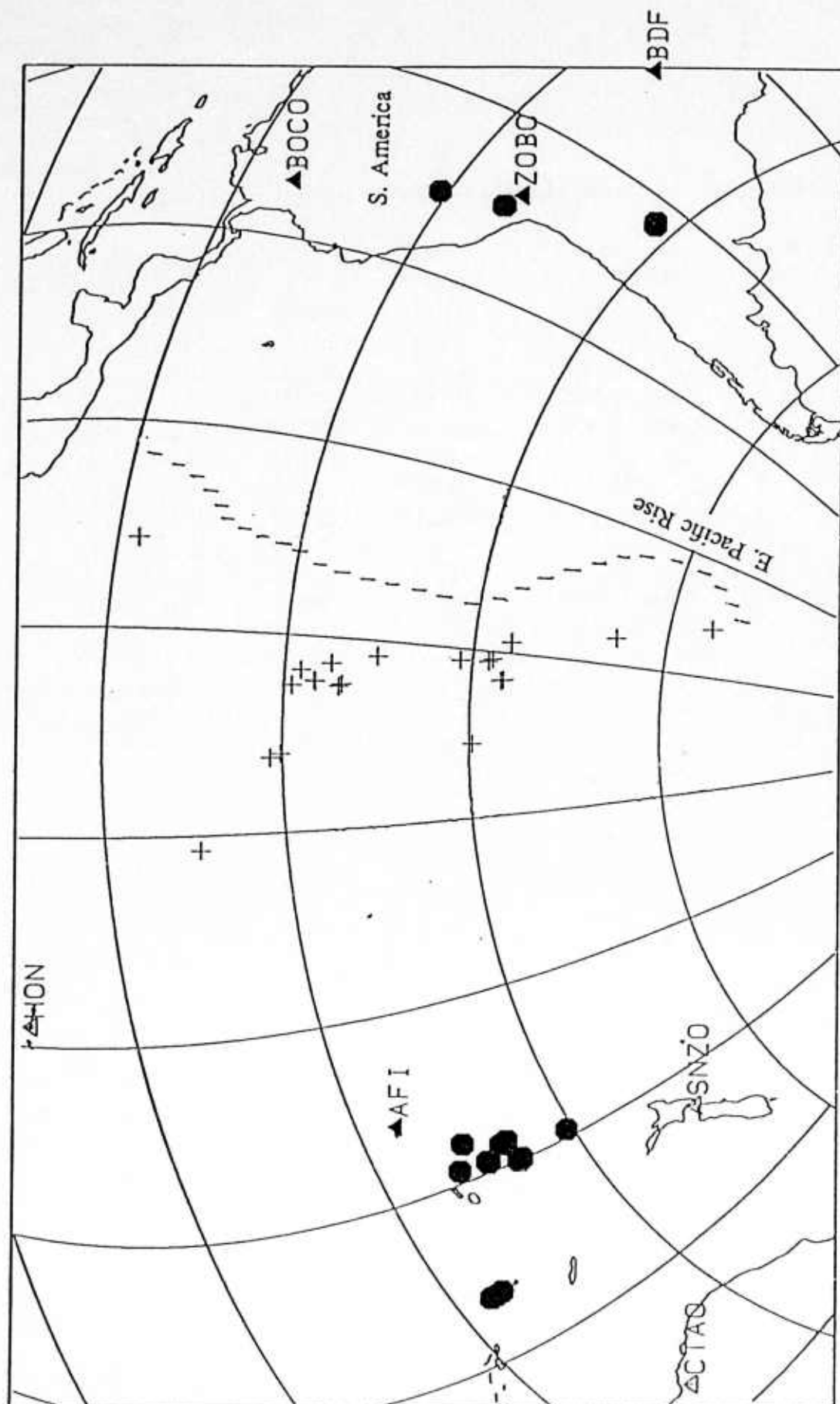


Figure 27. Map for E. Pacific showing locations of events used for the PP/PKP amplitude ratio study. The bounce points where the PP are sampling are indicated as + 's. They normally do not fall too close to the E. Pacific Rise.

Table 11

Parameters of earthquakes used in PP/PKP study of tectonic Pacific

Event #	date	latitude	longitude	depth	m_b
1	Nov 25, 1976	-19.50	-177.70	424	6.0
2	Sep 6, 1978	-13.35	+167.13	214	5.9
3	Sep 23, 1978	-13.94	+167.18	216	6.1
4	Nov 8, 1979	-32.26	+179.33	447	5.7
5	Jan 4, 1982	-23.17	-177.31	195	6.0
6	Sep 16, 1983	-24.03	-179.80	510	6.0
7	Nov 29, 1983	-19.50	-177.78	525	5.7
8	Apr 22, 1984	-21.87	-179.38	593	5.7
9	May 30, 1984	-04.84	+151.58	174	6.2
10	Jun 15, 1984	-15.82	-174.83	247	6.1
11	Nov 17, 1984	-18.79	-178.03	451	6.1
12	Oct 6, 1985	-18.96	169.43	273	5.7

PP/PKP RATIO

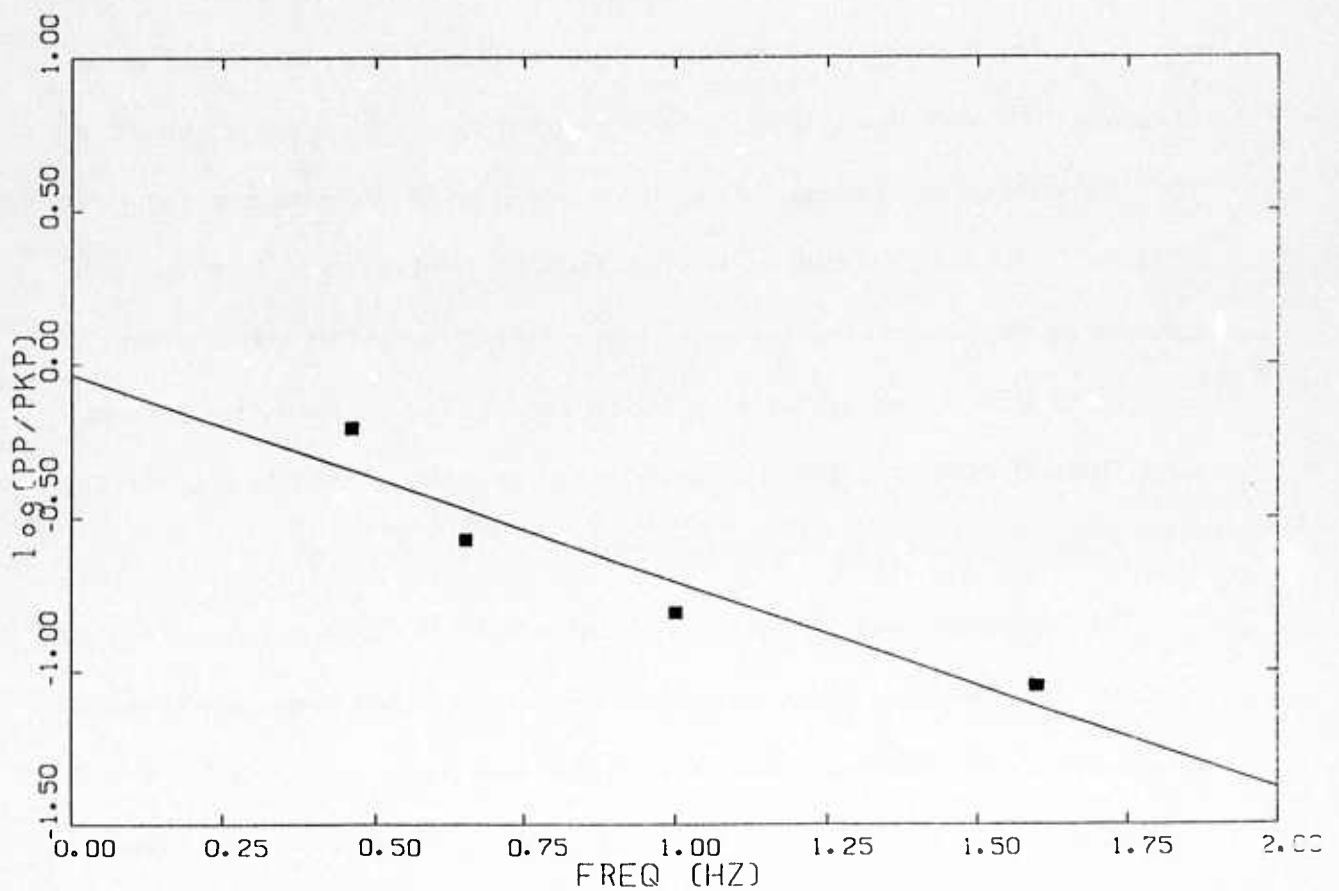


Figure 28. An example of a least squares fit to the PP/PKP amplitude ratios for a path across the E. Pacific. The ratios are plotted in $\log(\text{PP/PKP})$ against frequencies. The best fitting least squares line indicates a t_p^* of 0.67 sec.

SSS/SS Amplitude Ratios

In order to study the variations of long period t^* in Eastern Pacific, we have employed an amplitude ratio method between SS and SSS phases. The same approach has been used in other regions as discussed in our previous studies (Der *et al.*, 1985a). The SS phase has one surface bounce point whereas the SSS phase has two surface bounces along the path. The amplitude ratio between the two phases indicates the energy loss caused by a double passage of the S wave through the upper mantle anelastic structure.

We have examined deep focus events in Fiji-Tonga and S. America recorded at S. American and Western Pacific stations respectively. Both the SS and SSS are very difficult to identify due to the relatively low Q in the tectonic Pacific and contaminations due to other arrivals. The locations of the earthquake source and station used in the SS-SSS measurement are shown in Figure 29 and the parameters are listed in Table 12. The location of the bounce points shown in the figure indicate that they do not sample the East Pacific Rise spreading center but are scattered among various age regions within the Pacific. Since our interest is to estimate t^* for the broad E. Pacific, at this point we do not attempt to resolve the variation of Q within the different age regions due to the scatter of our data.

The amplitude ratios of the SSS/SS are plotted in Figure 30 fitted with various theoretical t_S^* curves. These theoretical curves are computed assuming an oceanic model and a t_S^* of 6 sec for the SS path. The δt^* between SS and SSS varies from 1 to 7 sec. From a rms fit to the data, we arrive at an estimate of 6 sec for t_S^* of shear waves across the E. Pacific. The values obtained here provide a constraint to the long period data in constructing a t^* curve for the Pacific.

PACIFIC

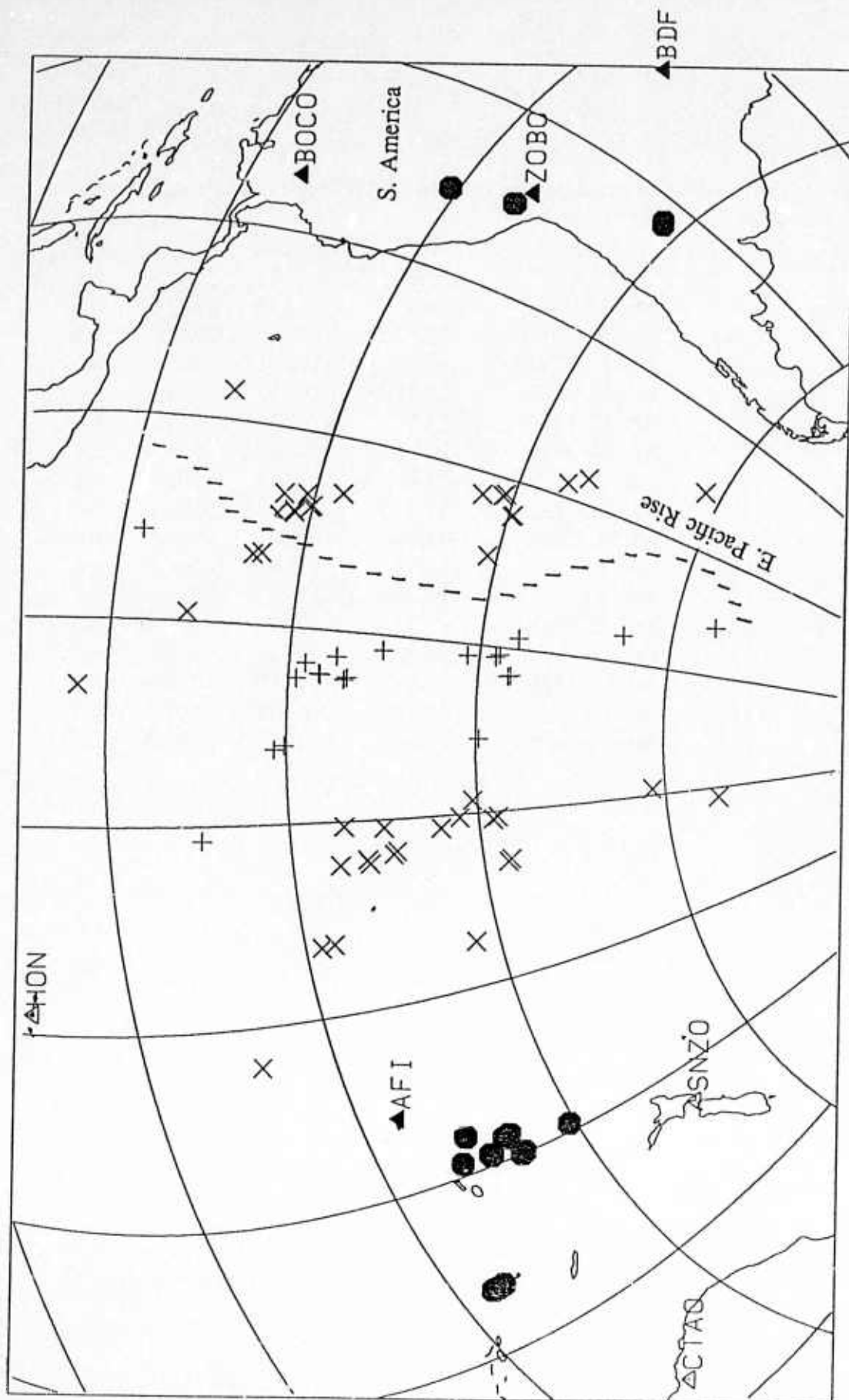


Figure 29. Map for E. Pacific showing locations of events used for the SSS/SS amplitude ratio study. The bounce points for the SSS are in X's while those for SS are +'s.

Table 12**Parameters of earthquakes used in SSS/SS study of tectonic Pacific**

Event #	date	latitude	longitude	depth	m_b
1	Oct 22, 1977	-27.96	-62.82	592.3	6.0
2	May 13, 1978	-14.60	+167.31	181.7	6.5
3	Jul 17, 1978	-14.95	-175.81	305.4	5.9
4	Jul 17, 1978	-14.95	-175.81	305.4	5.9
5	Sep 6, 1978	-13.35	+167.13	214.8	5.9
6	Sep 23, 1978	-13.94	+167.18	216.7	6.1
7	Apr 24, 1979	-20.82	-178.67	596.1	5.9
8	Aug 5, 1979	-22.86	-177.47	203.7	6.1
9	Apr 13, 1980	-23.53	-177.27	102.1	6.6
10	Jul 20, 1980	-17.88	-178.61	587.8	6.0
11	Nov 30, 1980	-19.43	-175.85	202.0	6.0
12	Nov 30, 1980	-19.43	-175.85	202.0	6.0
13	Sep 28, 1981	-29.33	-179.04	323.0	6.0
14	Nov 25, 1981	-20.94	-178.86	614.0	5.9
15	Sep 16, 1983	-24.03	-179.80	510.0	6.0
16	Dec 21, 1983	-28.19	-63.17	602.0	6.2
17	May 1, 1985	-09.20	-71.23	600.0	6.0

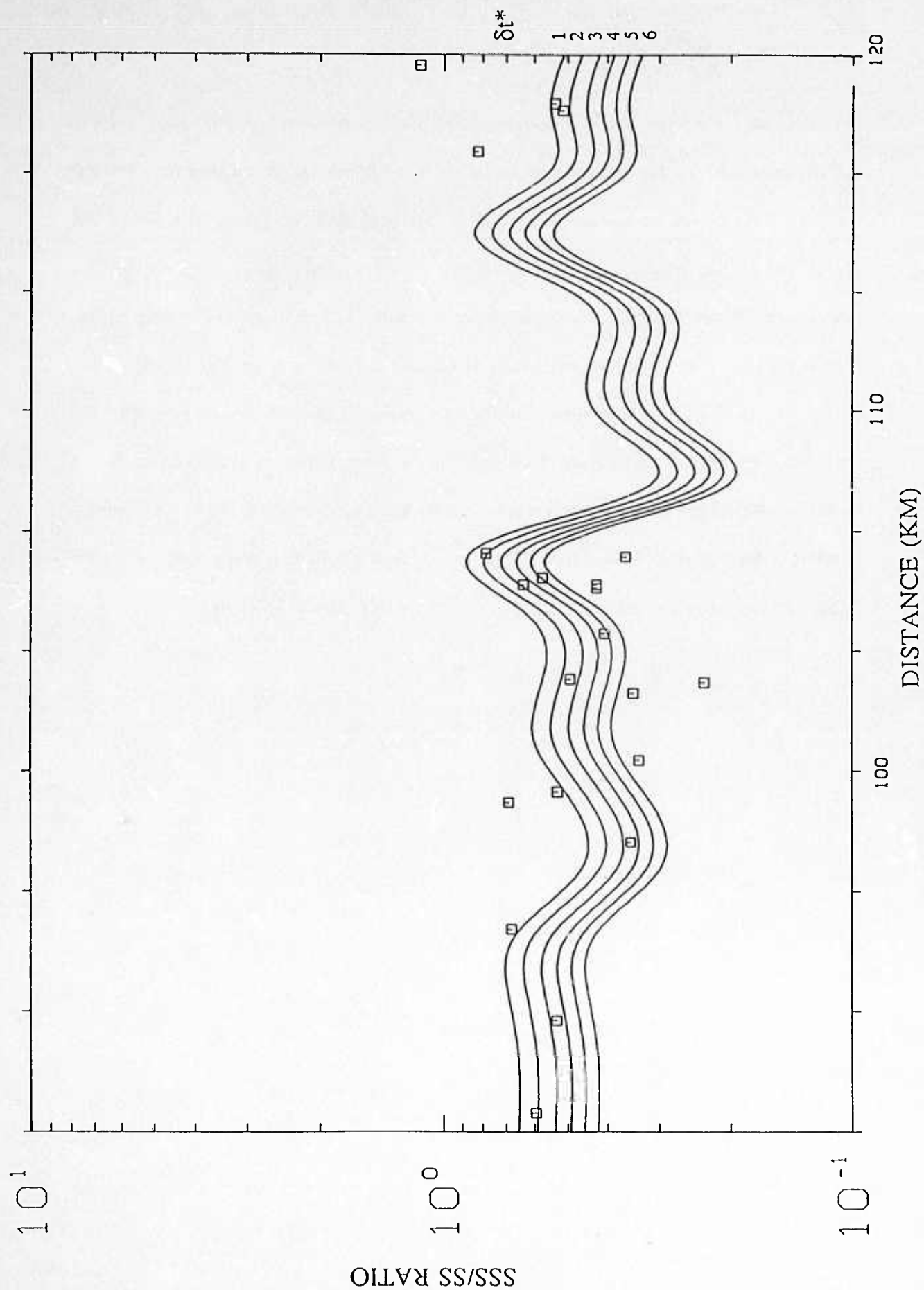


Figure 30. Plot of SSS/SS amplitude ratios versus distance. The theoretical fits to these data are obtained for a J-B oceanic model. A rms fit to the data points indicates an upper bound of t_s^* of 6 sec.

Final Model for E. Pacific

In general, the broad Pacific Ocean is characterized as tectonic, therefore only one curve will be constructed for the region. t^* values for the high frequencies are obtained from PP/PPK spectral ratios whereas the low frequency information is obtained from multiply reflected ScS phases and SS/SSS amplitude ratios. Combining the three sets of data, a broad-band $t^*(f)$ model is constructed for the E. Pacific as shown in Figure 31. This model is frequency dependent with higher t^* at the lower frequencies of 0.02 Hz and decreases towards the higher frequencies of up to 2 Hz, similar in form to the ones obtained earlier for the other regions. The long period estimates from ScS and SS/SSS are not in exact agreement to each other. This is most likely due to the scatter of bounce points within the E. Pacific and the different frequency contents of these phases. In constructing the curves, more emphasis is being put on using the ScS_N data since they are generally of higher quality than the SS and SSS data.

E TRANS-PACIFIC

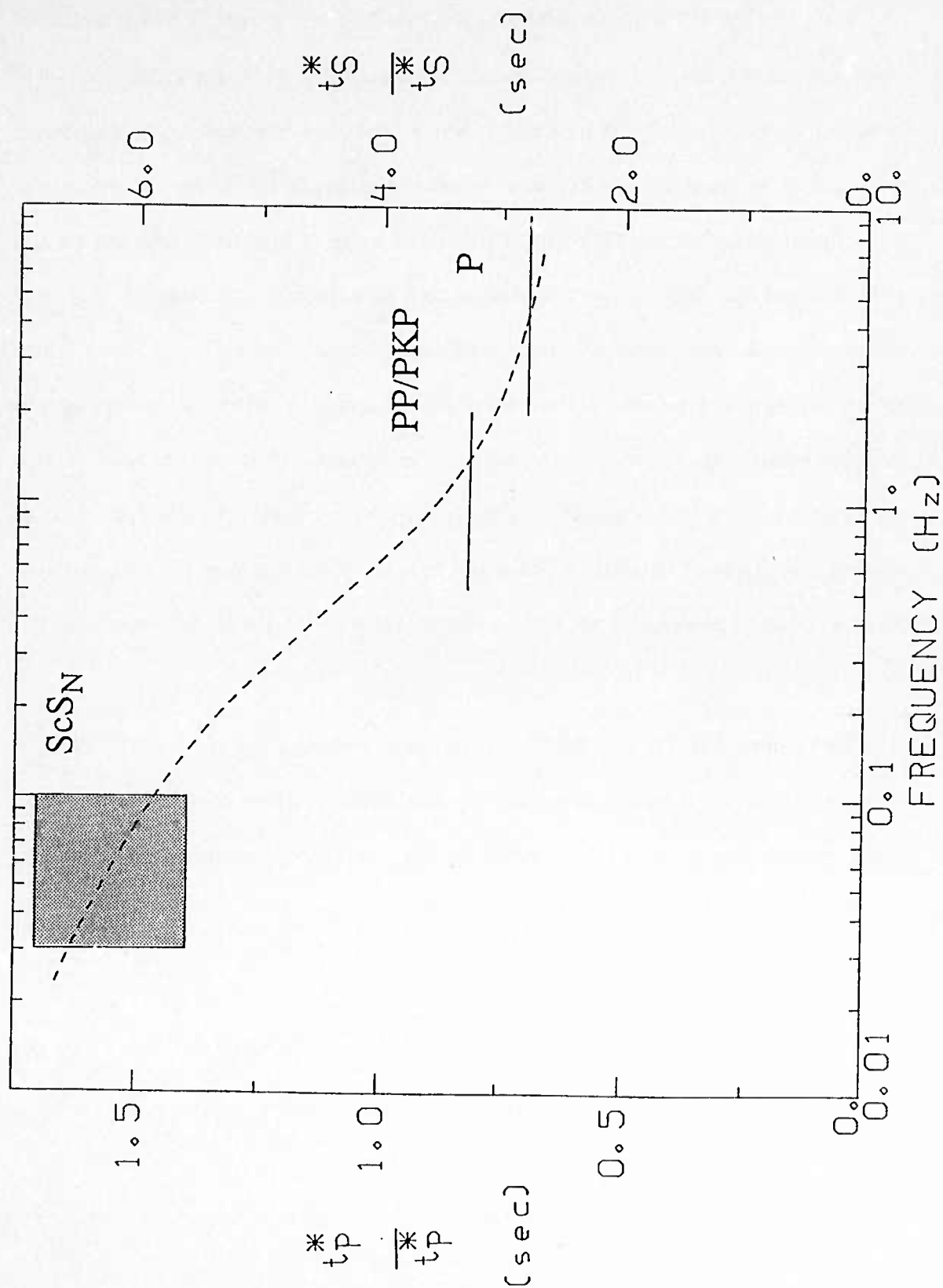


Figure 31. Summary of our results for E. Pacific as related to estimates of t^* obtained from amplitude waveform matching, spectral ratio study, and amplitude ratio method.

DISCUSSION OF THE BROAD-BAND RESULTS

Reviewing the ScS results together with the data presented for the individual regions of study earlier in this report, the pattern is evident: wherever the anelastic attenuation is shown to be high in the short period and intermediate period bands, it is also high in the long period band spanned by multiple S and ScS data. In areas where the t_p^* is low, the ScS phases have also a lower attenuation, the PP/P have a higher percentage of high frequencies and the rise times of P and S are also shorter. In areas of high attenuation just the reverse is true. The variations in wave characteristics in our "shield" and "tectonic" regions are similar in nature, but not as severe, to those observed in areas of anomalously high and low attenuation, such as spreading back-arc basins and spreading ridge axis respectively. This way our results fit into the framework of the picture provided by the "new global tectonics". In a way this is to be expected, since regional variations of Q are thought to be caused in a large part by lateral variations of temperature thus causing variations of Q which are of similar sign over wide frequency bands.

We summarize in Table 13 the t^* or $\overline{t^*}$ estimates, whichever one is the most applicable, for the various types of measurements and frequency bands in all the regions studied. These results give the raw material for inversions for $Q(f,r)$ and the definition of the "best" $t^*(f)$ models.

Table 13
Comparison of long period ScS and short period P
attenuation results

Region	t_{ScS}^* (.02-.1 Hz)	t_P^* (.5-10 Hz)
Tectonic Eurasia	3.0-3.9	0.5
Shield Eurasia	2.5	0.15-0.2
Tectonic N. America	4.0-4.5	0.4
Shield N. America	1.8-2.5	0.15
SE. tran-Pacific	5.5-7.0	0.8
W. Pacific	4.0-5.0	
Shield S. America	2.0-3.0	

POSSIBLE $t^*(f)$ and $Q(f,r)$ MODELS AND YIELD ESTIMATION

We are now ready to outline the $t^*(f)$ curves most appropriate to each of the regions studied. In Figure 32 we show these curves that have been obtained based on the data in Table 13. These curves apply to teleseismic paths confined entirely to the respective structures. In arriving at a gross estimates of $t^*(f)$, we do not attempt to resolve the lateral variation of Q within each region, for example, the different age regions within the E. Pacific. Curves for mixed paths can be constructed by linearly combining pairs of curves. The results do not favor the types of convergent or divergent models of $t^*(f)$ that could confound the spectral method in estimating *relative* attenuation corrections derived from spectra (Hadley and Mellman, 1983; Lay and Helmberger, 1981), rather they favor quasi-parallelism (Der and Lees, 1985). It is quite possible that more subtle, second order errors in attenuation may occur by weak convergence or divergence of such frequency dependent t^* curves. We also neglect here any distance dependence of t^* , yet another second order effect.

Our data do not allow us to make a strict inversion for $Q(f,r)$, since the depth dependence is not well constrained. Nevertheless, assuming that the lateral Q variations in the Earth is the most pronounced within a 200-300 km thick layer in the upper mantle, we can confidently state that Q may vary by about a factor of 5-10 laterally over wide frequency range of .01 to .1 Hz. Such a strong lateral variation in Q indicates that it is highly unlikely that $t^*(f)$ models converge at low frequencies.

With regards to yield estimation, the postulated types of $t^*(f)$ allow one to predict *relative* attenuation corrections for various source and receiver regions derived from shapes of P and S wave spectra as done before (Der *et al.*, 1985b). Mixed path attenuation may also be corrected by using a linear combination of the $t^*(f)$ values for different regions. On the other hand, since our data require that the Q be frequency dependent in all the regions studied the absolute

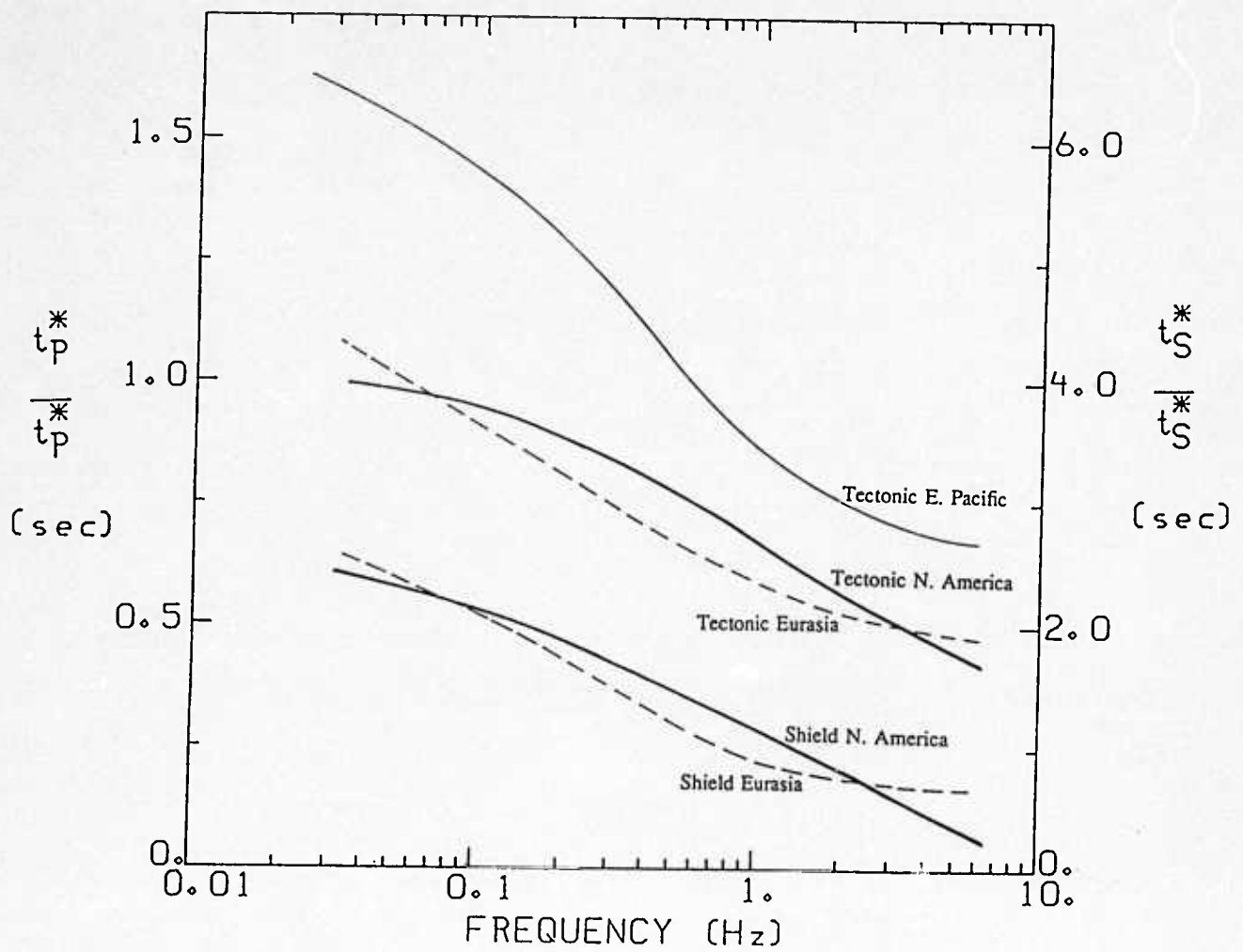


Figure 32. A summary of all models shown in this study for different tectonic and shield regions.

signal (P and S wave) amplitudes will be altered by the frequency-dependent Q models relative to those predicted by constant Q derived from short period data. This removes at least some of the apparent (but not real) discrepancies between absolute amplitudes and the so called "spectral Q" claimed (Burdick *et al.*, 1984).

CONCLUSIONS

Broad-band models of $t^*(f)$ are presented for different tectonic and shield regions. These regions include tectonic N. America, Eurasia, E. Pacific, W. Pacific and S. America and shield N. America, Eurasia, and S. America. These models are discussed in conjunction with each other in terms of the lateral variation and frequency dependence of Q in various parts of the world. The main question, from the point of view of practical consequences of this study in estimating attenuation is the approximate form of $t^*(f)$ for teleseismic paths crossing the mantle under various regions.

In Eurasia we are using the shield curve obtained previously as a basis of reference in order to estimate the Q structure under the tectonic regions of Eurasia. We have also presented some direct t^* estimates for the WWSSN stations located in "tectonic" areas. All of the observations for the tectonic areas are higher than the corresponding measurements under shields. The total picture that emerges from all this is that the relative attenuation changes among the two regions are similar in sign over the whole frequency band studied from .02 to 10 Hz.

There is no question that in the short period band at frequencies above 2 Hz, Q is quite high under the shield regions of Eurasia (Der and McElfresh, 1977; Der *et al.*, 1982b) with values not less than 500 for Q_p . The argument of Der and Lees (1985) uses the assumption of $t_s^* = 4 t_p^*$. Their conclusion that the two $t^*(f)$ curves do not converge at low frequencies would even be strengthened if we assume a lower ratio between the t^* appropriate to S waves and P waves (Taylor *et al.*, 1985). We do not believe, however, that the ratio is considerably less than 4.

A considerable amount of work has already been done on studying attenuation under continental North America. In this study we compile the results of past work and supplement them with additional long period data and address the issue in a broad-band context. The most

controversial question concerns the changes in Q applicable to long period band data. Solomon and Toksoz (1970) and Lee and Solomon (1975,1979) found large regional variations in Q in the long period band, while Lay and Helmberger (1981) expressed doubts about any such variations. In the short and intermediate period bands Taylor *et al.* (1985) and Der and Lees (1985) have studied P and S wave attenuation and found that significant Q differentials existed in the upper mantle among various regions of the United States that were detectable throughout the total range of the frequency bands utilized in these studies.

Der and Lees (1985) investigated some $t^*(f)$ curves that were proposed for purely shield and shield-to-tectonic paths involving the mantle of North America. Using spectral and waveform data, their study showed that only pairs of curves that are quasi-parallel (QP) can explain the results of both kinds of analyses. Several models that converged towards low frequencies can be rejected based on this kind of data. It was also concluded that using the short period data alone, it is not possible to specify the exact forms of frequency dependence since most pairs of quasi-parallel $t^*(f)$ curves can explain the kind of short period P and S data presented by Der and Lees (1985).

The E. Pacific attenuation model has the highest t^* among all regions. The curve also assumes the same frequency dependent pattern as the other regions being quasi-parallel to them. The low frequency t^* for the E. Pacific is up to a factor of three larger than that for the shield regions, strongly indicating that t^* does not converge towards the low frequencies. The $t^*(f)$ curve being higher than those for tectonic N. America and Eurasia suggests that regional variation in attenuation among tectonic regions are also inevitable. We have imposed constraints on our work by studying other regions and wherever possible reprocess data that were used in other published studies. These regions include tectonic and shield S. America, W. and NW. Pacific. Results from our study are similar to others, and being higher in some cases.

Lateral variations in low frequency t_{scs}^* are observed in these additional regions in support of our earlier conclusion.

Since our data do not have the resolution to warrant a full inversion on the $t^*(f)$ models, to obtain $Q(r,f)$ we can only say that the finding of Solomon and Toksoz (1970) that large Q differentials exist in the upper mantle at low frequencies across North America seems to be supported by our data thus far. The same is true for all other regions we have studied. Since the ratios of t^* are less than the ratios in Q in the upper mantle in order to cause the observed amplitude decay and spectral differences (in proportion to the travel times through the total mantle and the upper mantle).

In addition, in all the regions we have studied, the t^* estimates tend to rise towards lower frequencies supporting the idea of frequency dependence of Q (Lundquist and Cormier, 1978; Sipkin and Jordan, 1979; Anderson and Given, 1982). Invariably in the short period band, more high frequency energy is seen than that compatible with the Q estimates from long period data. With regards to yield estimation these results are important since they diminish the likelihood of the kinds of non-parallel $t^*(f)$ models that would make impossible estimation of magnitude bias from spectral data.

REFERENCES

- Anderson, D.L. and J.W. Given (1982). Absorption band Q model for the earth, *J. Geophys. Res.*, 87, 3893-3904.
- Bache, T.C., P.D. Marshall, and L.B. Bache (1985). Q for teleseismic P waves from Central Asia, *J. Geophys. Res.*, 90, 3575-3587.
- Booth, D.C, P.D. Marshall, and J. B. Young (1974). Long and short period P-wave amplitudes from earthquakes in the range 0°-114°, *Geophys. J. R. astr. Soc.*, 39, 523-537.
- Burdick, L., T. Wallace, and T. Lay (1984). Modeling near-field and teleseismic observations from the Amchitka Test Site, *J. Geophys. Res.*, 89, 4573-4388.
- Dahlman, O. and H. Israelson (1977). *Monitoring Underground Nuclear Explosions*, Elsevier Scientific Publishing Company, Amsterdam.
- Der, Z.A. (1986). Comments on the paper "Estimation of scalar moments from explosion-generated surface waves" by Jeffry L. Stevens *Bull. Seism. Soc. Am.* in press.
- Der, Z.A., and A.C. Lees (1985). Methodologies for estimating $t^*(f)$ from short period body waves and regional variations of $t^*(f)$ in the United States, *Geophys. J. R. astr. Soc.* in press.
- Der, Z.A., and T.W. McElfresh (1977). The relationship between anelastic attenuation and regional amplitude anomalies of short-period P waves in North America, *Bull. Seism. Soc. Am.*, 67, 1303-1317.
- Der, Z.A., A.C. Lees, L.M. Anderson, J.A. Burnetti, M.E. Marshall, T.W. McElfresh, and R. Wagner (1984). Frequency dependence of Q in the mantle underlying the shield areas of Eurasia, *AL-84-1*, Teledyne Geotech, Alexandria, VA.
- Der, Z.A., A.C. Lees, V.F. Cormier, L. Anderson, J. Burnetti and M. Marshall (1985b). Frequency dependence of Q in the mantle underlying the shield areas of Eurasia, Final Technical Report for the Air Force Office for Scientific Research. *AL-85-1*, Teledyne Geotech, Alexandria, VA.

- Der, Z.A., T.W. McElfresh, and A. O'Donnell (1982a). An investigation of the regional variations and frequency dependence of anelastic attenuation in the mantle under the United States in the 0.5-4 Hz band, *Geophys. J. R. Astr. Soc.*, 69, 67-100.
- Der, Z.A., T.W. McElfresh, T.W. and C.P. Mrazek (1979). Interpretation of short period P wave magnitude anomalies at selected LRSM stations. *Bull. Seism. Soc. Am.*, 69, 1149-1160.
- Der, Z.A., T.W. McElfresh, R. Wagner, and J. Burnetti (1985b). Spectral characteristics of P waves from nuclear explosions and yield estimation. *Bull. Seism. Soc. Am.*, 75, 379-390.
- Der, Z.A., W.D. Rivers, T.W. McElfresh, A. O'Donnell, P.J. Klouda, and M.E. Marshall (1982b). Worldwide variations in the attenuative properties of the upper mantle as determined from spectral studies of short-period body waves, *Phys. Earth Planet. Int.*, 30, 12-25.
- Der, Z.A., E. Smart, and A. Chaplin (1980). Short-period S-wave attenuation under the United States, *Bull. Seism. Soc. Am.*, 70, 101-125.
- Dziewonski, A. and D.L. Anderson (1981). Preliminary reference Earth model. *Phys. Earth. Planet. Int.*, 25, 297-356.
- Frankel, A. and R.W. Clayton (1984). A finite difference simulation of wave propagation in two-dimensional media, *Bull. Seism. Soc. Am.*, 74, 2167-2186.
- Grand, S.P. and D.V. Helmberger (1984). Upper mantle shear velocity structure beneath the Northwest Atlantic Ocean. *J. Geophys. Res.*, 89, 11465-11475.
- Hadley, D.M. and Mellman, G.R. (1983). Estimation of δm_b from δt^* measurements, (Topical Report), SGI-R-83-093, Sierra Geophysics, Redmond, WA.
- Jordan, T.H. (1975). The continental tectosphere. *Rev. Geophys. Space Phys.*, 13, 1-12.
- Jordan, T.H. and S.A. Sipkin (1977). Estimation of the attenuation operator for multiple ScS waves. *Geophys. Res. Letters*, 4, 167-170.
- Lay, T. and D.V. Helmberger (1981). Body wave amplitude patterns and upper mantle attenuation variations across North America, *Geophys. J. R. astr. Soc.*, 66, 691-726.

- Lee, W.B. and S.C. Solomon (1975). Inversion schemes for surface wave attenuation and Q in the crust and mantle, *Geophys. J. R. astr. Soc.*, 43, 47-71.
- Lee, W.B. and S.C. Solomon (1979). Simultaneous inversion of surface wave phase velocity and attenuation, Rayleigh and Love waves over continental and oceanic paths, *Bull. Seismol. Soc. Am.*, 69, 65-96.
- Lundquist, G.M., and V.F. Cormier (1980). Constraints on the absorption band model of Q, *J. Geophys. Res.*, 85, 5244-5265.
- McLaughlin, K.L. and L.M. Anderson (1986). Stochastic dispersion of short-period P wave due to scattering and multipathing, *Geophys. J. R. astr. Soc.*, in press.
- McLaughlin, K.L., L.M. Anderson, and Z.A. Der (1986). Investigation of scattering and attenuation of seismic waves using 2-dimensional finite difference calculations, in *Scattering of Waves in Random Media and Random Rough Surfaces*, edited by V. J. Varadan, and V. K. Varadan (in press).
- McLaughlin, K.L., R.H. Shumway, R.O. Ahner, M. Marshall, T. W. McElfresh, and R. Wagner (1986). Determination of Event Magnitudes with Correlated Data and Censoring: A Maximum Likelihood Approach, TGAL-86-01, USACDA Final Technical Report.
- Nakanishi, I. (1979). Attenuation of multiple ScS waves beneath the Japanese arc. *Phys. Earth Planet. Inter.*, 19, 337-347.
- Minster, J.B. (1978). Transient and impulse responses of a one-dimensional linearly attenuating medium. 2. A parametric study. *Geophys. J. R. astr. Soc.*, 52, 503-524.
- Minster, J.B. and D.L. Anderson (1980). Dislocation and nonelastic process in the mantle. *J. Geophys. Res.*, 85, 6347-6352.
- Richards, P.G. and W. Menke (1983). The apparent attenuation of a scattering medium, *Bull. Seism. Soc. Am.*, 73, 1005-1021.
- Sato, R. and A.F. Espinosa (1967). Dissipation in the Earth's mantle and rigidity and viscosity in the Earth's core determined from waves multiply reflected from the mantle-core boundary. *Bull. Seism. Soc. Am.*, 57, 829-856.

- Shore, M.J. (1983). Short period P-wave attenuation in the middle and lower mantle of the earth, *VSC-TR-83-7*, VELA Seismological Center, Alexandria, Virginia. 829-856.
- Sipkin, S.A., and T.H. Jordan (1979). Frequency dependence of Q_{Scs} , *Bull. Seismo. Soc. Am.*, 69, 1055-1079.
- Sipkin, S. and T.H. Jordan (1980). Regional variations of Q_{Scs} . *Bull. Seism. Soc. Am.*, 70, 1071-1102.
- Solomon, S.C. (1972). Seismic-wave attenuation and partial melting in the upper mantle of North America, *J. Geophys. Res.*, 77, 1483-1502.
- Solomon, S.C. and M.N. Toksoz (1970). Lateral variation of attenuation of P and S waves beneath the United States, *Bull. Seism. Soc. Am.*, 60, 819-838.
- Stevens, J.L. (1986). Estimation of scalar moments from explosion-generated surface waves. *Bull. Seism. Soc. Am.*, 76, 123-151.
- Stewart, R.C. (1984). Q and the rise and fall of a seismic pulse, *Geophys. J. R. Astr. Soc.*, 76, 793-805.
- Taylor, S.R., B.P. Bonner, and G. Zandt (1985). Attenuation and scattering of broadband P and S waves across North America, submitted to *J. Geophys. Res.*
- von Seggern, D.H., and R.R. Blandford (1972). Source time functions and spectra from underground nuclear explosions, *Geophys. J. R. Astr. Soc.*, 31, 83-97.
- Yoshida, M. and M. Tsujiura (1975). Spectrum and attenuation of multiply-reflected core phases. *J. Phys. Earth*, 23, 31-42.

(THIS PAGE INTENTIONALLY LEFT BLANK)

APPENDIX A

Time Domain Analyses of Multiple ScS Phases.

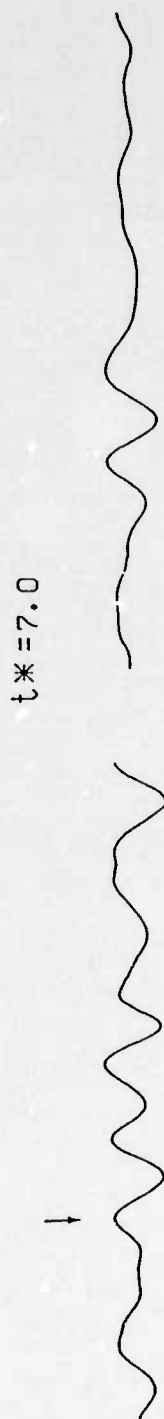
ZOB0

FIJ-76330 SH

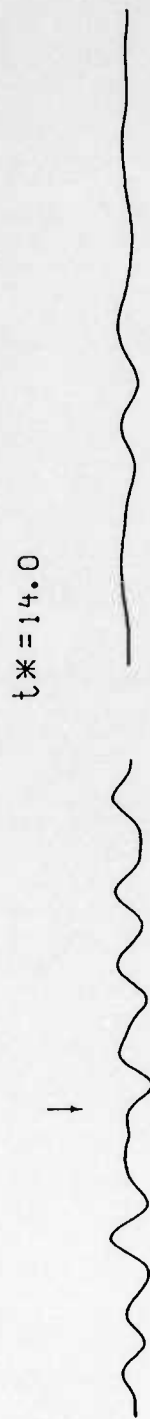
ScS2



ScS3



ScS4



ScS5

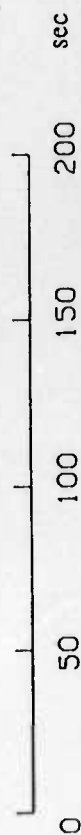
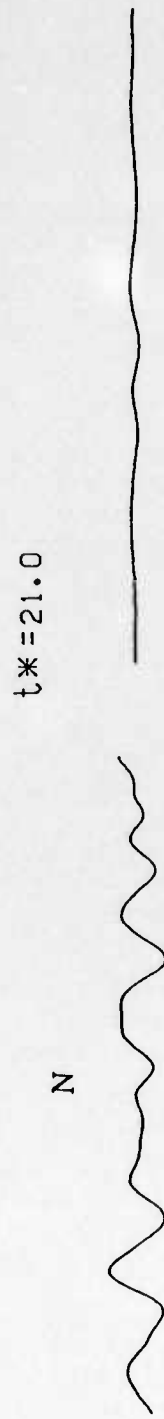


Figure A1. Observed ScS_N phases displayed on the left matched with the first observable ScS_N phase convolved with multiples of t^* shown on the right for Fiji-S. America path (event 1). The arrow indicates the arrival of the ScS_N phase and N's indicates that the ScS_N is in the noise level.

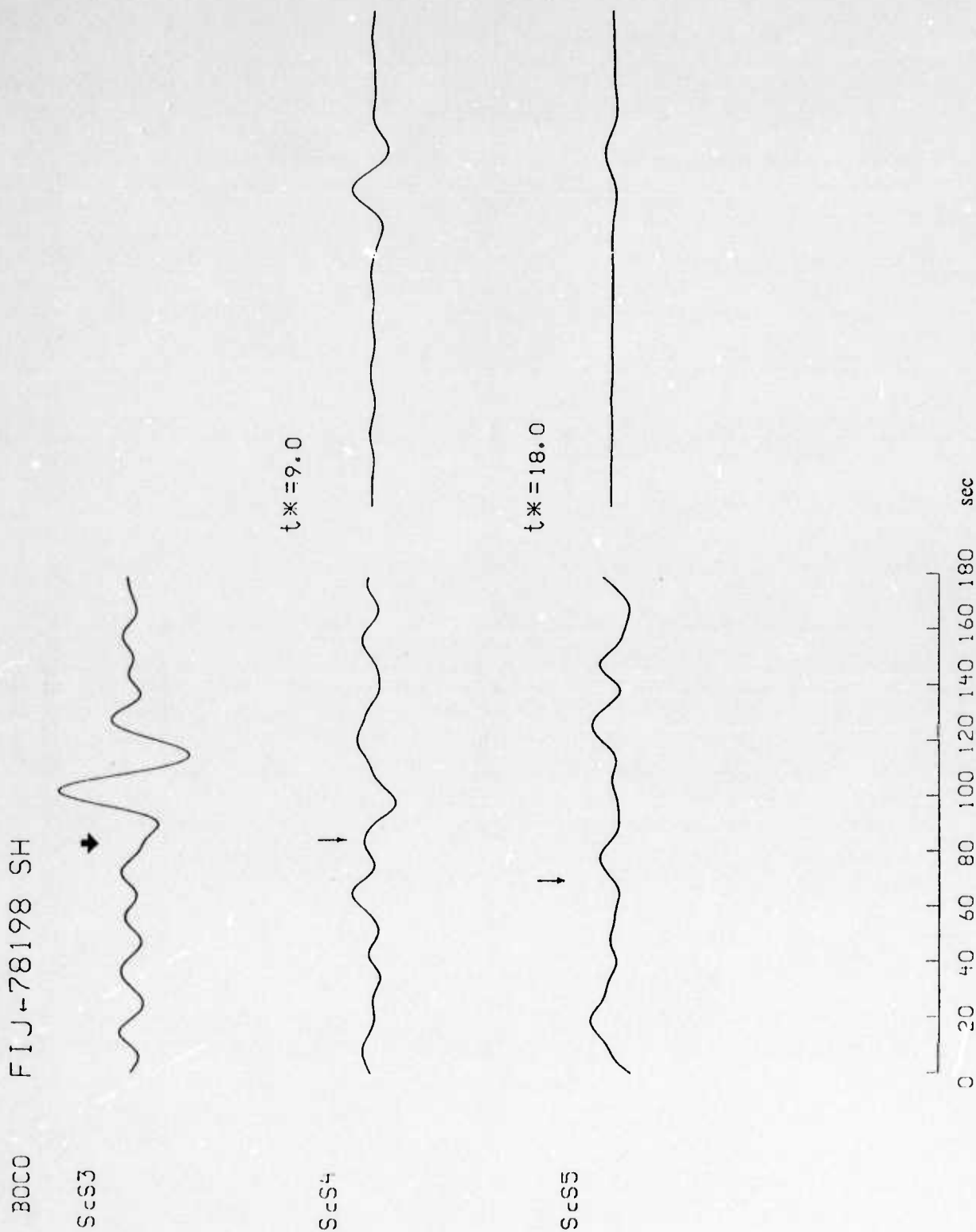


Figure A2. Observed ScS_N phases displayed on the left matched with the first observable ScS_N phase convolved with multiples of t^* shown on the right for Fiji-S. America path (event 2).

ZOB0

FIJ-78198 SH

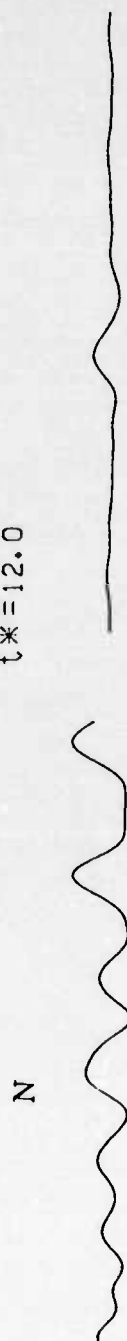
ScS3



ScS4

 $t^* = 6.0$ 

ScS5

 $t^* = 12.0$ 

N

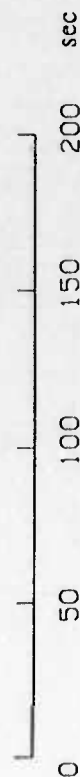


Figure A3. Observed ScS_N phases displayed on the left matched with the first observable ScS_N phase convolved with multiples of t^* shown on the right for Fiji-S. America path (event 2).

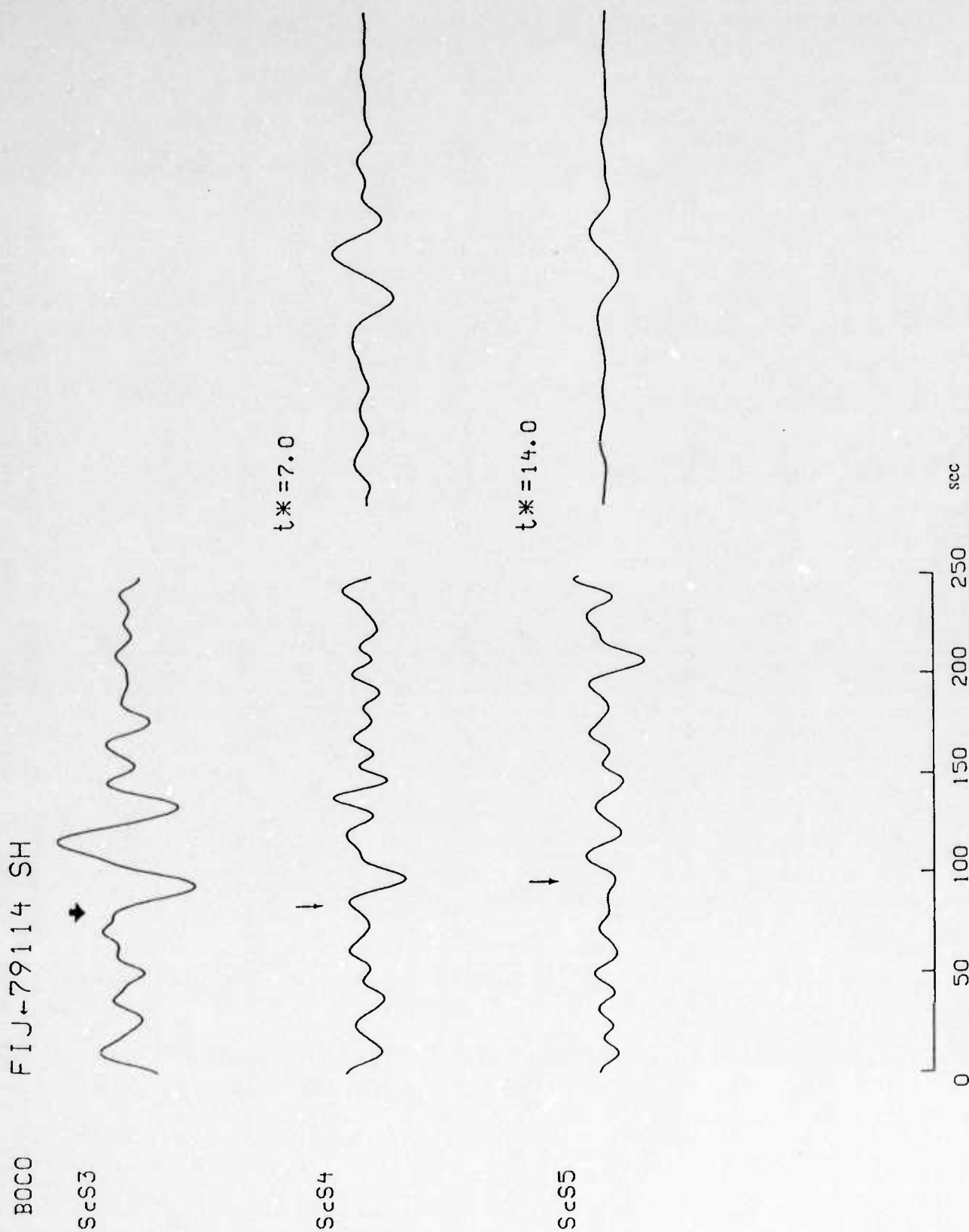


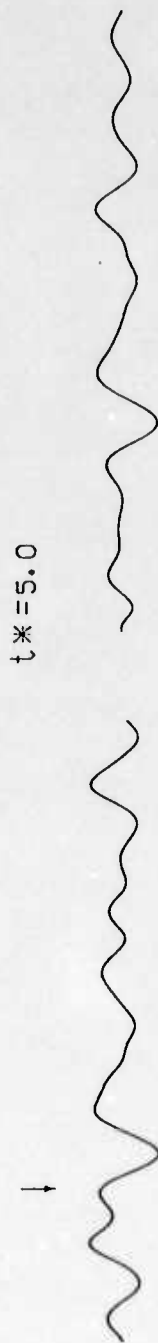
Figure A4. Observed ScS_N phases displayed on the left matched with the first observable ScS_N phase convolved with multiples of t^* shown on the right for Fiji-S. America path (event 3).

FIJ-80202 SH

BOC0

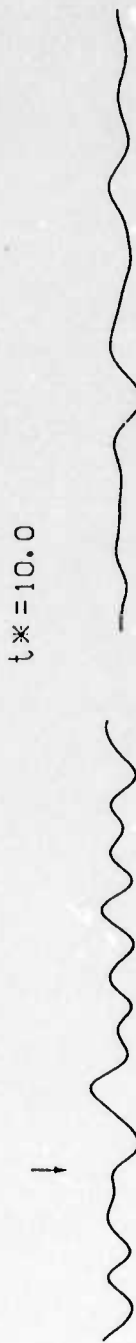


SCS2



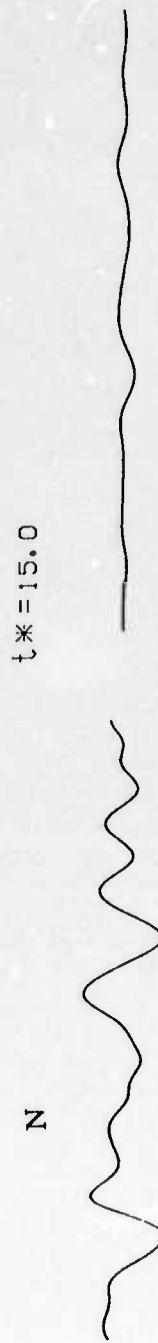
$t^* = 5.0$

SCS3



$t^* = 10.0$

SCS4



$t^* = 15.0$

SCS5

N



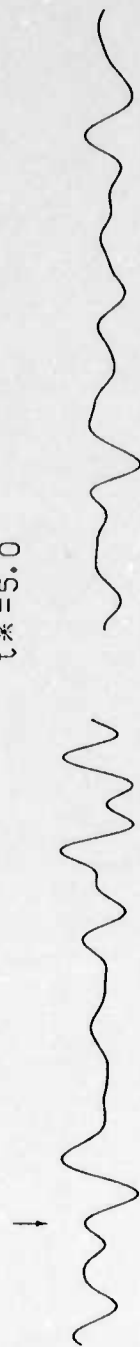
Figure A5. Observed ScS_N phases displayed on the left matched with the first observable ScS_N phase convolved with multiples of t^* shown on the right for Fiji-S. America path (event 4).

BOCO

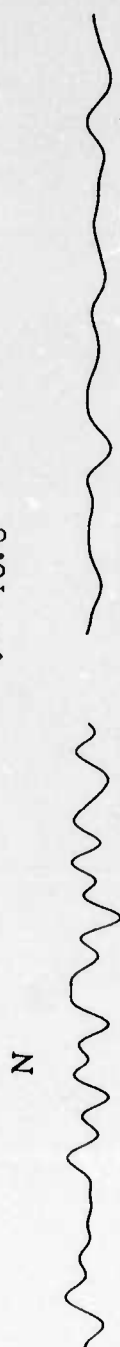
FIJ-81271 SH



ScS3

 $t^* = 5.0$ 

ScS4

 $t^* = 10.0$ 

ScS5

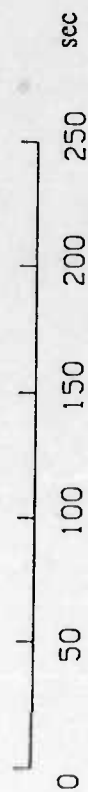
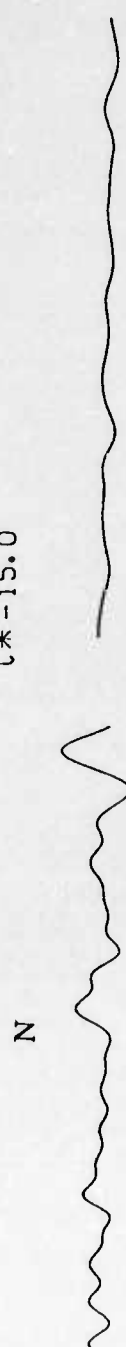
 $t^* = 15.0$ 

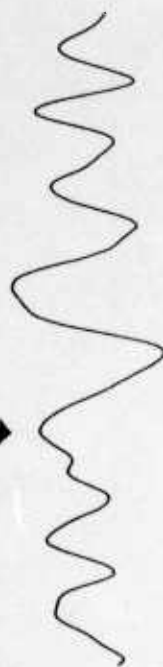
Figure A6. Observed ScS_N phases displayed on the left matched with the first observable ScS_N phase convolved with multiples of t^* shown on the right for Fiji-S. America path (event 5).

FIJ-81329 SH

BOC0



ScS3



$t^* = 7.0$



ScS4



$t^* = 14.0$

N

ScS5

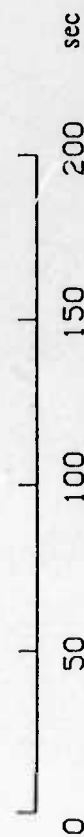
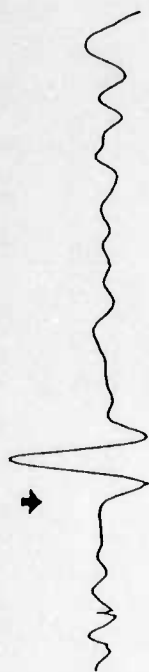


Figure A7. Observed ScS_N phases displayed on the left matched with the first observable ScS_N phase convolved with multiples of t^* shown on the right for Fiji-S. America path (event 6).

FIJ-83259 SH

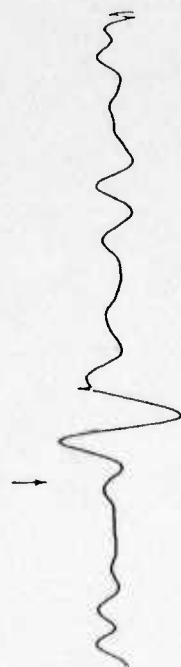
ZOB0

ScS2



ScS3

$t^* = 3.5$



ScS4

$t^* = 7.0$



ScS5

$t^* = 10.5$

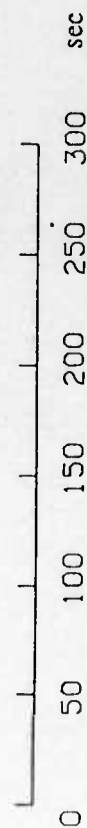


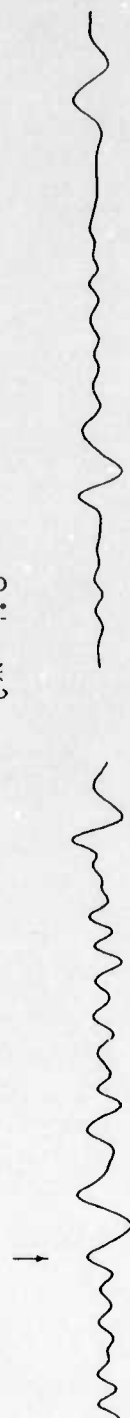
Figure A8. Observed ScS_N phases displayed on the left matched with the first observable ScS_N phase convolved with multiples of t^* shown on the right for Fiji-S. America path (event 7).

FIJ-81271 SH

AFI



$t^* = 4.0$



$t^* = 8.0$

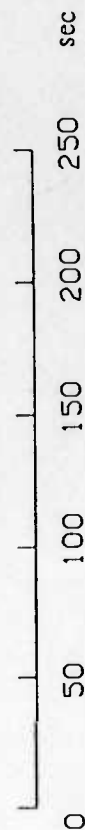
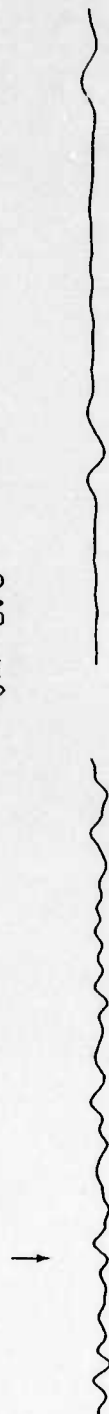


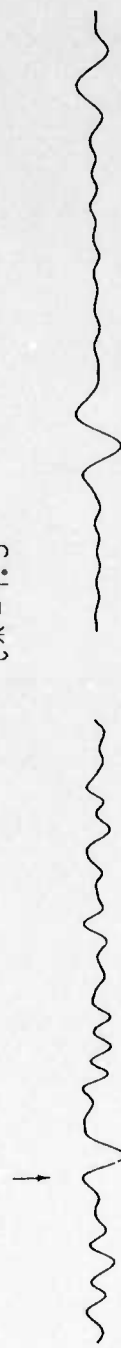
Figure A9. Observed ScS_N phases displayed on the left matched with the first observable ScS_N phase convolved with multiples of t^* shown on the right for SW Pacific path (event 8).

FIJ-84019 SH



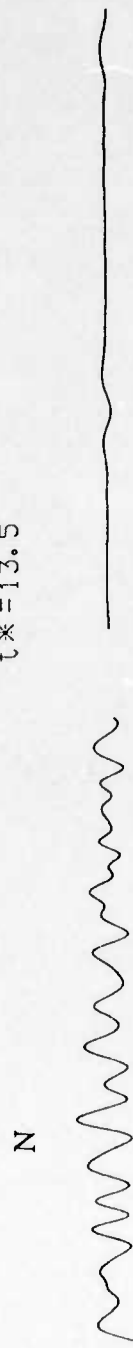
ScS

$t^* = 4.5$



ScS2

$t^* = 13.5$



ScS4

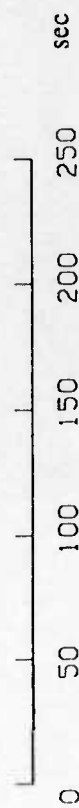


Figure A10. Observed ScS_N phases displayed on the left matched with the first observable ScS_N phase convolved with multiples of t^* shown on the right for SW Pacific path (event 9).

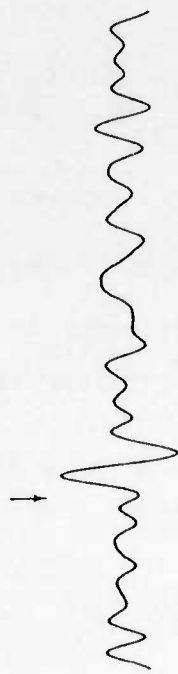
FIJ-84151 SH

HON

ScS2



$t^* = 2.5$



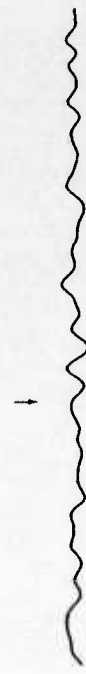
ScS3

$t^* = 5.0$



ScS4

$t^* = 7.5$



ScS5

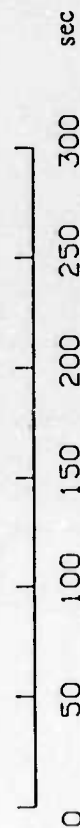


Figure A11. Observed ScS_N phases displayed on the left matched with the first observable ScS_N phase convolved with multiples of t^* shown on the right for SW Pacific path (event 10).

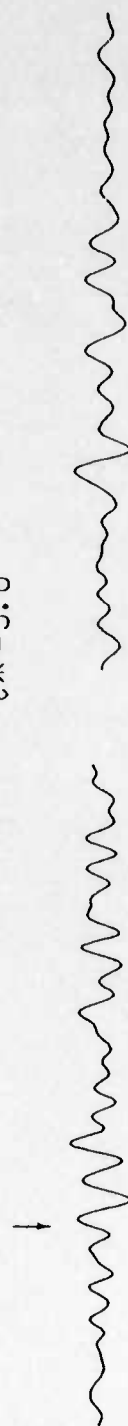
GUM0

FIJ-84151 SH

ScS2

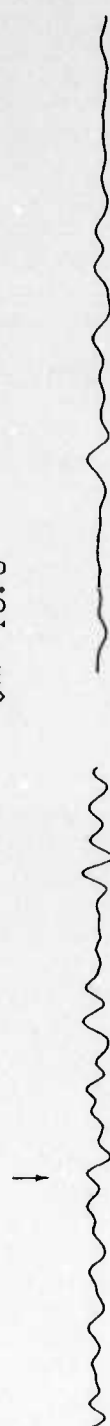


ScS3



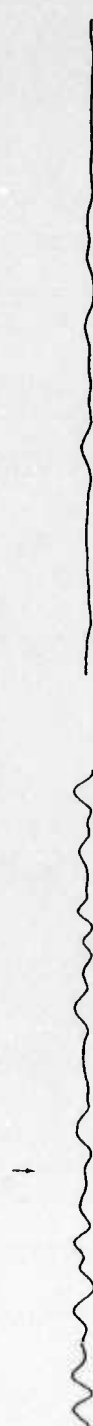
$t^* = 5.0$

ScS4



$t^* = 10.0$

ScS5



$t^* = 15.0$

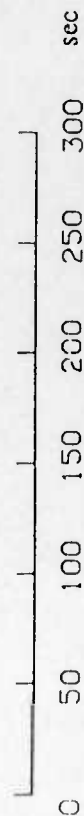


Figure A12. Observed ScS_N phases displayed on the left matched with the first observable ScS_N phase convolved with multiples of t^* shown on the right for SW Pacific path (event 10).

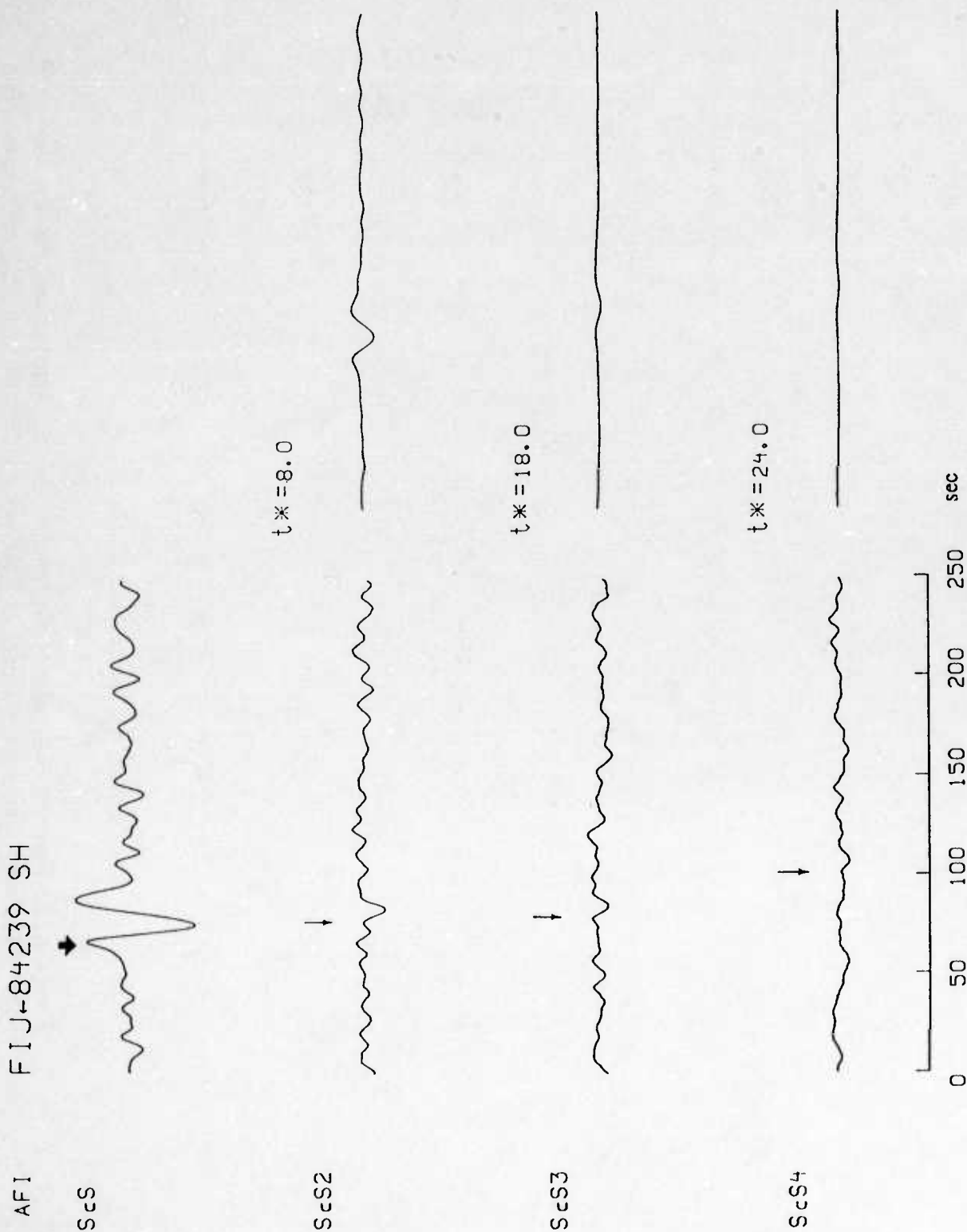


Figure A13. Observed ScS_N phases displayed on the left matched with the first observable ScS_N phase convolved with multiples of t^* shown on the right for SW Pacific path (event 11).

FIJ-84322 SH

AFI

ScS



$t^* = 3.0$

ScS2



$t^* = 6.0$

ScS3



$t^* = 9.0$

ScS4

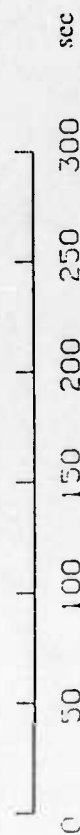
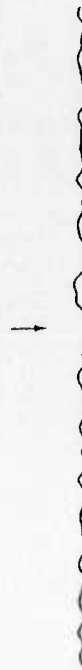
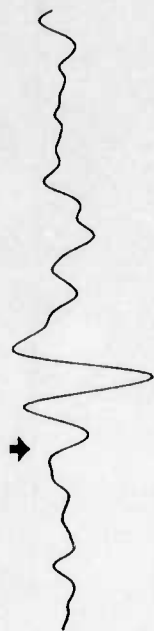


Figure A14. Observed ScS_N phases displayed on the left matched with the first observable ScS_N phase convolved with multiples of t^* shown on the right for SW Pacific path (event 12).

FIJ-84327 SH

HON

ScS



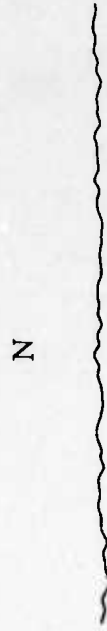
ScS2

$t^* = 7.0$



ScS3

$t^* = 14.0$



ScS4

$t^* = 21.0$

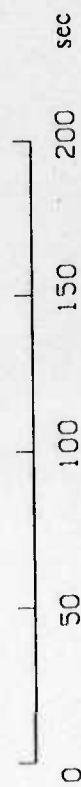
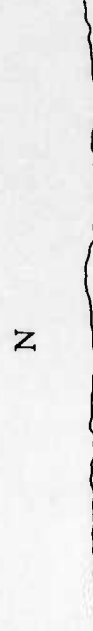
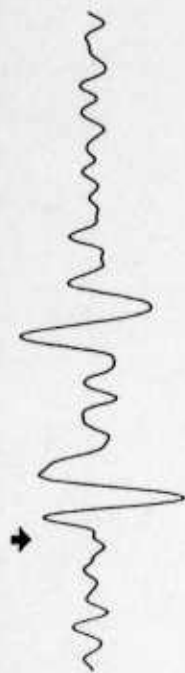


Figure A15. Observed ScS_N phases displayed on the left matched with the first observable ScS_N phase convolved with multiples of t^* shown on the right for SW Pacific path (event 13).

AFI

FIJ-85285 SH

ScS



ScS2

 $t^* = 5.0$

ScS3

 $t^* = 10.0$

ScS4

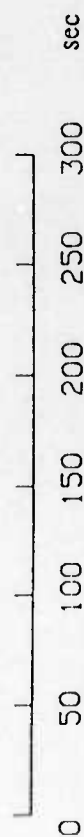
 $t^* = 15.0$ 

Figure A16. Observed ScS_N phases displayed on the left matched with the first observable ScS_N phase convolved with multiples of t^* shown on the right for SW Pacific path (event 14).

HON

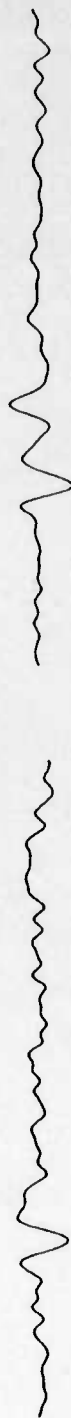
FIJ-85240 SH

ScS



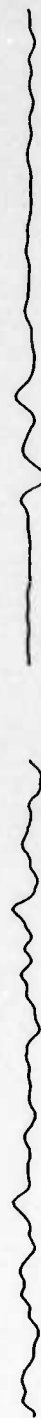
ScS2

↓

 $t^* = 2.5$ 

ScS3

↓

 $t^* = 5.0$ 

ScS4

N

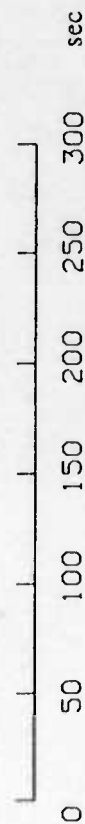
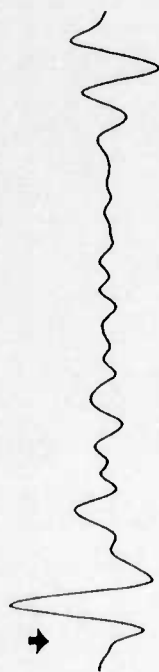
 $t^* = 7.5$ 

Figure A17. Observed ScS_N phases displayed on the left matched with the first observable ScS_N phase convolved with multiples of t^* shown on the right for SW Pacific path (event 15).

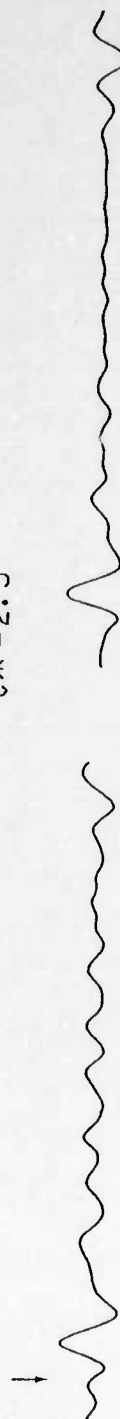
ZOB0

SAM 77035 SH

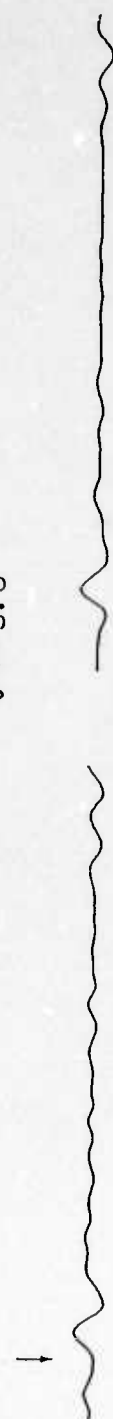
ScS



ScS2

 $t^* = 2.5$

ScS3

 $t^* = 5.0$

ScS4

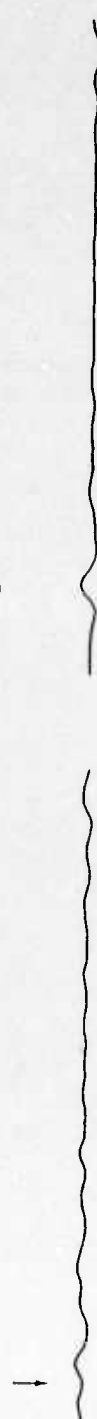
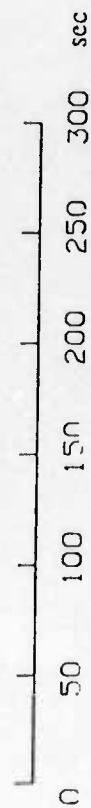
 $t^* = 7.5$ 

Figure A18. Observed ScS_N phases displayed on the left matched with the first observable ScS_N phase convolved with multiples of t^* shown on the right for shield S. America path (event 16).

SAM 79141 SH

ZOB0

ScS



ScS2

$t^* = 4.0$



ScS3

$t^* = 8.0$



ScS4

$t^* = 12.0$

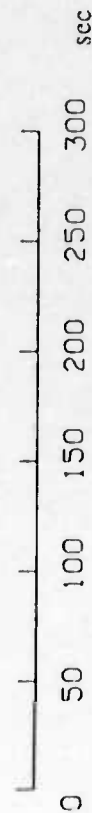


Figure A19. Observed ScS_N phases displayed on the left matched with the first observable ScS_N phase convolved with multiples of t^* shown on the right for shield S. America path (event 17).

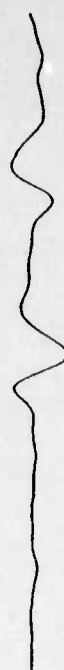
ZOB0

SAM 83010 SH

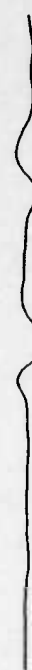
ScS



ScS2

 $t^* = 2.5$ 

ScS3

 $t^* = 5.0$ 

ScS4

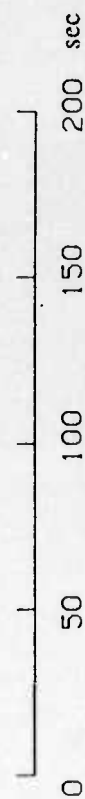
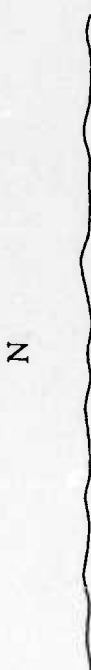
 $t^* = 7.5$ 

Figure A20. Observed ScS_N phases displayed on the left matched with the first observable ScS_N phase convolved with multiples of t^* shown on the right for shield S. America path (event 18).

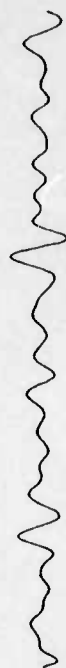
ZOB0

SAM 83153 SH

ScS



ScS2

 $t^* = 2.5$ 

ScS3

 $t^* = 5.0$ 

ScS4

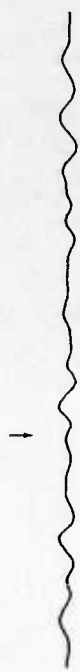
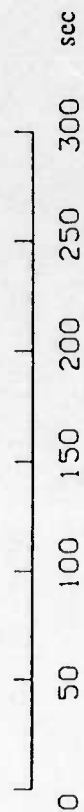
 $t^* = 7.5$ 

Figure A21. Observed ScS_N phases displayed on the left matched with the first observable ScS_N phase convolved with multiples of t^* shown on the right for shield S. America path (event 19).

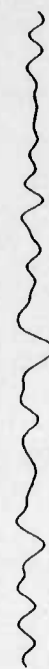
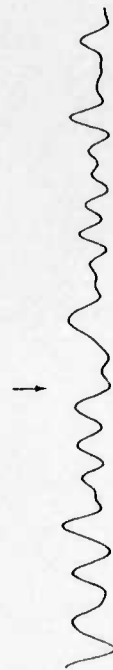
BDF

SAM 83355 SH

ScS2



ScS3

 $t^* = 2.5$ 

ScS4

 $t^* = 5.0$ 

ScS5

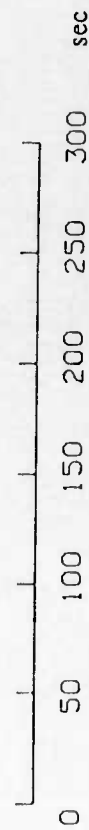
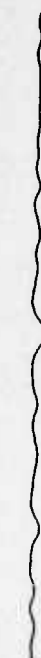
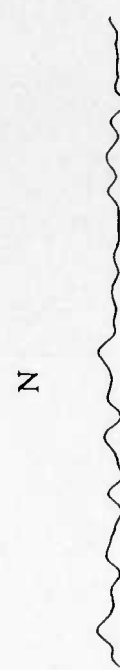
 $t^* = 7.5$ 

Figure A22. Observed ScS_N phases displayed on the left matched with the first observable ScS_N phase convolved with multiples of t^* shown on the right for shield S. America path (event 20).

SAM 83355 SH



ScS2

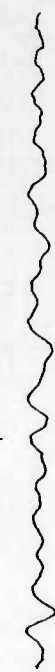
$t^* = 2.5$



ScS3



$t^* = 5.0$



ScS4



$t^* = 7.5$



ScS5

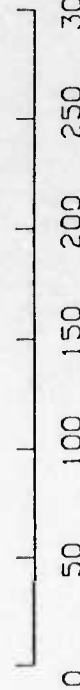


Figure A23. Observed ScS_N phases displayed on the left matched with the first observable ScS_N phase convolved with multiples of t^* shown on the right for shield S. America path (event 20).

ZOBO

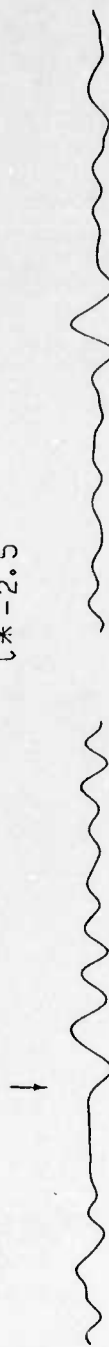
SAM 85161 SH

ScS



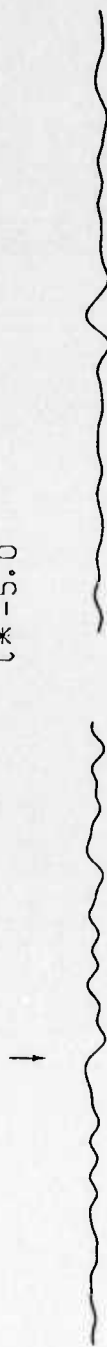
ScS2

$t^* = 2.5$



ScS3

$t^* = 5.0$



ScS4

$t^* = 7.5$

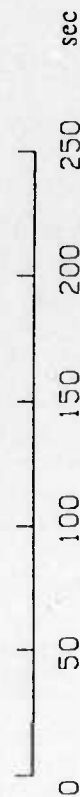
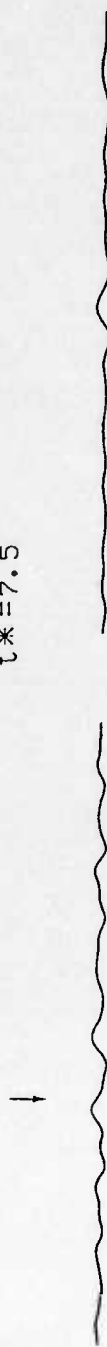


Figure A24. Observed ScS_N phases displayed on the left matched with the first observable ScS_N phase convolved with multiples of t^* shown on the right for shield S. America path (event 22).

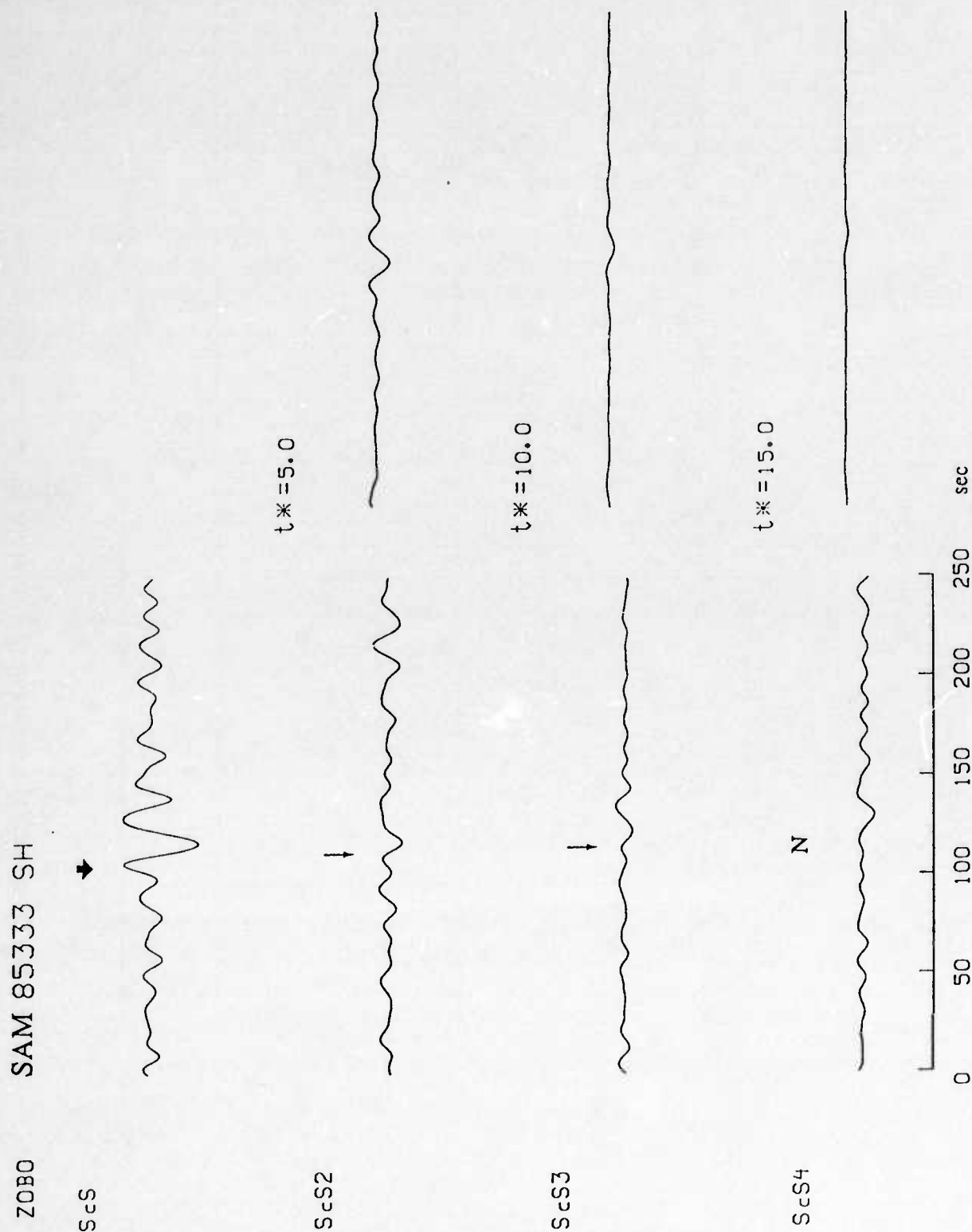
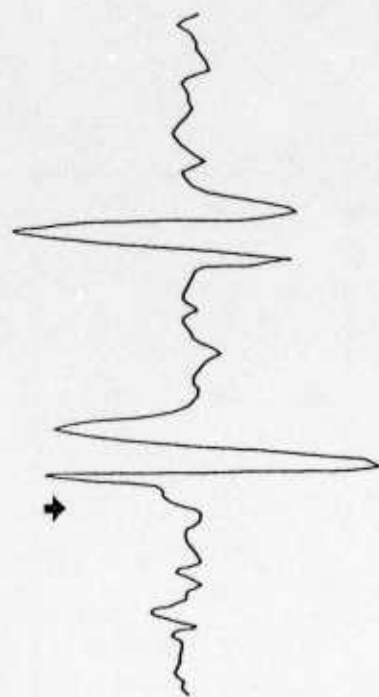


Figure A25. Observed ScS_N phases displayed on the left matched with the first observable ScS_N phase convolved with multiples of t^* shown on the right for shield S. America path (event 23).

mat

MAT-750626 EW

ScS



$t^* = 5.5$

ScS2

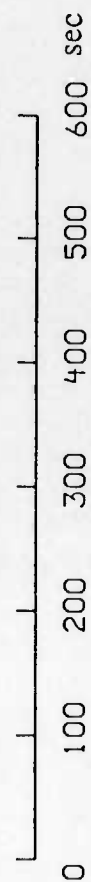


Figure A26. Observed ScS_N phases displayed on the left matched with the first observable ScS_N phase convolved with multiples of t^* shown on the right for NW Pacific path (event 24).

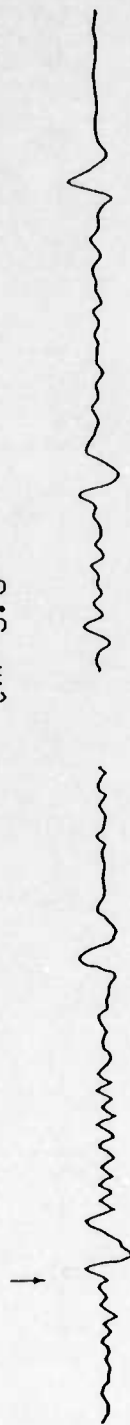
mat le MAT-751221 EW

ScS



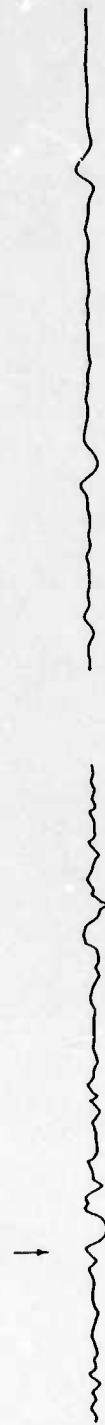
ScS2

$t^* = 5.0$



ScS3

$t^* = 10.0$



ScS4

$t^* = 15.0$

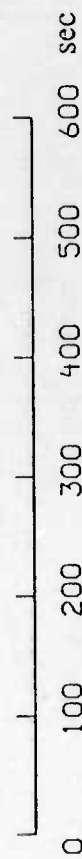
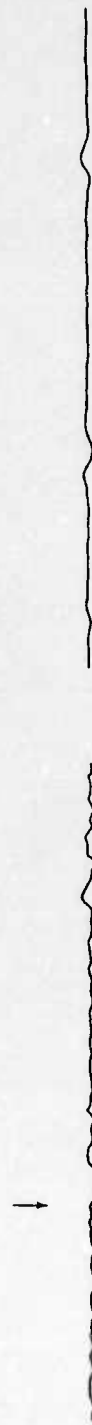


Figure A27. Observed ScS_N phases displayed on the left matched with the first observable ScS_N phase convolved with multiples of t^* shown on the right for NW Pacific path (event 25).

mat

MAT-750812 EW

ScS2



$t^* = 7.0$

ScS3

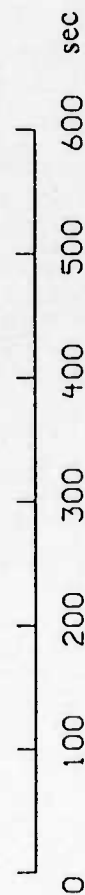
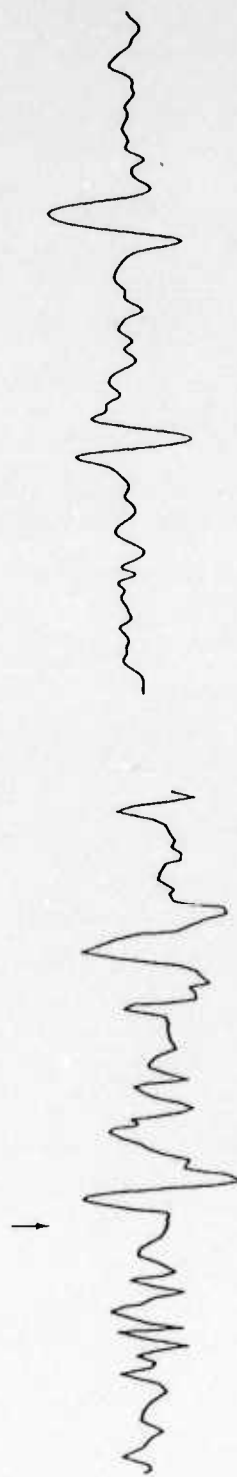
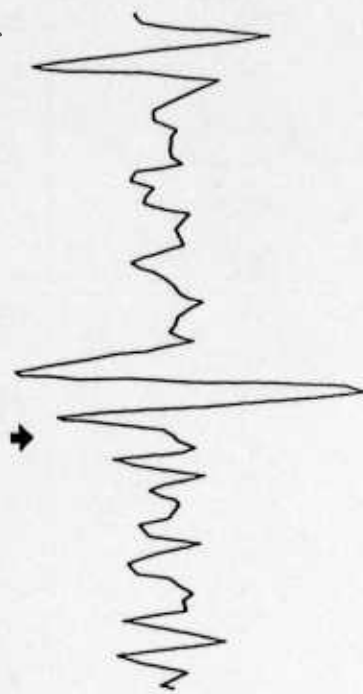


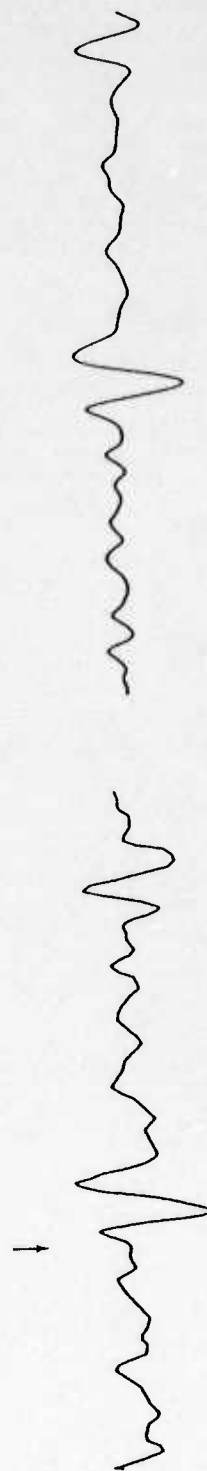
Figure A28. Observed ScS_N phases displayed on the left matched with the first observable ScS_N phase convolved with multiples of t^* shown on the right for NW Pacific path (event 26).

mat ← 730728 EW



ScS

$t^* = 7.0$



ScS2

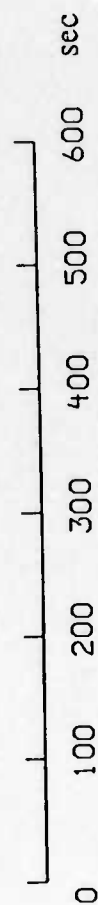


Figure A29. Observed ScS_N phases displayed on the left matched with the first observable ScS_N phase convolved with multiples of t^* shown on the right for NW Pacific path (event 27).

WPAC-76101 SH

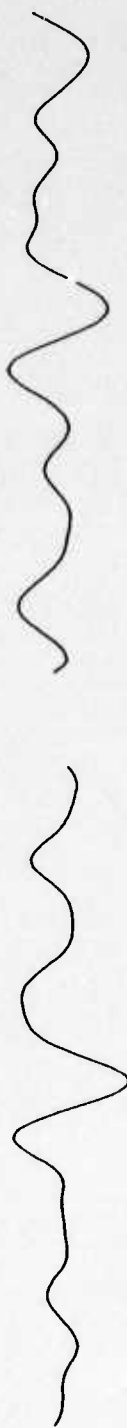
MAT



ScS2

$t^* = 2.0$

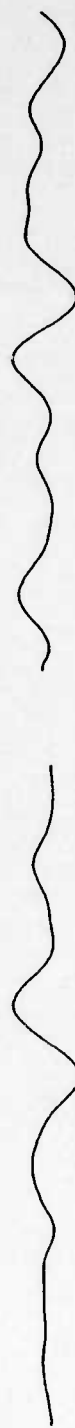
↓



ScS3

$t^* = 4.0$

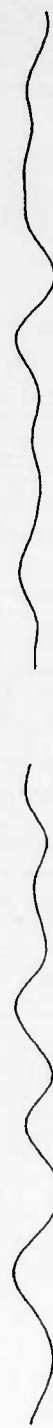
↓



ScS4

$t^* = 8.0$

↓



ScS5

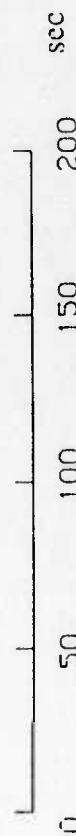


Figure A30. Observed ScS_N phases displayed on the left matched with the first observable ScS_N phase convolved with multiples of t^* shown on the right for NW Pacific path (event 28).

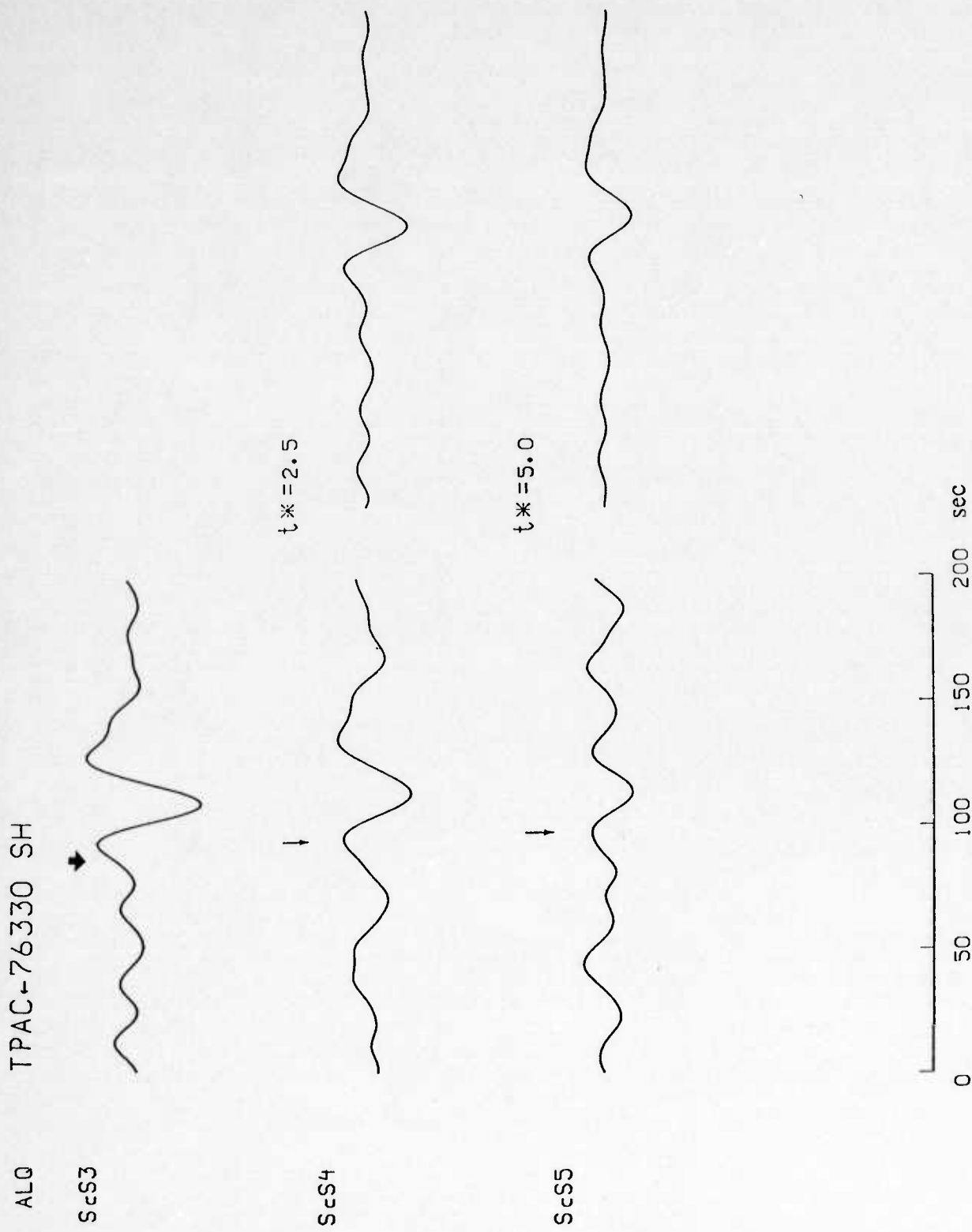
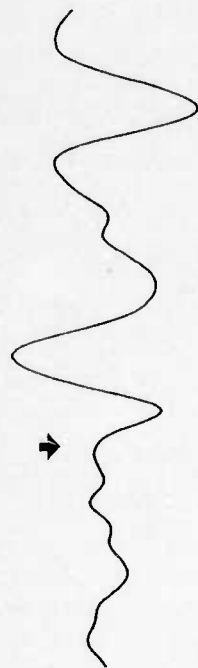


Figure A31. Observed ScSN phases displayed on the left matched with the first observable ScSN phase convolved with multiples of t^* shown on the right for N. Trans-Pacific path (event 29).

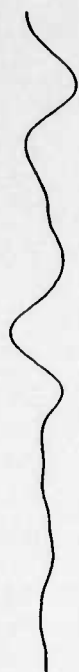
CTA

AUST-76009 SH

ScS



ScS2

 $t^* = 5.0$ 

ScS3

 $t^* = 10.0$ 

ScS4

 $t^* = 15.0$ 

Figure A32. Observed ScS_N phases displayed on the left matched with the first observable ScS_N phase convolved with multiples of t^* shown on the right for W Pacific path (event 30).

(THIS PAGE INTENTIONALLY LEFT BLANK)

APPENDIX B

Analyses of PP/P and PP/PKP Spectral Ratios.

1979230 KONO

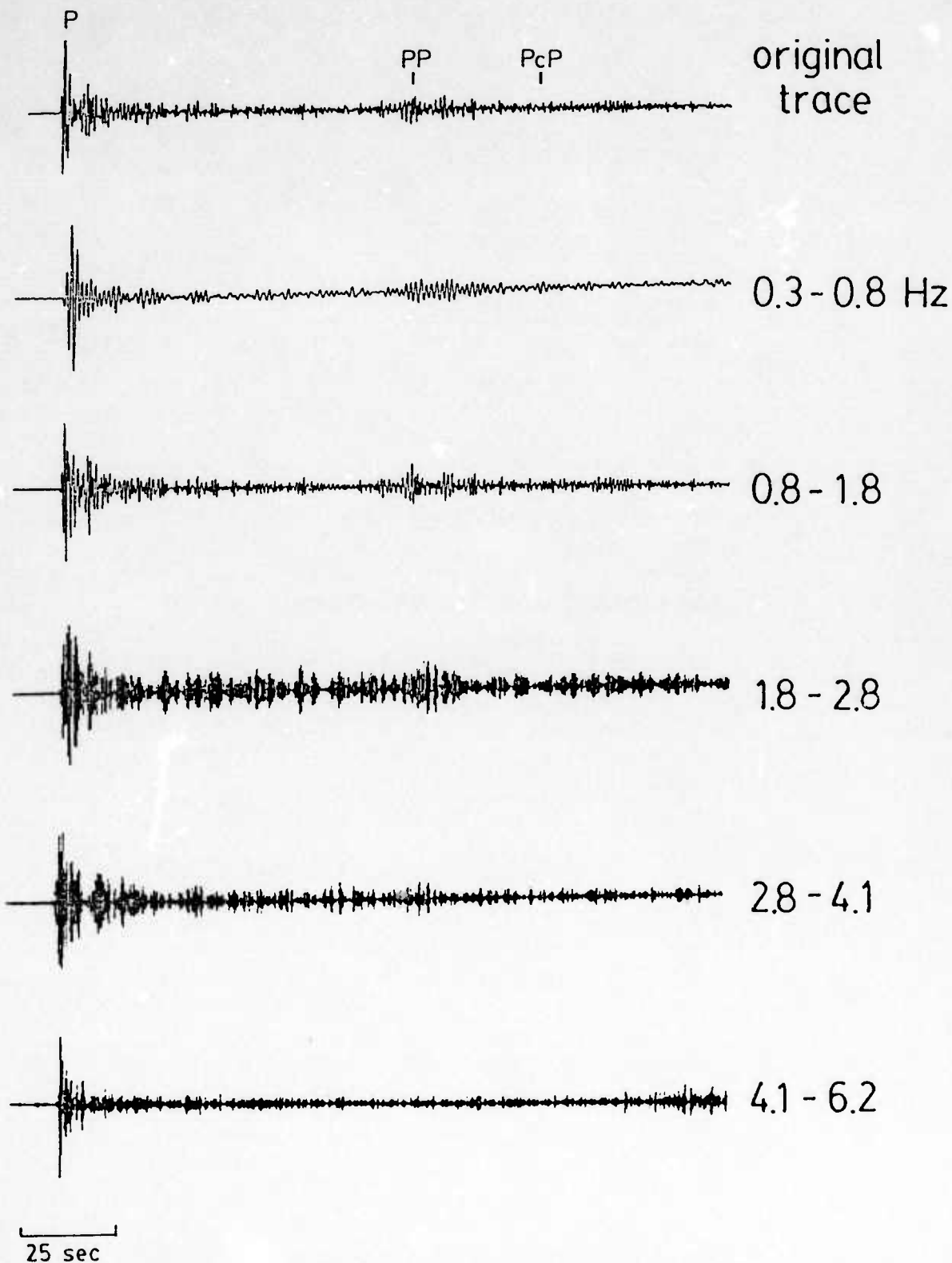


Figure B1. Band-pass filtered P and PP phases on vertical component for a Kazakh nuclear explosion at KONO. The PP phase is observable up to 6 Hz indicating high Q surface reflection region.

1980349 GRFO

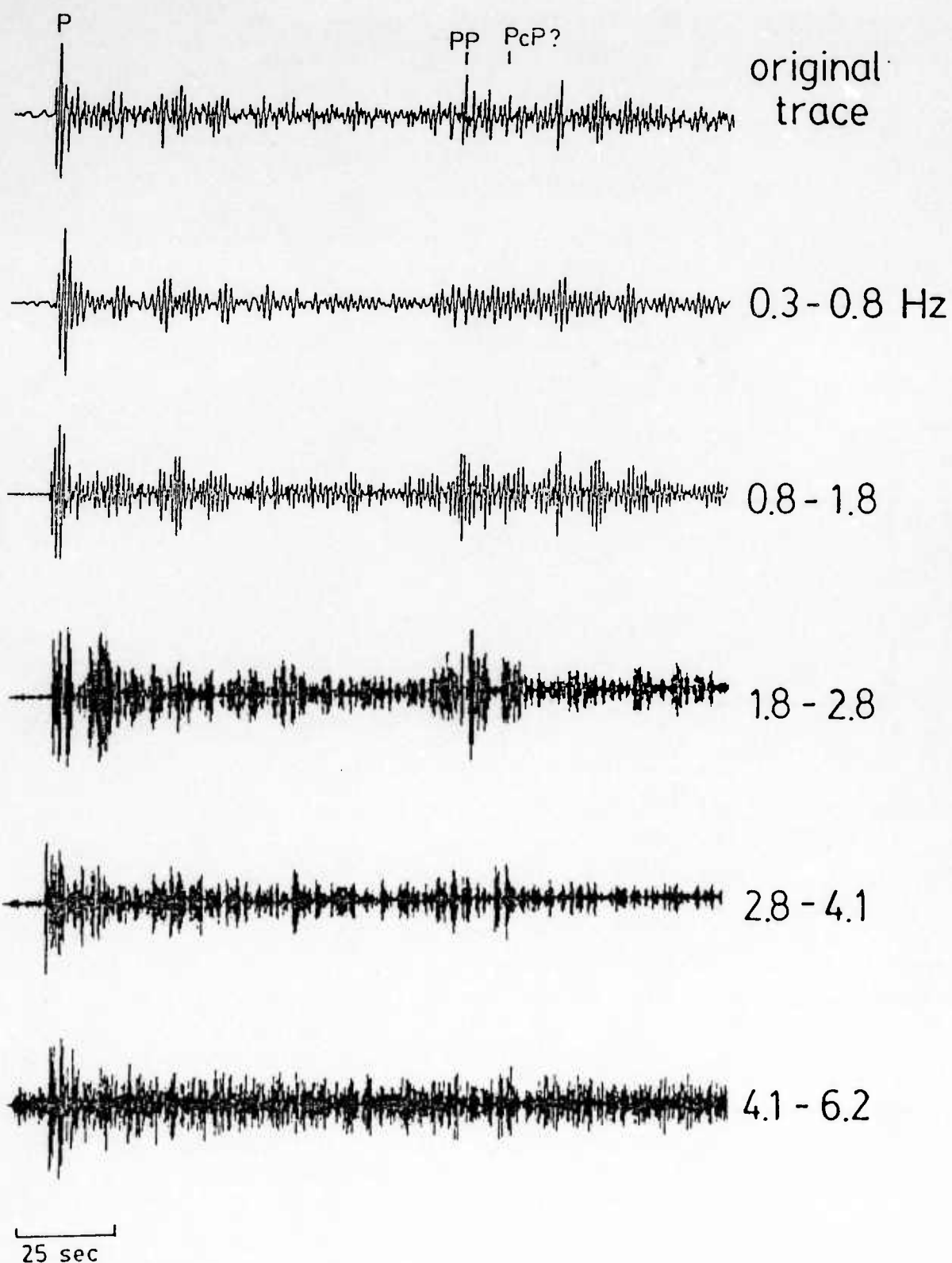


Figure B2. Band-pass filtered P and PP phases on vertical component for a Kazakh nuclear explosion at GRFO. The PP phase is observable up to 2.8 Hz.

1980349 ANTO

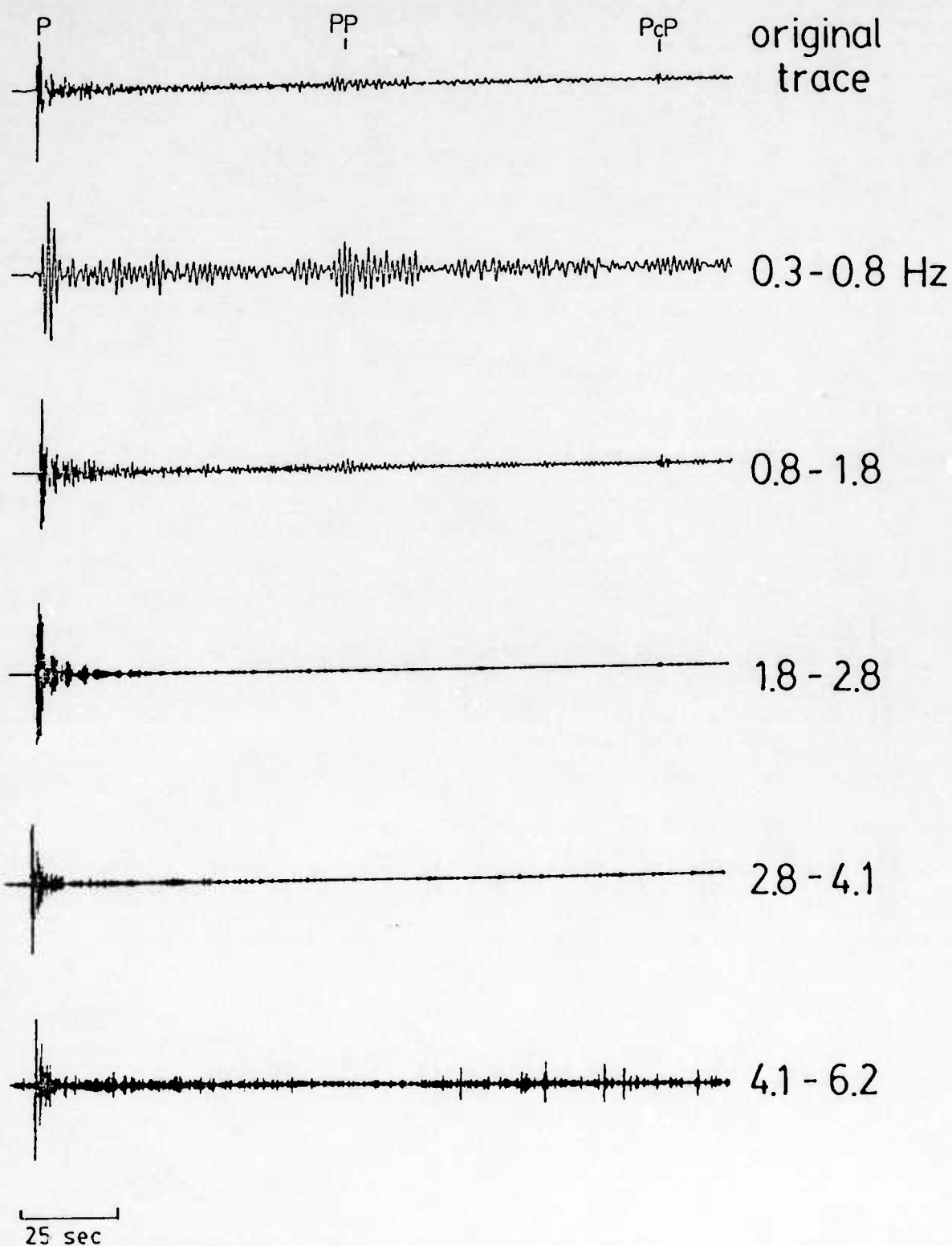


Figure B3. Band-pass filtered P and PP phases on vertical component for a Kazakh nuclear explosion at ANTO. The PP phase is observable up to 1.8 Hz.

1979336 SHIO

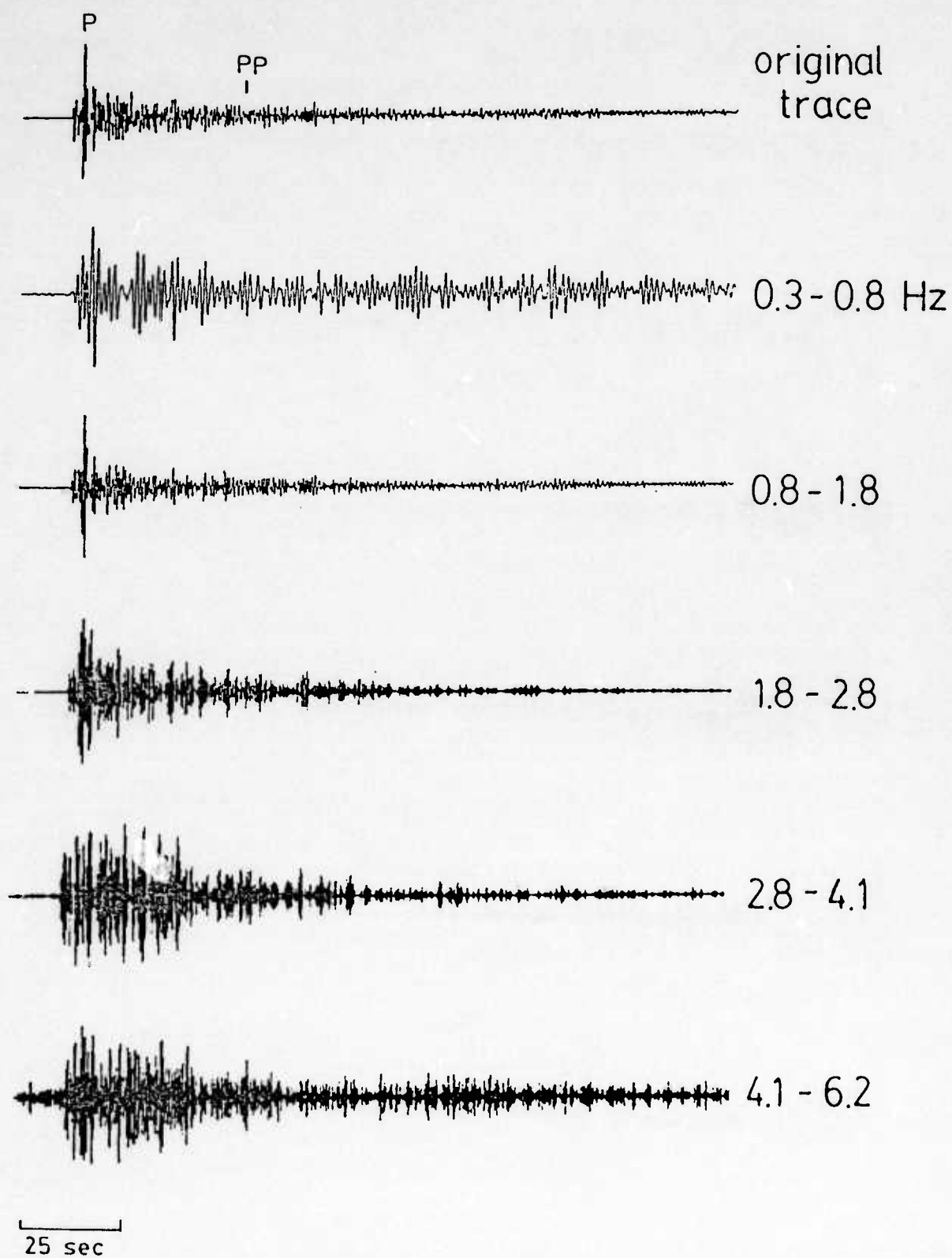


Figure B4. Band-pass filtered P and PP phases on vertical component for a Kazakh nuclear explosion at SHIO. The PP phase is questionable.

1978241

SHIO

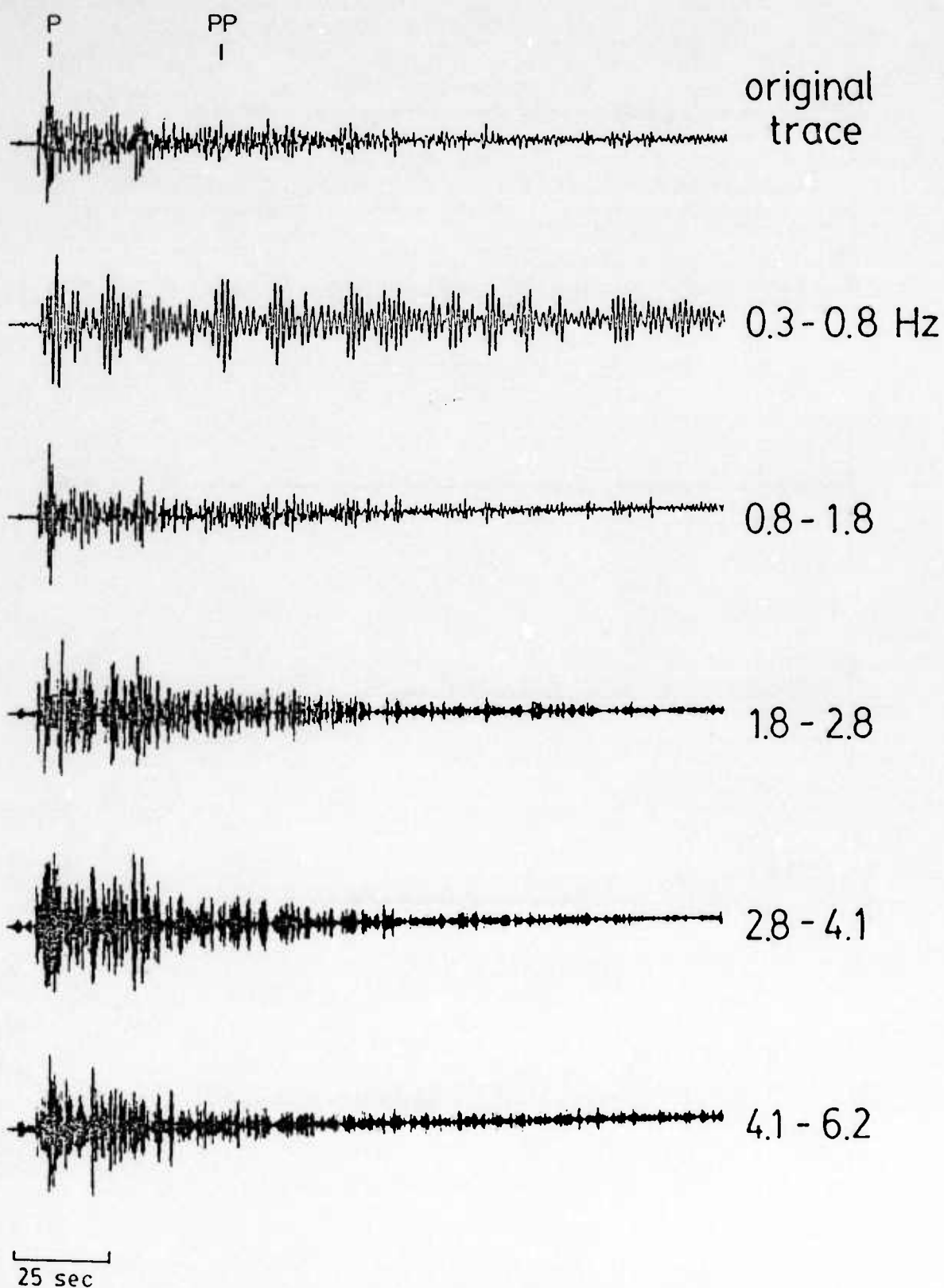


Figure B5. Band-pass filtered P and PP phases on vertical component for a Kazakh nuclear explosion at SHIO. The PP phase observable up to 1.8 Hz.

1978186 MAJO

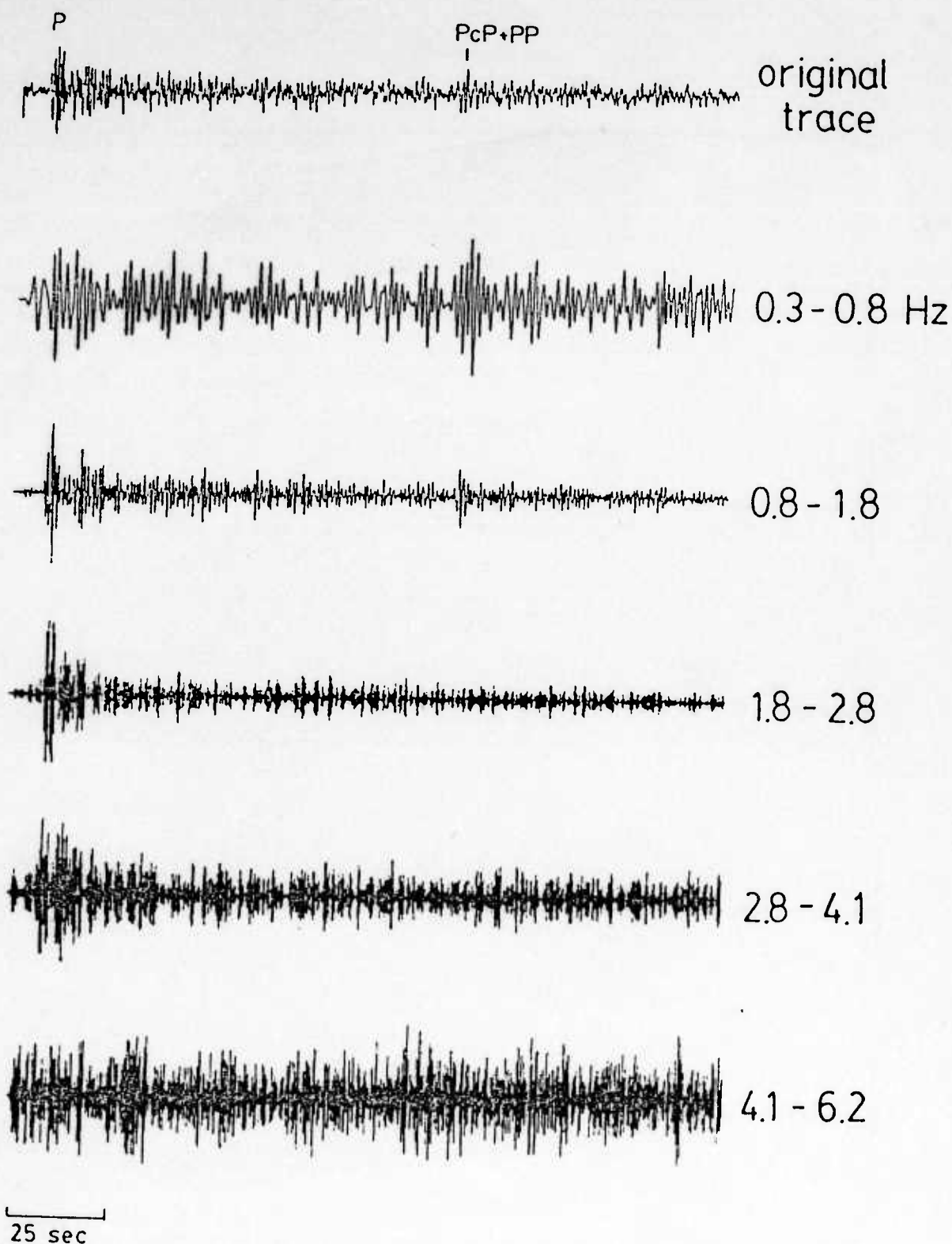


Figure B6. Band-pass filtered P and PP phases on vertical component for a Kazakh nuclear explosion at MAJO. The PP phase observable up to 2.8 Hz.

1981112 CHTO

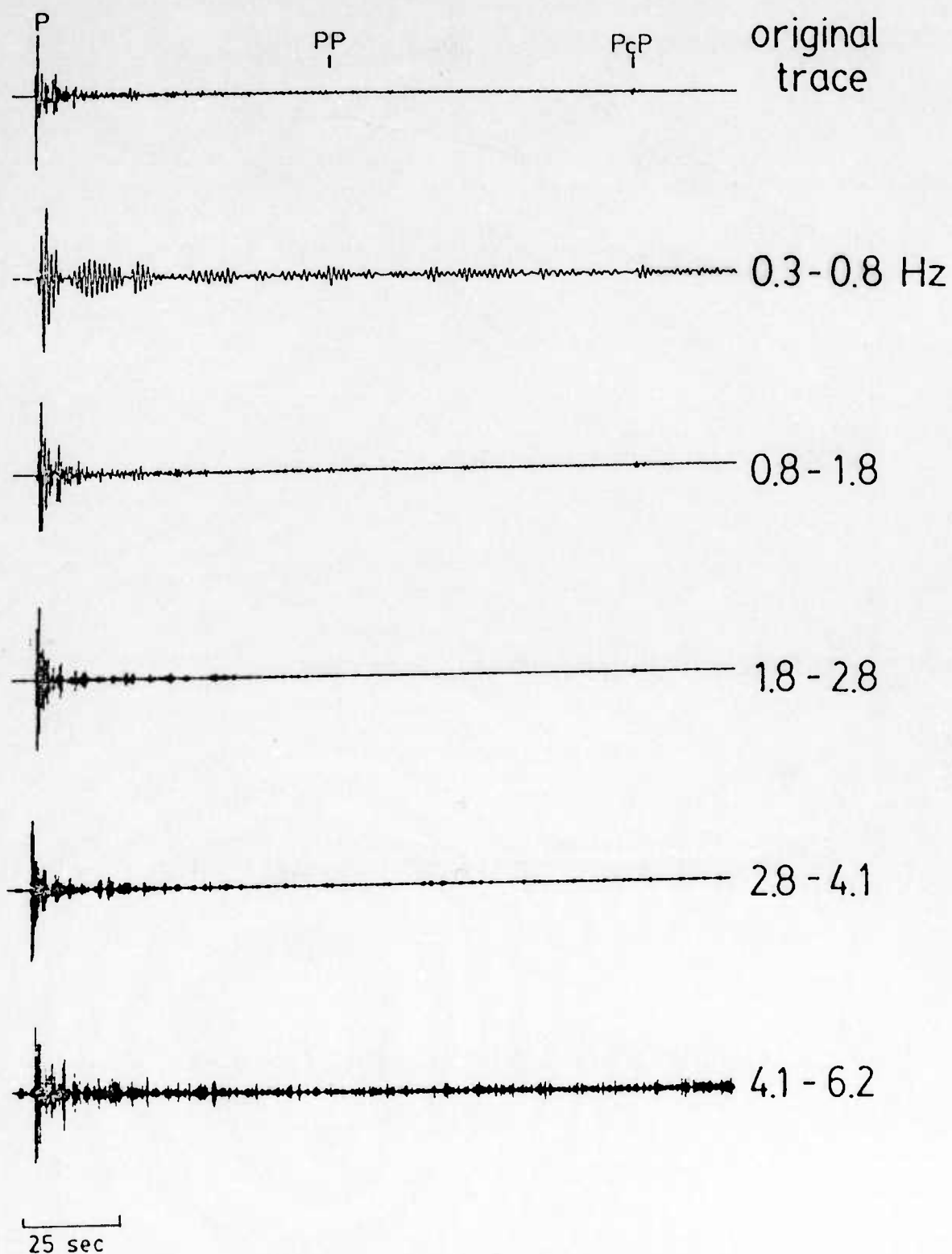


Figure B7. Band-pass filtered P and PP phases on vertical component for a Kazakh nuclear explosion at CHTO. The PP phase may not be seen above 0.8 Hz.

1980258 TATO

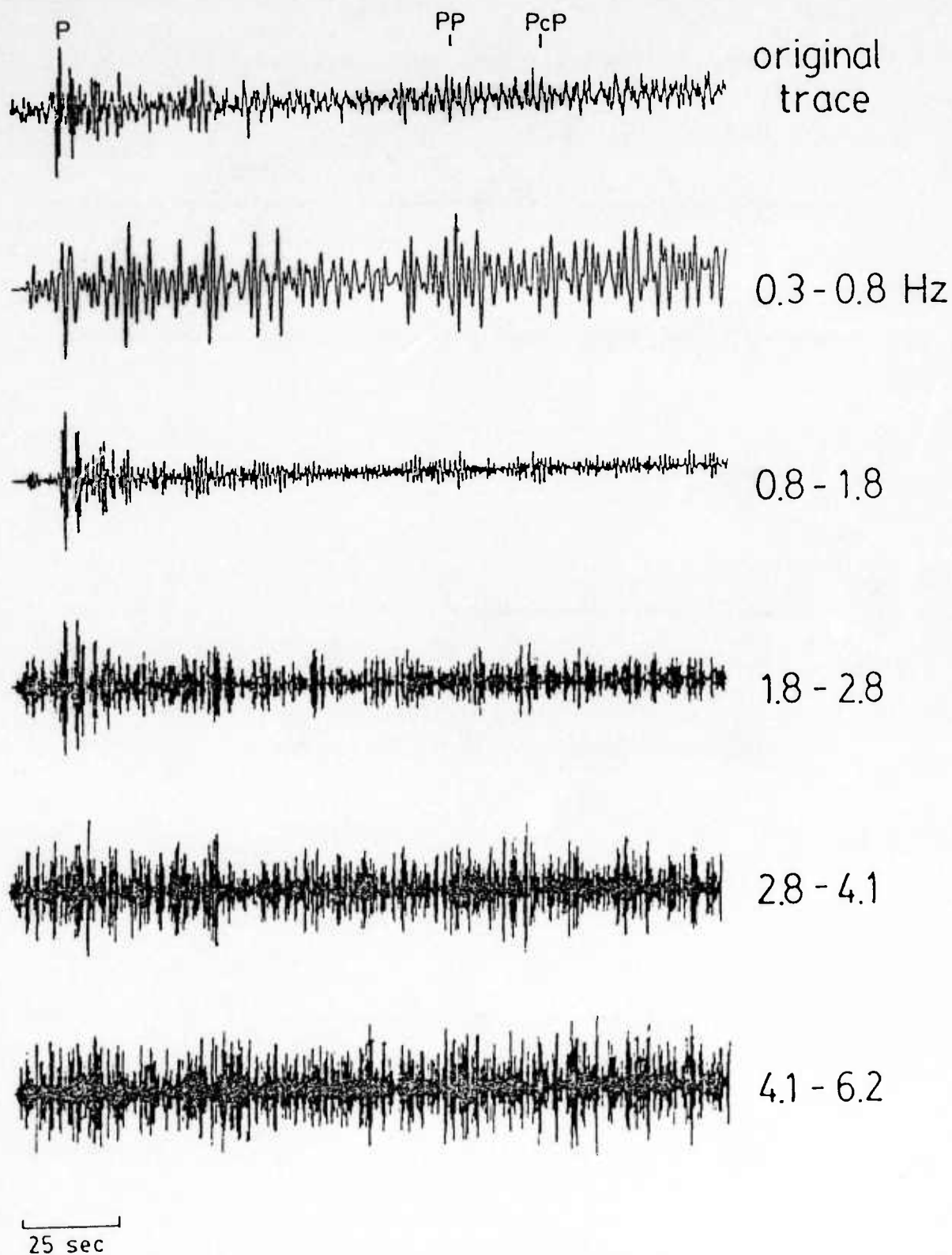


Figure B8. Band-pass filtered P and PP phases on vertical component for a Kazakh nuclear explosion at TATO. The PP phase is observable up to 1.8 Hz.

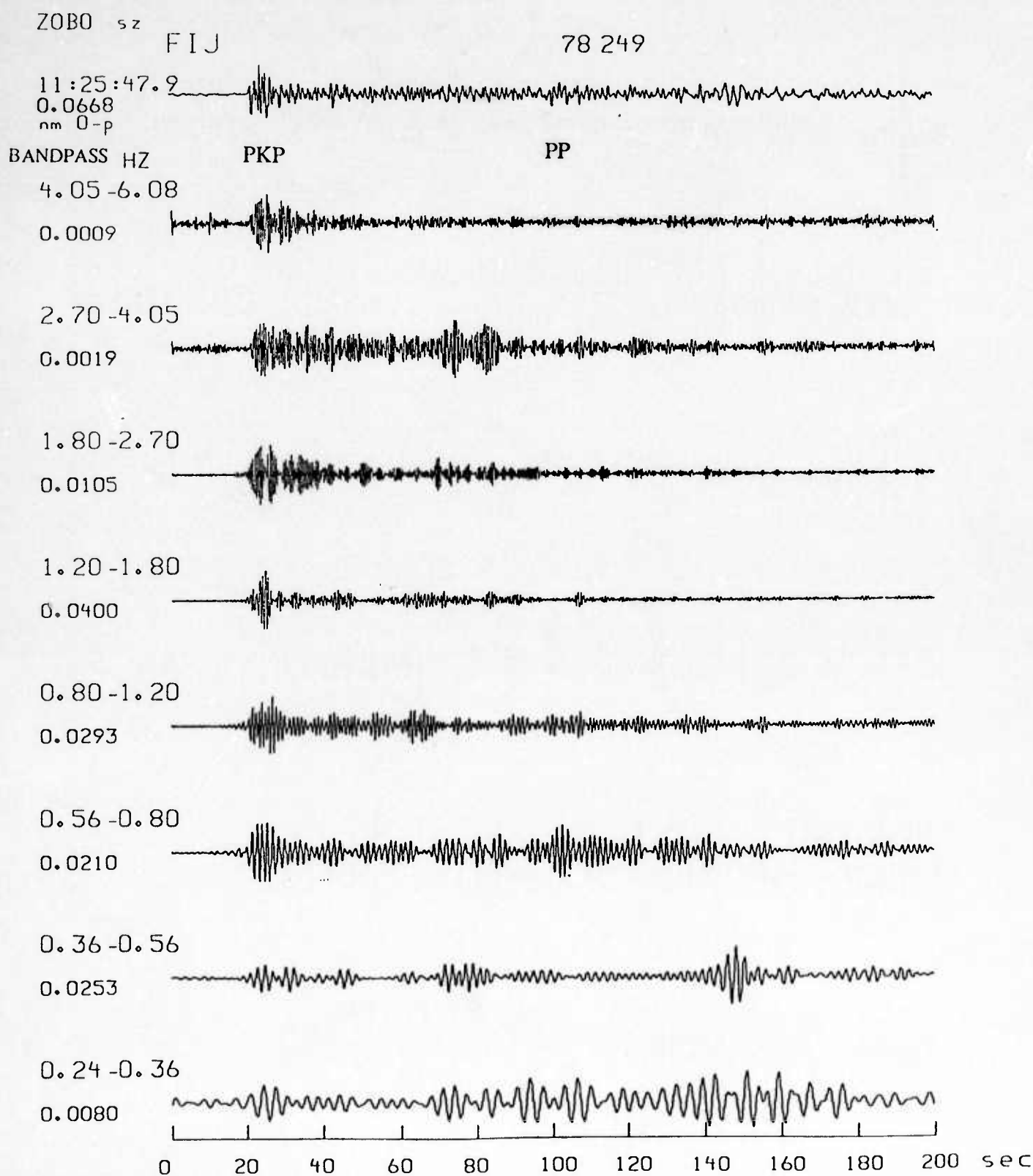


Figure B9. Band-pass filtered vertical component seismograms for path across E. Pacific with arrival times of PKP and PP identified. Absence of high frequency PP phase indicates a low Q bounce region.

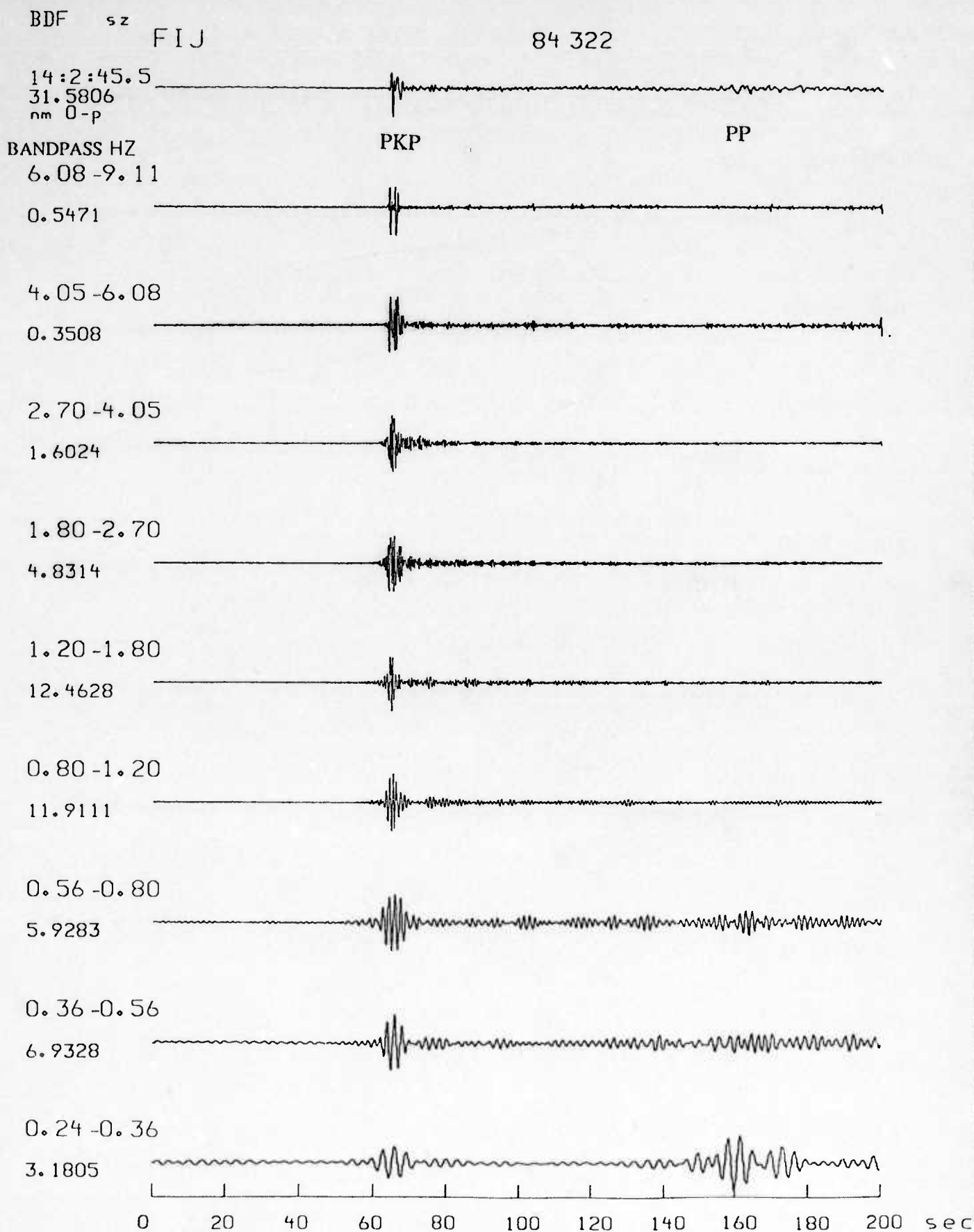


Figure B10. Band-pass filtered vertical component seismograms for path across E. Pacific with arrival times of PKP and PP identified. Absence of high frequency PP phase indicates a low Q bounce region.

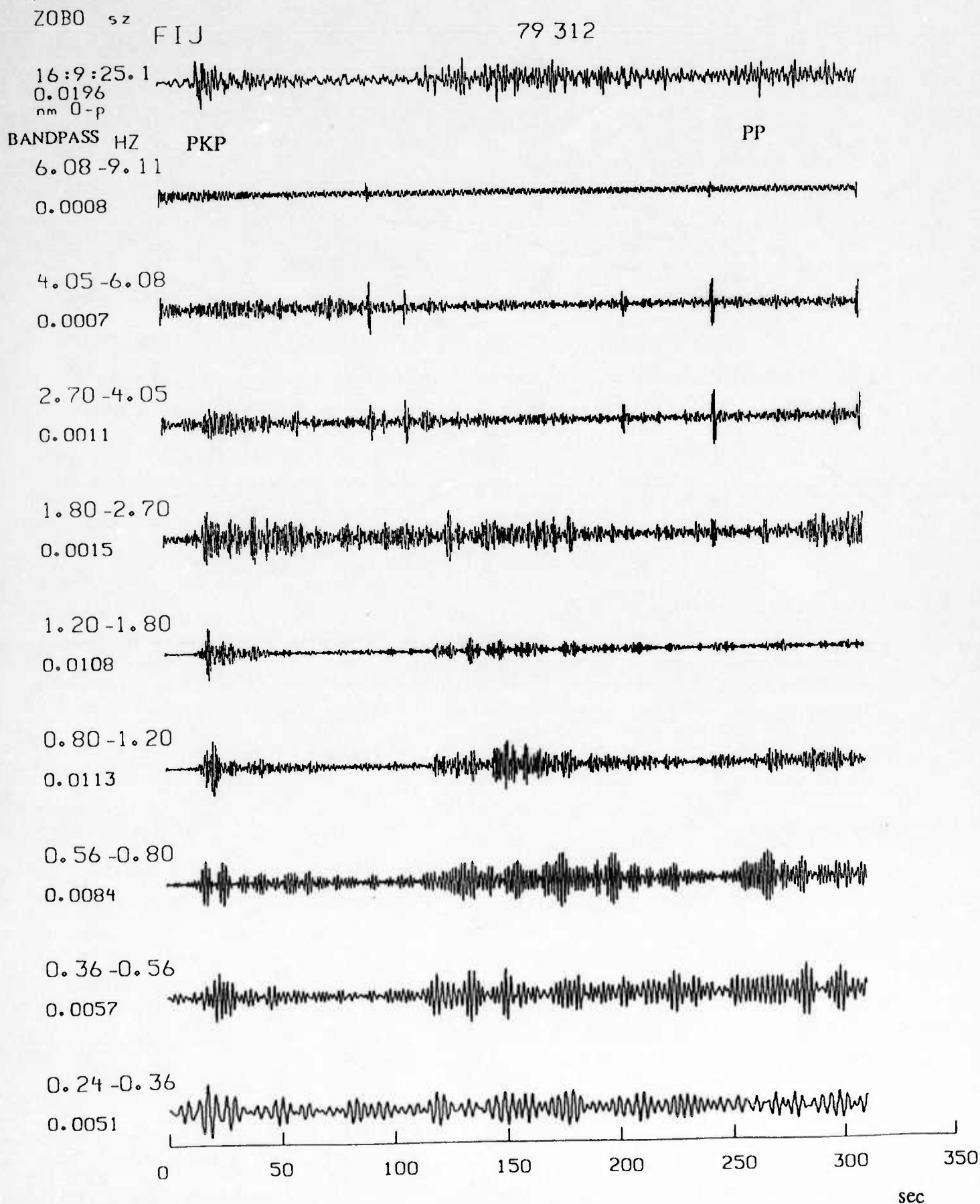


Figure B11. Band-pass filtered vertical component seismograms for path across E. Pacific with arrival times of PKP and PP identified. Absence of high frequency PP phase indicates a low Q bounce region.

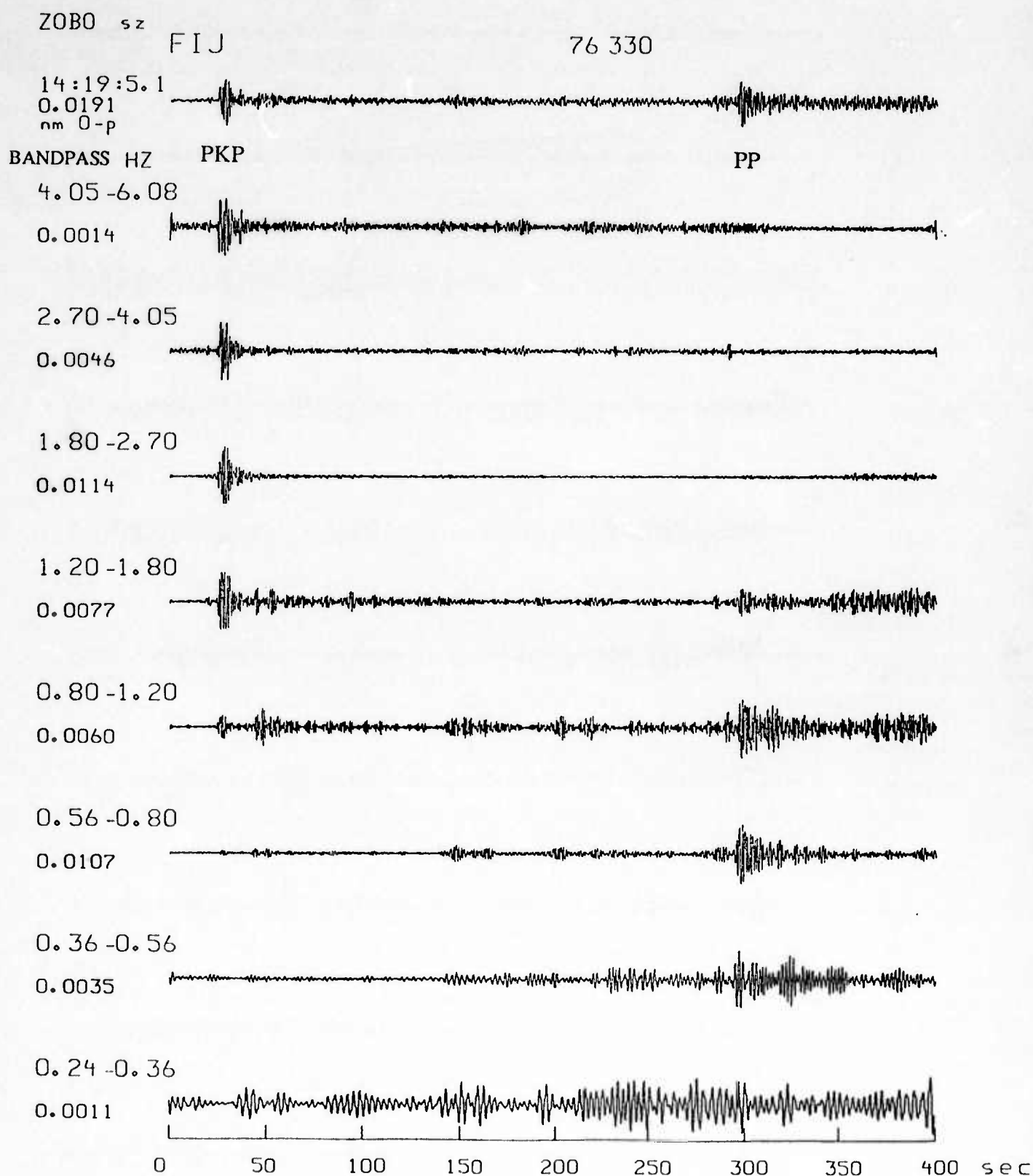


Figure B12. Band-pass filtered vertical component seismograms for path across E. Pacific with arrival times of PKP and PP identified. Absence of high frequency PP phase indicates a low Q bounce region.

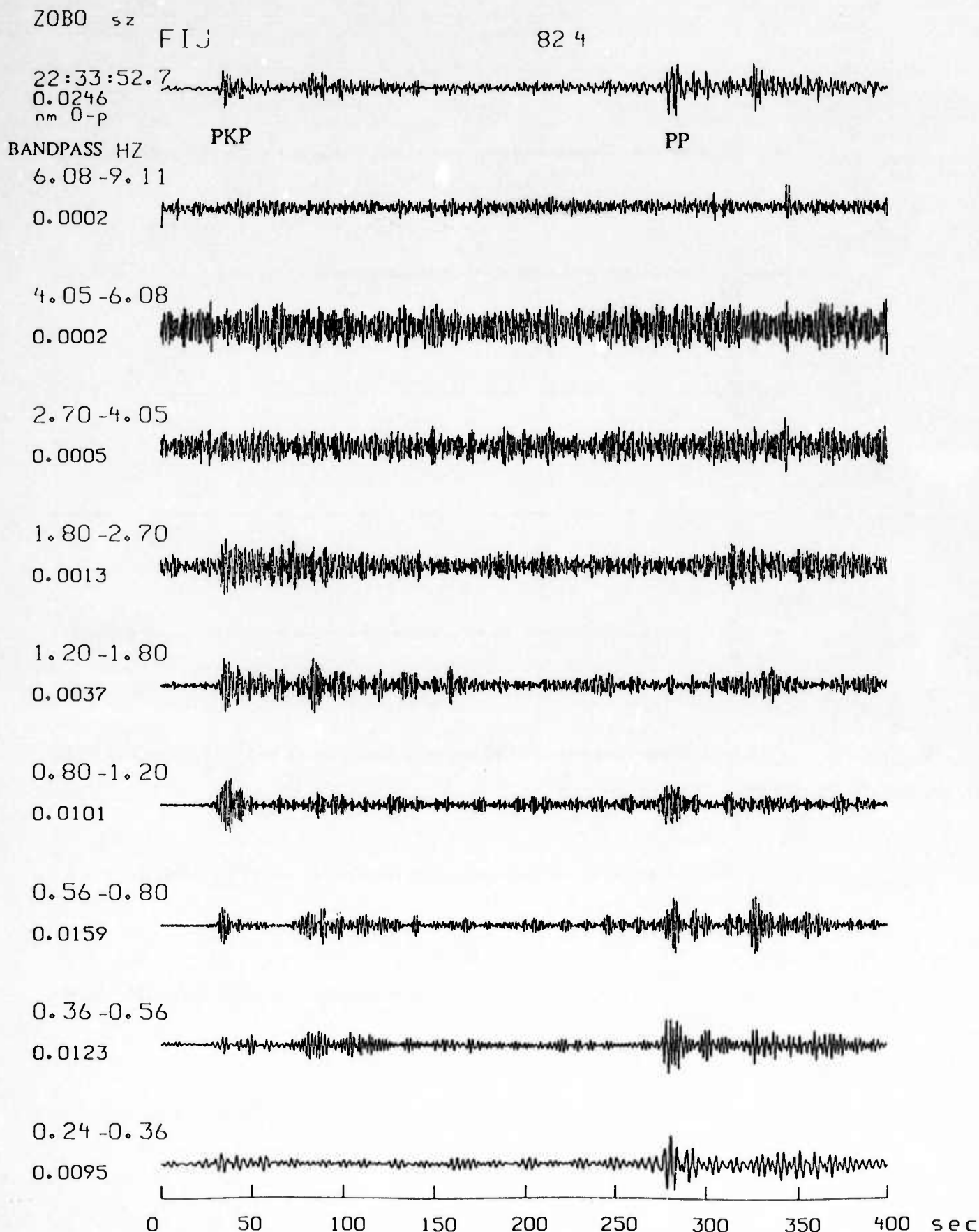


Figure B13. Band-pass filtered vertical component seismograms for path across E. Pacific with arrival times of PKP and PP identified. Absence of high frequency PP phase indicates a low Q bounce region.

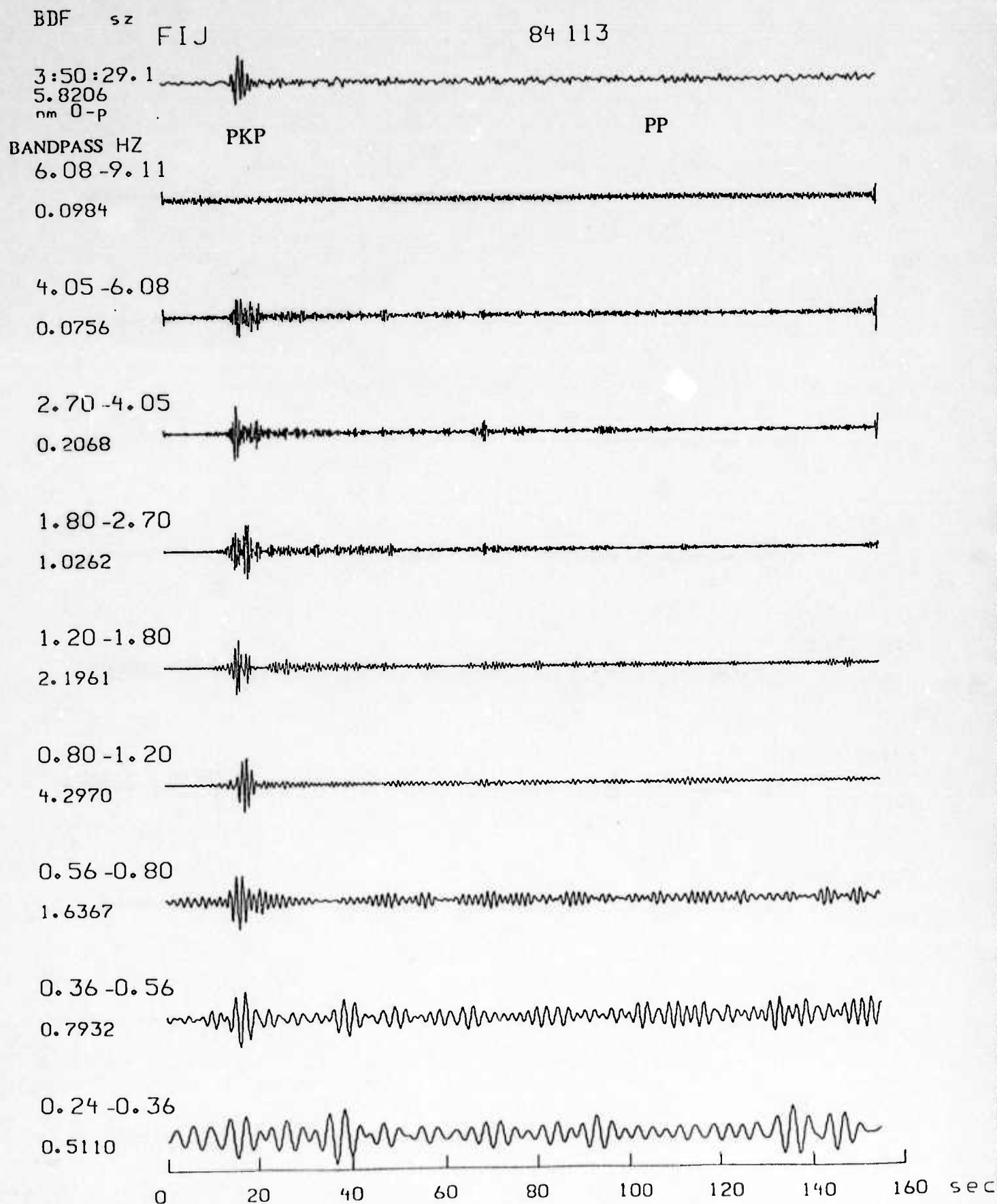


Figure B14. Band-pass filtered vertical component seismograms for path across E. Pacific with arrival times of PKP and PP identified. Absence of high frequency PP phase indicates a low Q bounce region.

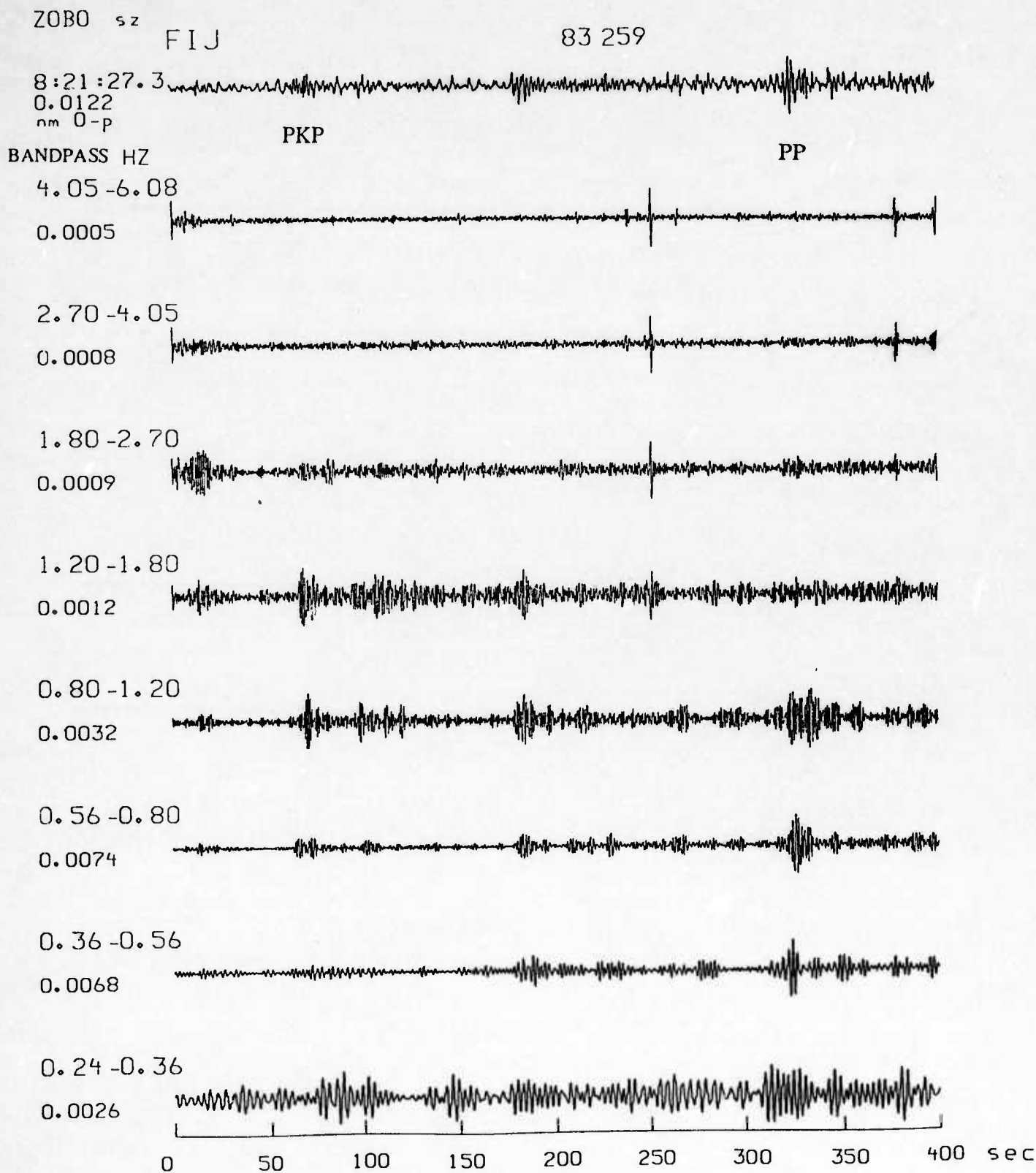


Figure B15. Band-pass filtered vertical component seismograms for path across E. Pacific with arrival times of PKP and PP identified. Absence of high frequency PP phase indicates a low Q bounce region.

BDF sz FIJ

85 279

12:18:33.9
7.4204
nm 0-p

BANDPASS HZ

6.08 -9.11

0.0900

PKP

PP

4.05 -6.08

0.0595

2.70 -4.05

0.2914

1.80 -2.70

1.1351

1.20 -1.80

2.3054

0.80 -1.20

2.5893

0.56 -0.80

3.1251

0.36 -0.56

1.8215

0.24 -0.36

0.5549

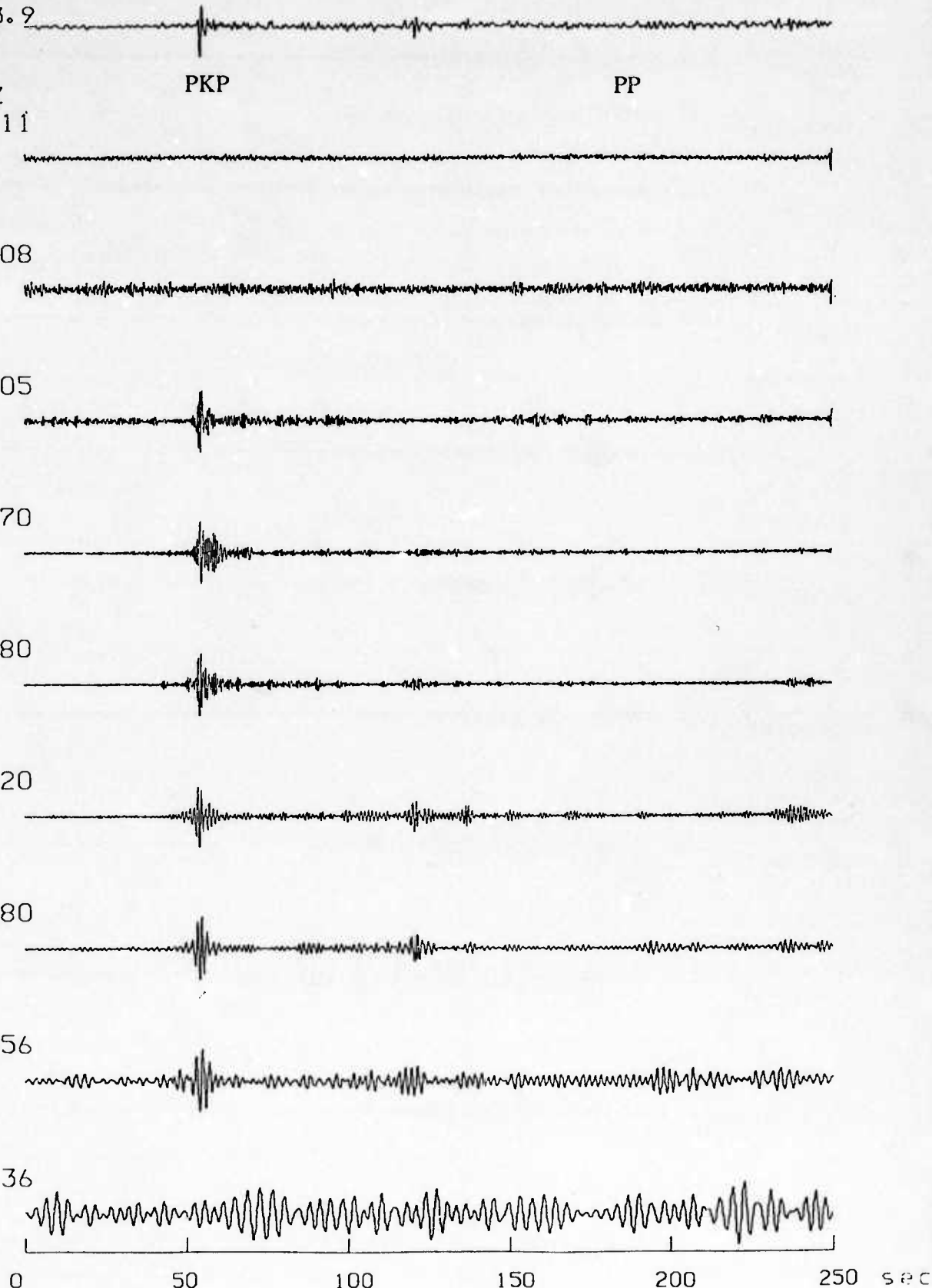


Figure B16. Band-pass filtered vertical component seismograms for path across E. Pacific with arrival times of PKP and PP identified. Absence of high frequency PP phase indicates a low Q bounce region.

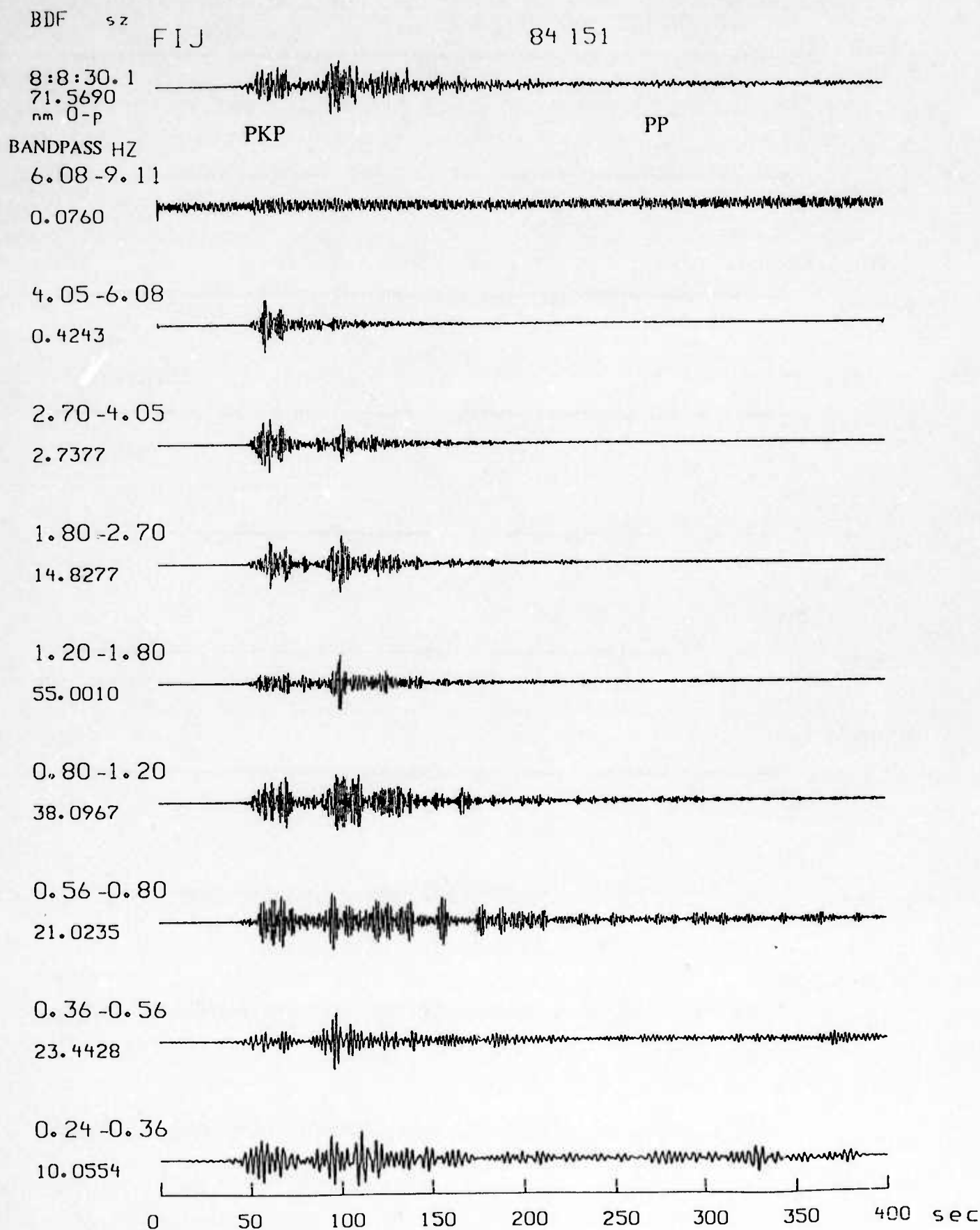


Figure B17. Band-pass filtered vertical component seismograms for path across E. Pacific with arrival times of PKP and PP identified. Absence of high frequency PP phase indicates a low Q bounce region.

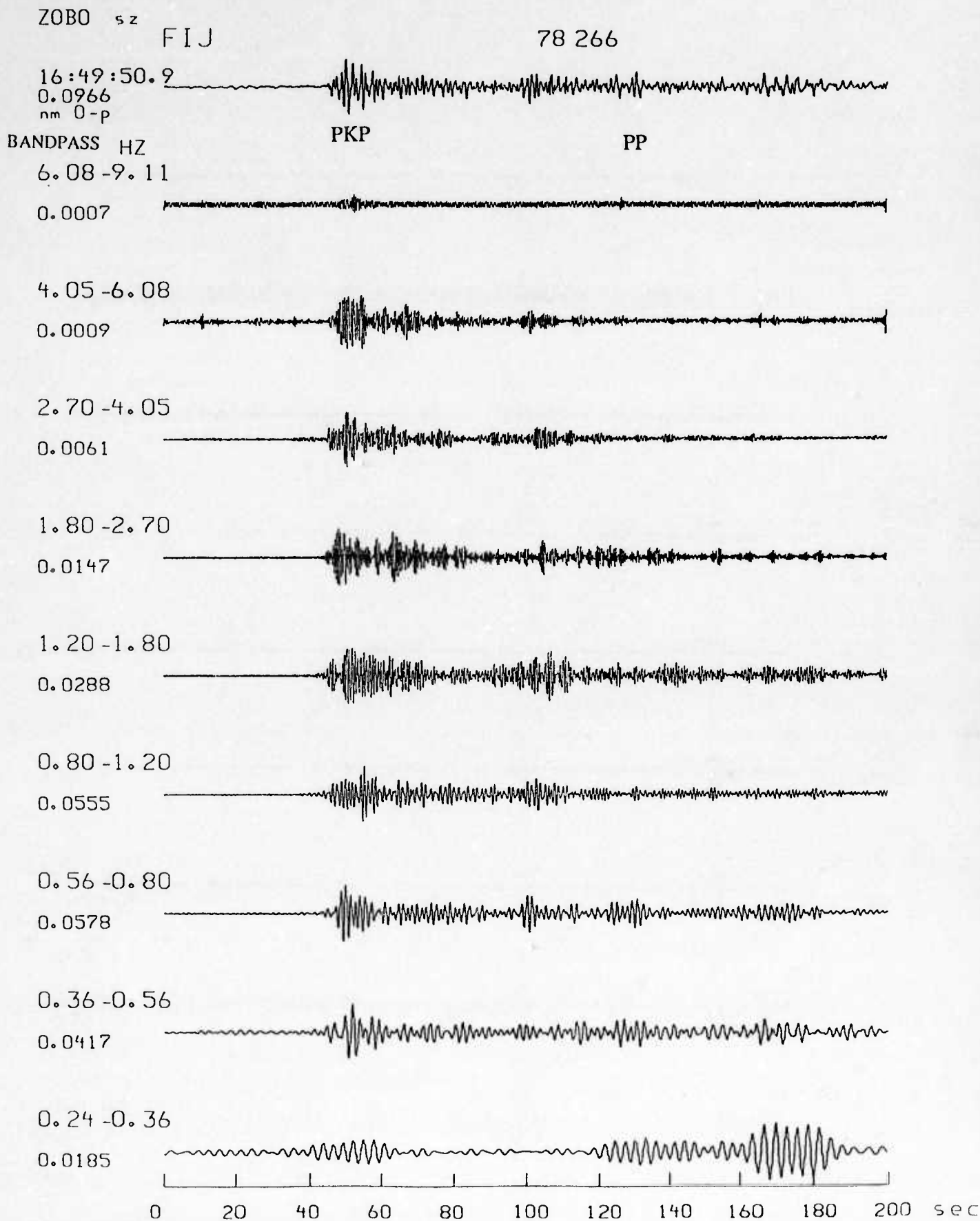


Figure B18. Band-pass filtered vertical component seismograms for path across E. Pacific with arrival times of PKP and PP identified. Absence of high frequency PP phase indicates a low Q bounce region.

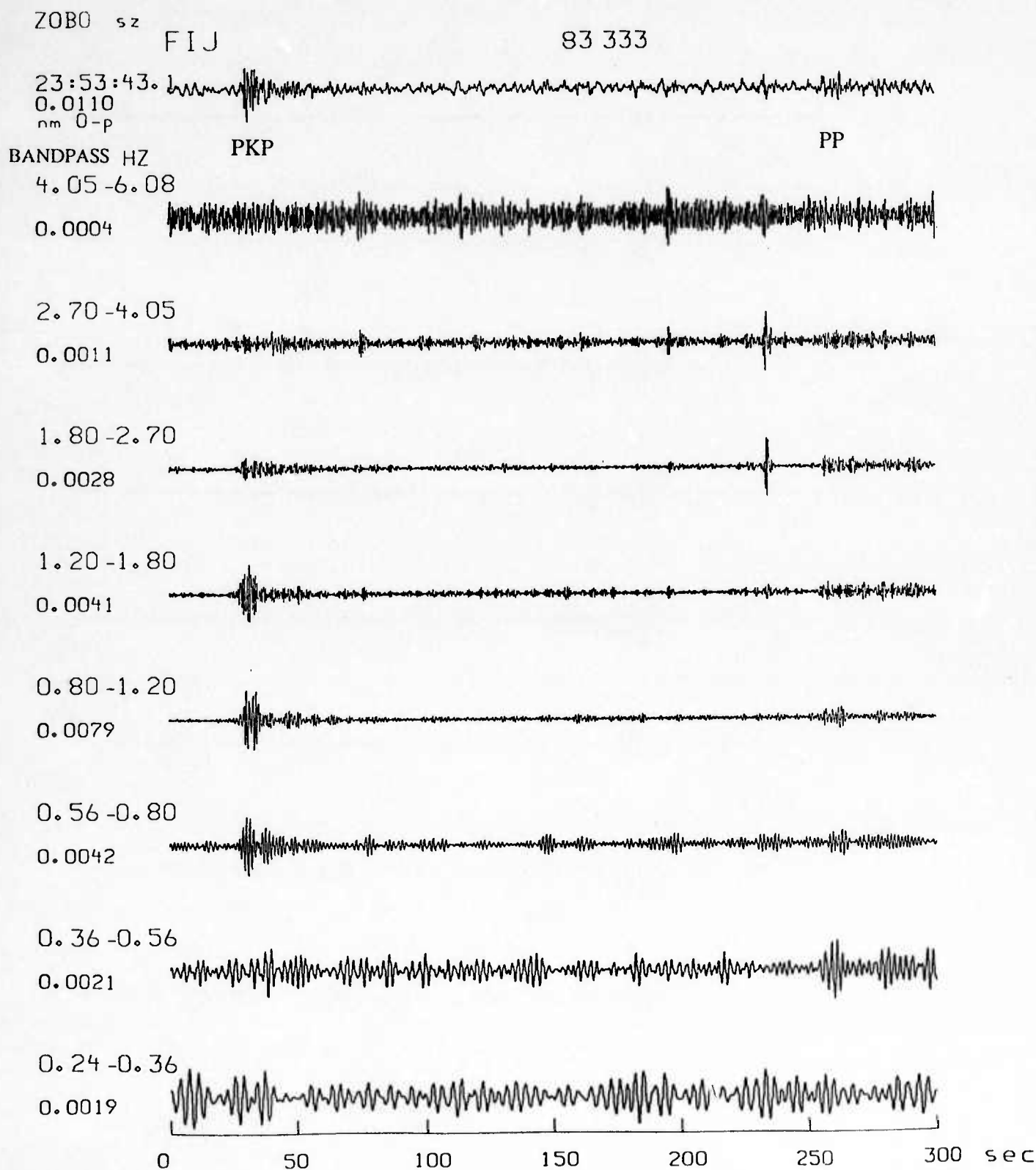


Figure B19. Band-pass filtered vertical component seismograms for path across E. Pacific with arrival times of PKP and PP identified. Absence of high frequency PP phase indicates a low Q bounce region.

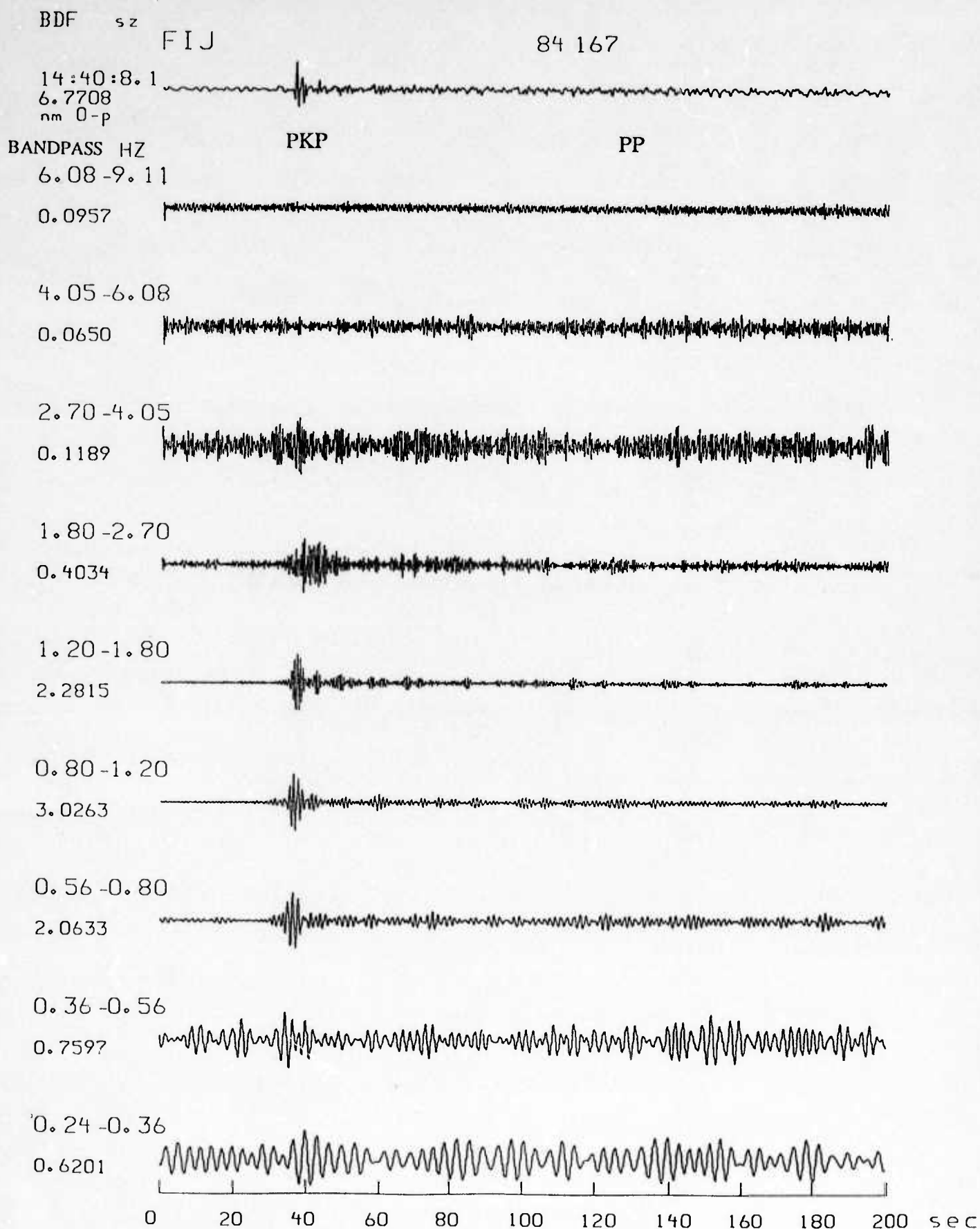


Figure B20. Band-pass filtered vertical component seismograms for path across E. Pacific with arrival times of PKP and PP identified. Absence of high frequency PP phase indicates a low Q bounce region.

(THIS PAGE INTENTIONALLY LEFT BLANK)

APPENDIX C

Rise Time Analyses.

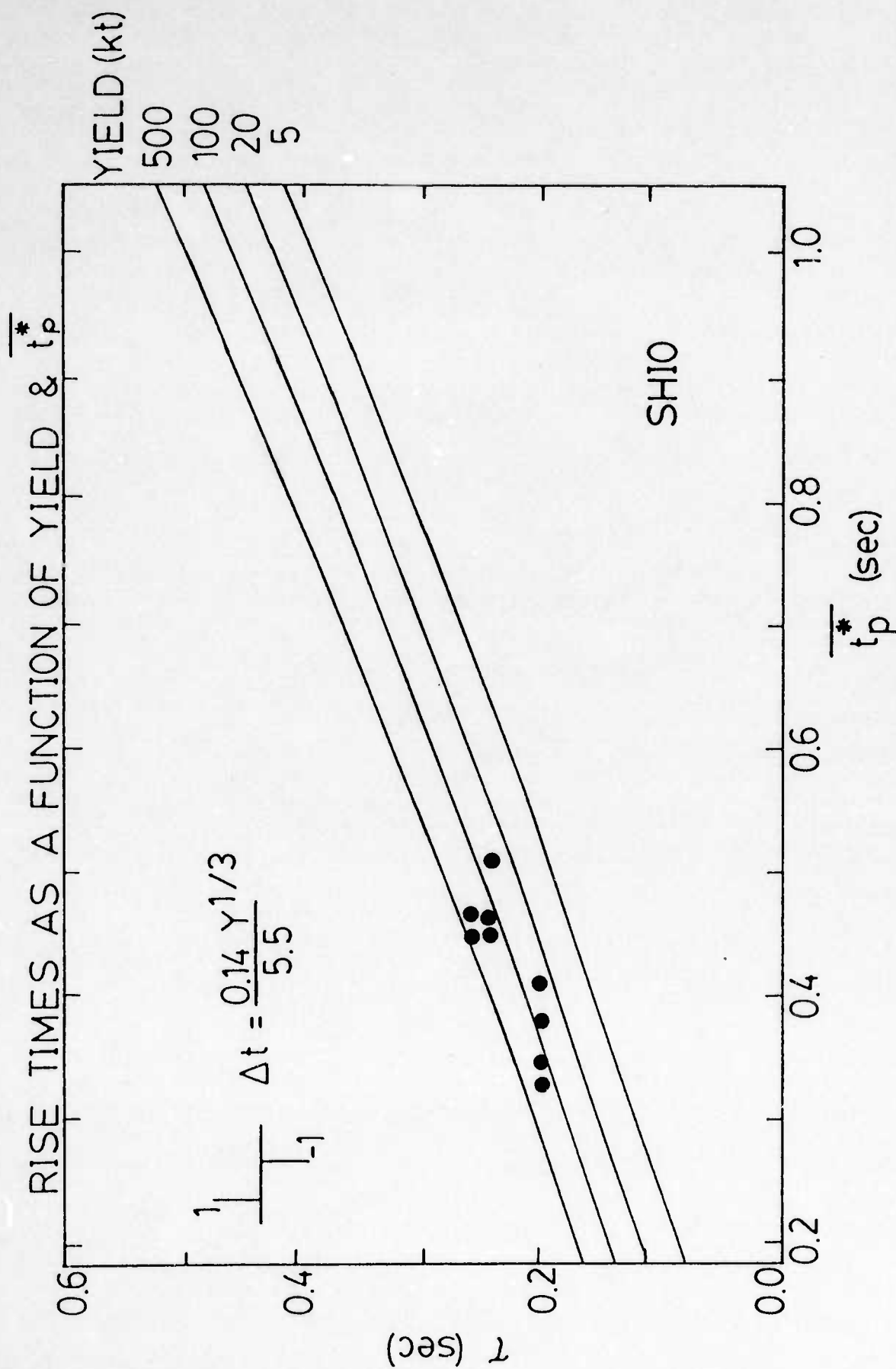


Figure C1. Rise times of P waves from Kazakh nuclear explosions recorded at SHIO. The maximum t_p^* for P waves for this path is around 0.4 sec.

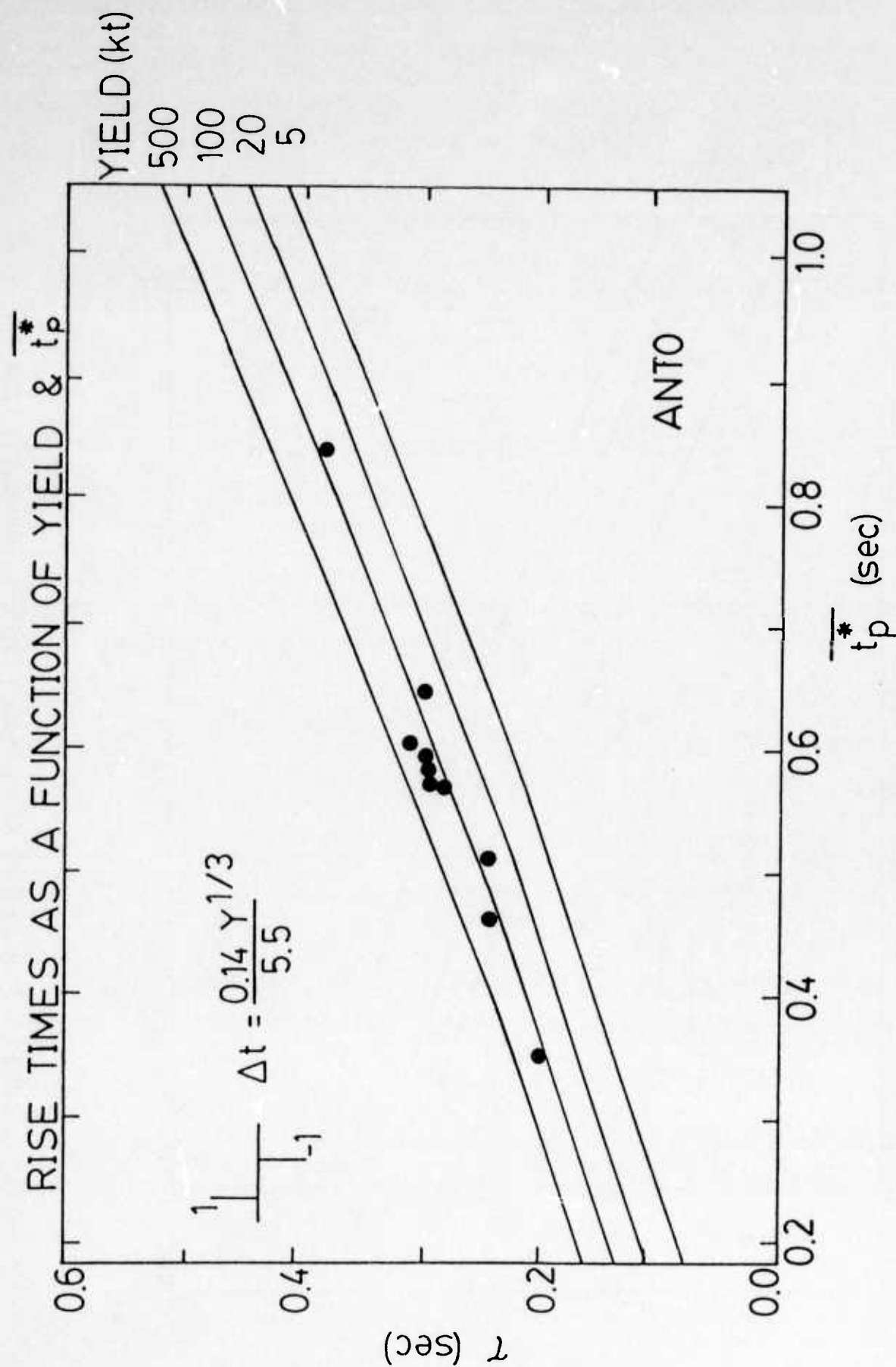


Figure C2. Rise times of P waves from Kazakh nuclear explosions recorded at ANTO. The maximum t_p^* for P waves for this path is around 0.55 sec.

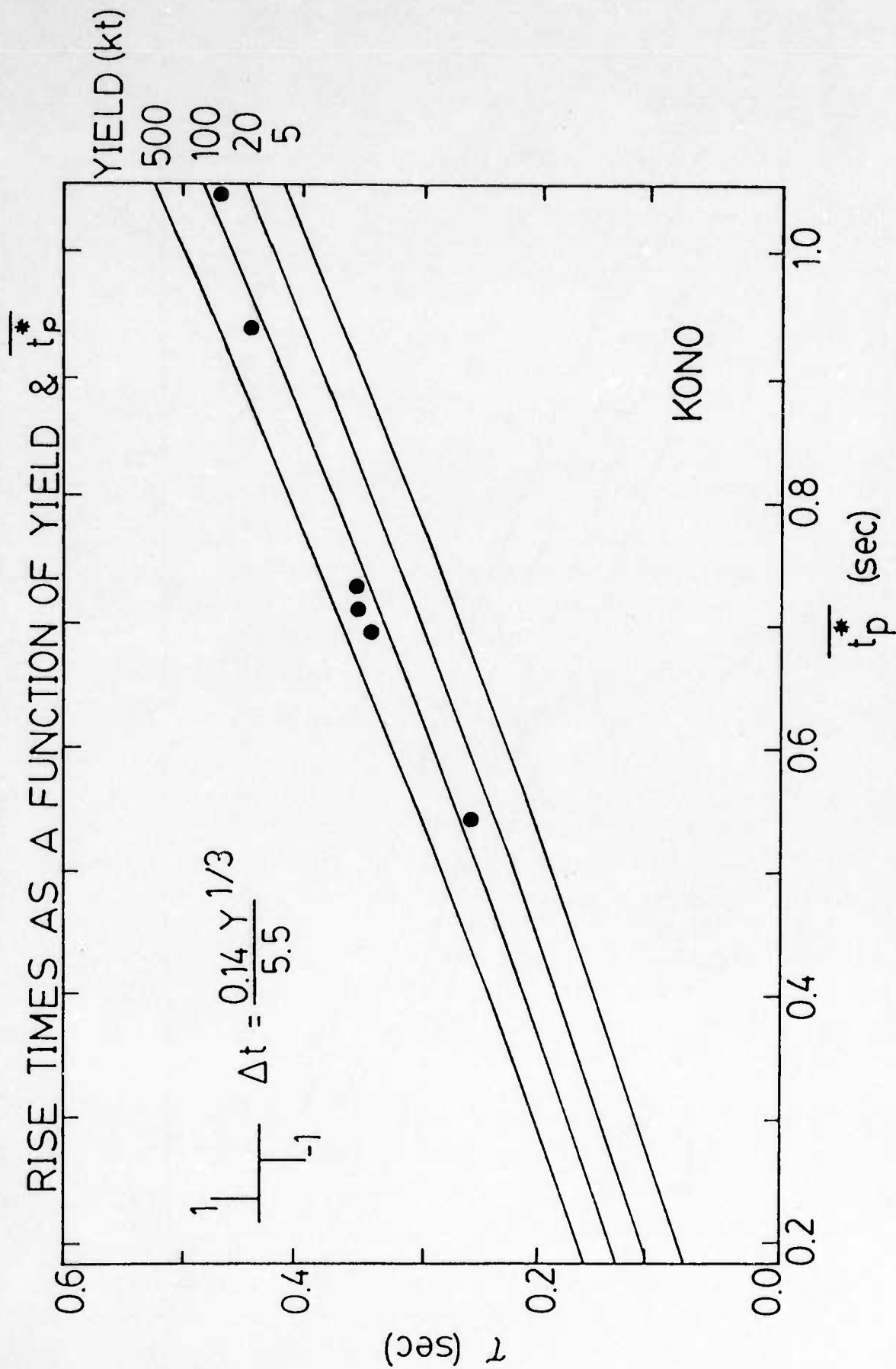


Figure C3. Rise times of P waves from Kazakh nuclear explosions recorded at KONO. The maximum $\overline{t_p^*}$ values for P waves center around 0.8 sec with the lowest at 0.5 sec.

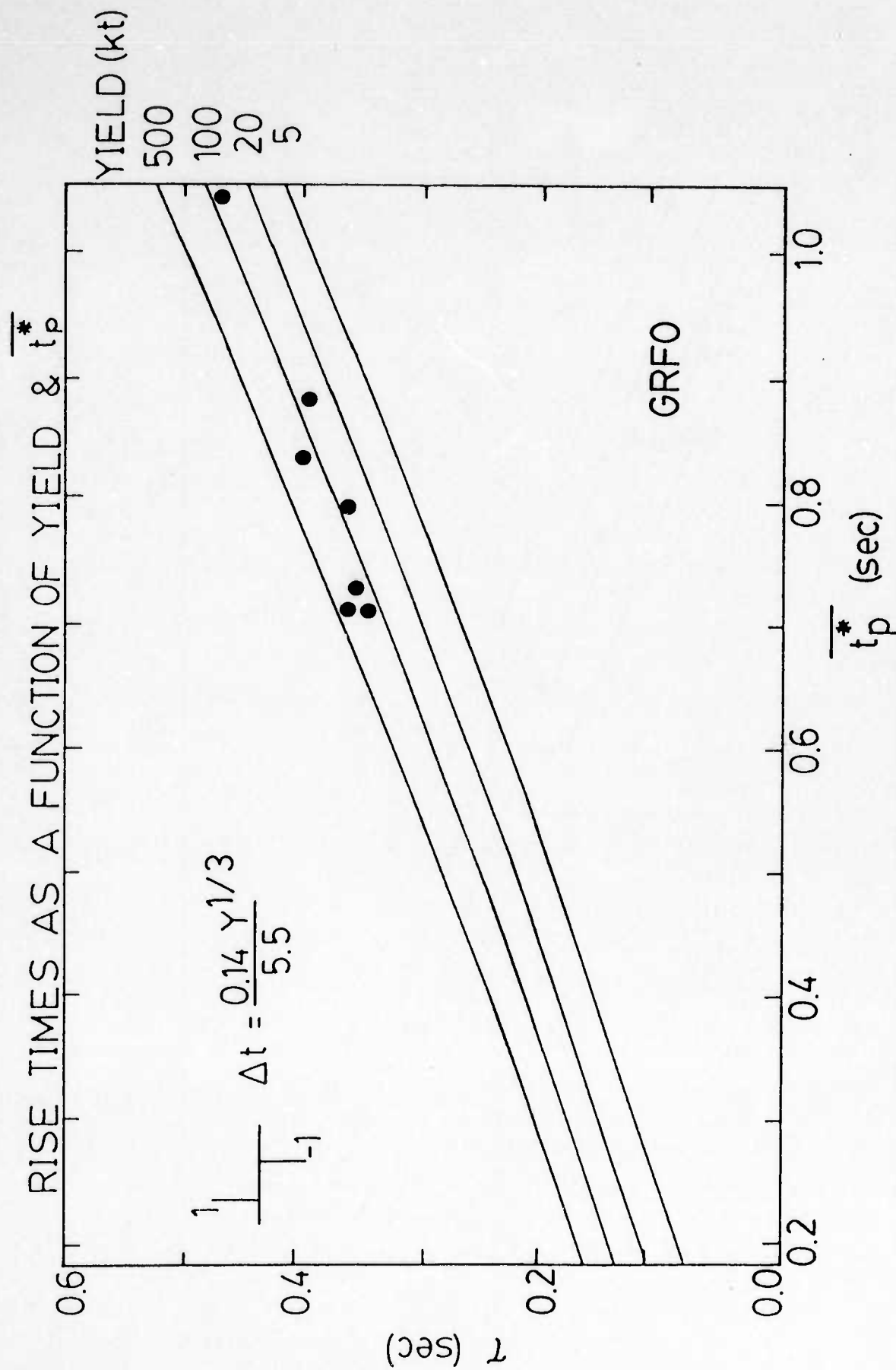


Figure C4. Rise times of P waves from Kazakh nuclear explosions recorded at GRFO. The maximum $\overline{t_p^*}$ for P waves for this path is around 0.8 sec.

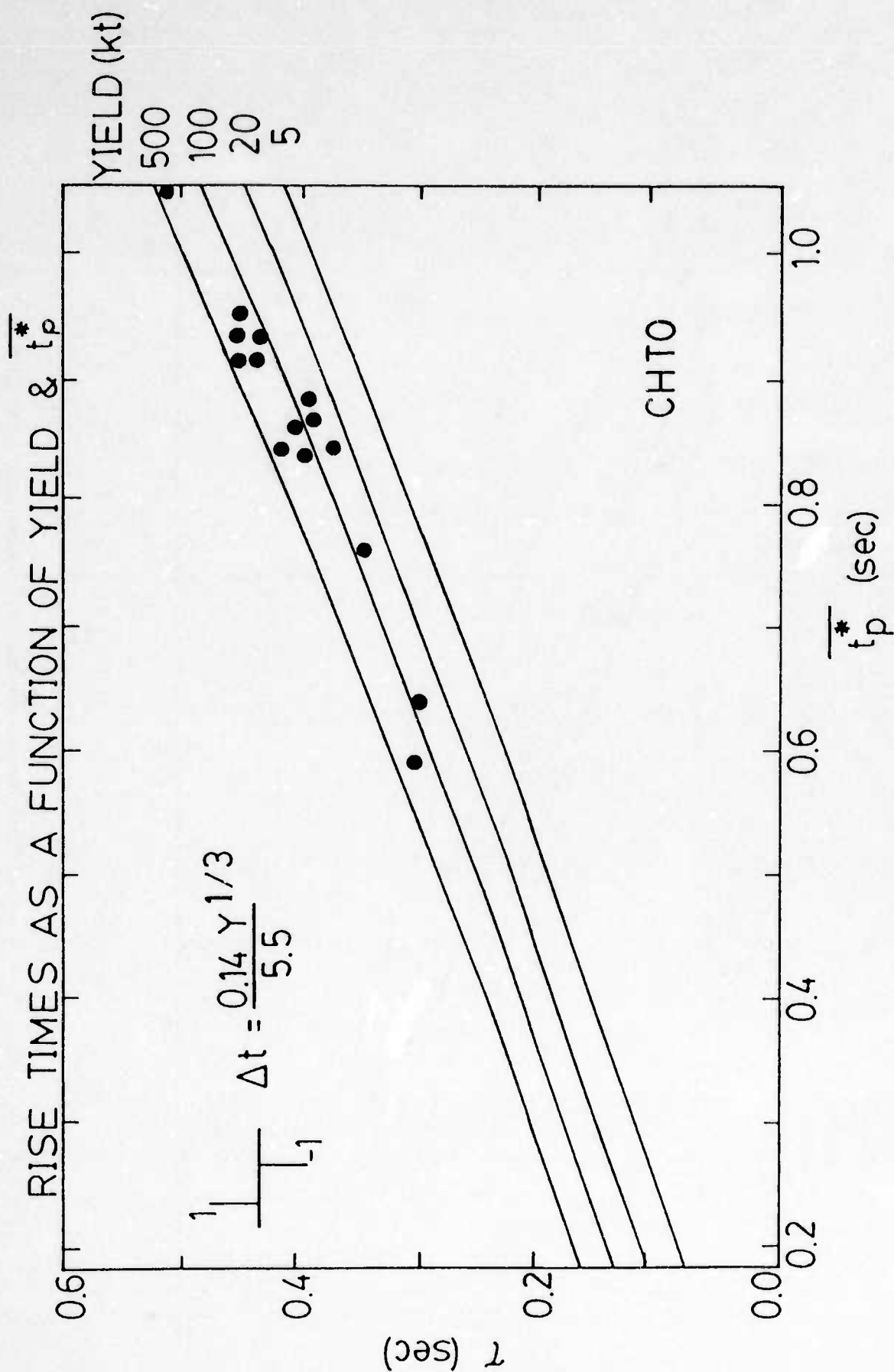


Figure C5. Rise times of P waves from Kazakh nuclear explosions recorded at CHTO. The maximum t_p^* values for P waves center around 0.85 sec with the lowest value near 0.6 sec indicating high attenuation for this path.

DISTRIBUTION LIST
FOR UNCLASSIFIED REPORTS
DARPA-FUNDED PROJECTS
(Last Revised: 5 Jan 1987)

<u>RECIPIENT</u>	<u>NO. OF COPIES</u>
DEPARTMENT OF DEFENSE	
DARPA/GSD ATTN: Dr. R. Alewine and Dr. R. Blandford 1400 Wilson Boulevard Arlington, VA 22209-2308	2
DARPA/PM 1400 Wilson Boulevard Arlington, VA 22209-2308	1
Defense Intelligence Agency Directorate for Scientific and Technical Intelligence Washington, D.C. 20301	1
Defense Nuclear Agency Shock Physics Washington, D.C. 20305-1000	1
Defense Technical Information Center Cameron Station Alexandria, VA 22314	12
DEPARTMENT OF THE AIR FORCE	
AFGL/LWH ATTN: Dr. J. Cipar and Mr. J. Lewkowicz Terrestrial Sciences Division Hanscom AFB, MA 01731-5000	2
AFOSR/NPG ATTN: Director Bldg. 410, Room C222 Bolling AFB, Washington, D.C. 20332	1

AFTAC/CA 1
ATTN: STINFO Officer
Patrick AFB, FL 32925-6001

AFTAC/TG 3
Patrick AFB, FL 32925-6001

AFWL/NTESG 1
Kirtland AFB, NM 87171-6008

DEPARTMENT OF THE NAVY

NORDA 1
ATTN: Dr. J.A. Ballard
Code 543
NSTL Station, MS 39529

DEPARTMENT OF ENERGY

Department of Energy 1
ATTN: Mr. Max A. Koontz (DP-52)
International Security Affairs
1000 Independence Avenue
Washington, D.C. 20545

Lawrence Livermore National Laboratory 2
ATTN: Dr. J. Hannon and Dr. M. Nordyke
University of California
P.O. Box 808
Livermore, CA 94550

Los Alamos Scientific Laboratory 2
ATTN: Dr. K. Olsen and Dr. T. Weaver
P.O. Box 1663
Los Alamos, NM 87544

Sandia Laboratories 1
ATTN: Mr. P. Stokes
Geosciences Department 1255
Albuquerque, NM 87185

OTHER GOVERNMENT AGENCIES

Central Intelligence Agency 1
ATTN: Dr. L. Turnbull
OSI/NED, Room 5G48
Washington, D.C. 20505

U.S. Arms Control and Disarmament Agency 1
ATTN: Dr. M. Fimer
Verification and Intelligence Bureau, Rm 4953
Washington, D.C. 20451

U.S. Arms Control and Disarmament Agency 1
ATTN: Mrs. M. Hoinkes
Multilateral Affairs Bureau, Rm 5499
Washington, D.C. 20451

U.S. Geological Survey 1
ATTN: Dr. T. Hanks
National Earthquake Research Center
345 Middlefield Road
Menlo Park, CA 94025

U.S. Geological Survey 1
ATTN: Dr. R. Masse
Global Seismology Branch
Box 25046, Stop 967
Denver Federal Center
Denver, CO 80225

UNIVERSITIES

Boston College 1
ATTN: Dr. A. Kafka
Western Observatory
381 Concord Road
Weston, MA 02193

California Institute of Technology 1
ATTN: Dr. D. Harkrider
Seismological Laboratory
Pasadena, CA 91125

Columbia University 1
ATTN: Dr. L. Sykes
Lamont-Doherty Geological Observatory
Palisades, NY 10964

Cornell University 1
ATTN: Dr. M. Barazangi
INSTOC
Snee Hall
Ithaca, NY 14853

Harvard University ATTN: Dr. J. Woodhouse Hoffman Laboratory 20 Oxford Street Cambridge, MA 02138	1
Massachusetts Institute of Technology ATTN: Dr. S. Solomon, Dr. N. Toksoz, and Dr. T. Jordan Department of Earth and Planetary Sciences Cambridge, MA 02139	3
Southern Methodist University ATTN: Dr. E. Herrin Geophysical Laboratory Dallas, TX 75275	1
State University of New York at Binghamton ATTN: Dr. F. Wu Department of Geological Sciences Vestal, NY 13901	1
St. Louis University ATTN: Dr. O. Nuttli and Dr. R. Herrmann Department of Earth and Atmospheric Sciences 3507 Laclede St. Louis, MO 63156	2
The Pennsylvania State University ATTN: Dr. S. Alexander Geosciences Department 403 Deike Building University Park, PA 16802	1
University of Arizona ATTN: Dr. T. Wallace Department of Geosciences Tucson, AZ 85721	1
University of California, Berkeley ATTN: Dr. T. McEvilly Department of Geology and Geophysics Berkeley, CA 94720	1
University of California Los Angeles ATTN: Dr. L. Knopoff 405 Hilgard Avenue Los Angeles, CA 90024	1

University of California, San Diego ATTN: Dr. J. Orcutt Scripps Institute of Oceanography La Jolla, CA 92093	1
University of Colorado ATTN: Dr. C. Archambeau CIRES Boulder, CO 80309	1
University of Illinois ATTN: Dr. S. Grand Department of Geology 1301 West Green Street Urbana, IL 61801	1
University of Michigan ATTN: Dr. T. Lay Department of Geological Sciences Ann Arbor, MI 48109-1063	1
University of Nevada ATTN: Dr. K. Priestley Mackay School of Mines Reno, NV 89557	1
University of Southern California ATTN: Dr. K. Aki Center for Earth Sciences University Park Los Angeles, CA 90089-0741	1

DEPARTMENT OF DEFENSE CONTRACTORS

Applied Theory, Inc. ATTN: Dr. J. Trulio 930 South La Brea Avenue Suite 2 Los Angeles, CA 90036	1
Center for Seismic Studies ATTN: Dr. C. Romney and Mr. R. Perez 1300 N. 17th Street, Suite 1450 Arlington, VA 22209	2
ENSCO, Inc. ATTN: Mr. G. Young 5400 Port Royal Road Springfield, VA 22151	1

<p> ENSCO, Inc. ATTN: Dr. R. Kemerait 445 Pineda Court Melbourne, FL 32940 </p>	1
<p> Gould Inc. ATTN: Mr. R. J. Woodard Chesapeake Instrument Division 6711 Baymeado Drive Glen Burnie, MD 21061 </p>	1
<p> Pacific Sierra Research Corp. ATTN: Mr. F. Thomas 12340 Santa Monica Boulevard Los Angeles, CA 90025 </p>	1
<p> Rockwell International ATTN: B. Tittmann 1049 Camino Dos Rios Thousand Oaks, CA 91360 </p>	1
<p> Rondout Associates, Inc. ATTN: Dr. P. Pomeroy P.O. Box 224 Stone Ridge, NY 12484 </p>	1
<p> Science Applications, Inc. ATTN: Dr. T. Bache, Jr. P.O.Box 2351 La Jolla, CA 92038 </p>	1
<p> Science Horizons ATTN: Dr. T. Cherry and Dr. J. Minster 710 Encinitas Blvd. Suite 101 Encinitas, CA 92024 </p>	2
<p> Sierra Geophysics, Inc. ATTN: Dr. R. Hart and Dr. G. Mellman 11255 Kirkland Way Kirkland, WA 98124 </p>	2
<p> SRI International ATTN: Dr. A. Florence 333 Ravensworth Avenue Menlo Park, CA 94025 </p>	1
<p> S-Cubed, A Division of Maxwell Laboratories Inc. ATTN: Dr. S. Day P.O. Box 1620 La Jolla, CA 92038-1620 </p>	1

S-Cubed, A Division of
Maxwell Laboratories Inc.
ATTN: Mr. J. Murphy
11800 Sunrise Valley Drive
Suite 1212
Reston, VA 22091 1

Teledyne Geotech
ATTN: Dr. Z. Der and Mr. W. Rivers
314 Montgomery Street
Alexandria, VA 22314 2

Woodward-Clyde Consultants
ATTN: Dr. L. Burdick and Dr. J. Barker
556 El Dorado St.
Pasadena, CA 91105 2

NON-U.S. RECIPIENTS

National Defense Research Institute
ATTN: Dr. O. Dahlman
Stockholm 80, Sweden 1

Blacknest Seismological Center
ATTN: Mr. P. Marshall
Atomic Weapons Research Establishment
UK Ministry of Defence
Brimpton, Reading RG7-4RS
United Kingdom 1

NTNF NORSAR
ATTN: Dr. F. Ringdal
P.O. Box 51
N-2007 Kjeller
Norway 1

OTHER DISTRIBUTION

To be determined by the project office 9